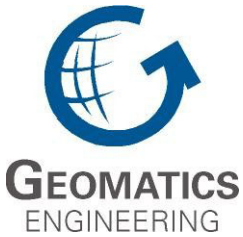

UCGE Reports
Number 20181

Department of Geomatics Engineering

Terrain Effects on Geoid Determination

(URL: http://www.geomatics.ucalgary.ca/links/GradTheses.html)

by

Sujan Bajracharya

September 2003

Calgary, Alberta, Canada

UNIVERSITY OF CALGARY

Terrain Effects on Geoid Determination

by

Sujan Bajracharya

A THESIS

SUBMITTED TO THE FACULTY OF GRADUATE STUDIES

IN PARTIAL FULFILMENT OF THE REQUIREMENTS FOR THE

DEGREE OF MASTER OF SCIENCE

DEPARTMENT OF GEOMATICS ENGINEERING

CALGARY, ALBERTA

September, 2003

Abstract

Gravimetric reduction schemes play an important role on precise geoid determination, especially in rugged areas. The main theme of this research is to explore different gravimetric reduction schemes in the context of precise geoid determination, in addition to the usual Helmert's second method of condensation and residual terrain model (RTM). A numerical investigation is carried out in the rugged area of the Canadian Rockies to study gravimetric geoid solutions based on the Rudzki inversion scheme, Helmert's second method of condensation, RTM, and the topographic-isostatic reduction methods of Airy-Heiskanen (AH) and Pratt-Hayford (PH). The mathematical formulations of each of these techniques are presented. This study shows that the Rudzki inversion scheme, which had neither been used in practice in the past nor is it used at present, can become a standard tool for gravimetric geoid determination since the Rudzki geoid performs as well as the Helmert and RTM geoids (in terms of standard deviation and range of maximum and minimum values) when compared to the GPS-levelling geoid of the test area. Also, it is the only gravimetric reduction scheme which does not change the equipotential surface and thus does not require the computation of the indirect effect.

In addition, this thesis investigated two important topics for precise geoid determination; the density and gravity interpolation effects on Helmert geoid determination and the terrain aliasing effects on geoid determination using different mass reduction schemes. The study of first topic shows that the topographic-isostatic gravimetric reduction schemes like the PH or AH models or the topographic reduction of RTM, should be applied for smooth gravity interpolation for precise Helmert geoid determination instead of the commonly used Bouguer reduction scheme. The density information should be incorporated not only for the computation of terrain corrections (TC), but also in all other steps of the Helmert geoid computational process. The study of the second topic suggests that a DTM grid resolution of 6″ or higher is required for precise geoid determination with an accuracy of a decimetre or higher for any gravimetric reduction method chosen in rugged areas.

Acknowledgements

I would like to express my gratitude to my supervisor, Dr. Michael Sideris, for his guidance and support throughout my graduate studies, as well as his constructive criticism of my research. This thesis would not have been possible without him. I am grateful to Dr. N. Sneeuw, Dr. P. Wu and Dr. Y. Gao for their suggestions on my thesis as members of the examination committee.

I would like to thank Dr. Christopher Kotsakis for his suggestions and criticism of my work at the beginning of this research. I thank Georgia Fotopoulos for her continuous help and suggestions on academic and professional issues. Thank you Rossen, for being a very good friend of mine.

I would like to thank George Vergos and Fadi Bayoud from the "gravity group" for creating an enjoyable working environment. I acknowledge the Department of Geomatics Engineering for its help on various academic matters and NSERC and the GEOIDE NCE for providing financial support for this research.

Finally, I am grateful to my parents and my family for their support and patience during my stay at the University of Calgary.

Contents

Chapter

List of Tables

List of Figures

LIST OF SYMBOLS

N	geoid undulation
h	orthometric height
h_n	normal height
h_e	ellipsoidal height
G	gravitational constant
E	integration area
S	Stokes's kernel
φ, λ	geodetic latitude and longitude
R	radius of reference sphere
T	gravitational potential
T'	gravitational potential of inverted topography
T_{Cond}	gravitational potential of condensed topography
T_{Comp}	gravitational potential of compensated masses
ρ	Earth's crust density
ρ_c	density of water
ρ'	density of the inverted topography
ρ_1	density of upper mantle
a	radius of the cylinder
b	thickness of cylinder
g	measured gravity value
$\overline{g}$	mean gravity
$\overline{\gamma}$	mean normal gravity
γ	normal gravity
F	free-air reduction
c	terrain correction
$\mathbf{F}$	Fourier transform
$\mathbf{F}^{-1}$	inverse Fourier transform

ψ	spherical distance
κ	surface density of condensation layer
D	compensation depth
t	root depth
$\Delta\rho$	density contrast
Δg	gravity anomaly
$\bar{C}_{nm}$,$\bar{S}_{nm}$	fully normalized coefficients
N_{ind}	indirect effect on geoid
N_{GM}	long wavelength part of the geoid
$N_{\Delta g}$	residual geoid
ΔT	change in the potential
ζ	quasigeoid
δA	the attraction change
Δx, Δy, Δz	grid spacing in x, y, and z directions
Δg_T	direct topographical effect on gravity
Δg_F	free-air anomaly
Δg_{GM}	reference gravity anomaly
Δg_B	Bouguer anomalies
A	gravitational attraction due to topography
A_{Inv}	gravitational attraction due to inverted masses
A_{Com}	gravitational attraction due to compensated masses
δg	indirect topographical effect on gravity
$\bar{P}_{nm}$	fully normalized associate Legendre functions.

LIST OF ABBREVIATIONS

BVP	boundary value problem
TC	terrain correction
AH	Airy-Heiskanen
PH	Pratt-Hayford
DTM	digital terrain model
DDM	digital density model
FFT	fast Fourier transform
RTM	residual terrain model
IUGG	International Union of Geodesy and Geodynamics
GRS	geodetic reference system
MP	mass prism
ML	mass line
GPS	global positioning system
FA	free-air anomalies
RMS	root mean square (error)
EGM96	Earth geopotential model 96

Chapter 1
Introduction

1.1 Background

The topographical effect is one of the most important components in the solution of the geodetic boundary value problem (BVP), and should be treated properly in the determination of a precise geoid. The classical solution of the geodetic BVP using Stokes's formula for geoid determination assumes that there should be no masses outside the geoid. The input gravity anomalies should refer to the geoid, which requires the actual Earth's topography to be regularized in some way. The mathematical and physical treatment of this issue play an important role in the computation of a precise (local or regional) gravimetric geoid solution. There are several reduction techniques, which all differ depending on how these topographical masses outside the geoid are dealt with. Each gravity reduction scheme treats the topography in a different way. In theory, gravimetric solution for geoid determination using different mass reduction methods should give the same results, provided that the corresponding indirect effect is taken into account properly and consistently (Heiskanen and Moritz, 1967; Heiskanen and Vening Meinesz, 1958).

The specific choice of gravity reduction method depends on the magnitude of its indirect effect, the smoothness and the magnitude of the resulting gravity anomalies, and their associated geophysical interpretation. The complete Bouguer reduction, for example, removes all topographic masses above the geoid producing smooth gravity anomalies, but introduces excessively large indirect effects. Topographic-isostatic gravity reductions (for example, Airy-Heiskanen and Pratt-Hayford), on the other hand, remove the topographic masses by shifting them into the interior of the geoid according to some model of isostasy, and they exhibit all the characteristics of a 'good' gravity reduction scheme. These methods introduce indirect effects of the order of several metres, which are much smaller than those of the Bouguer scheme, but still larger than those of Helmert's second

method of condensation, and thus have not been used in geoid determination since the late seventies. In Helmert's second method, the topographic masses between geoid and the Earth's surface are condensed on the geoid forming a surface layer. The direct topographic effects and indirect effects using this condensation reduction method have been discussed in the literature; see, for example, Heiskanen and Moritz (1967), Wichiencharoen (1982), Wang and Rapp (1990), Sideris (1990), Heck (1993), and Vanicek and Martinec (1994). The residual terrain model (RTM) scheme, which is not a topographic-isostatic reduction but gives anomalies similar to topographic-isostatic anomalies, has been used for almost two decades as a common tool for terrain reduction in quasigeoid computation (Forsberg, 1984). The recent studies on Helmert's first method of condensation by Heck (2003) and on topographic-isostatic reductions by Kuhn (2000) can be considered as an exploration of different gravimetric reduction techniques for geoid determination, in addition to RTM and Helmert's second method of condensation. Theoretical and practical research on direct and indirect effects is very important to be carried out for different gravimetric reduction schemes in addition to Helmert's second method of condensation in the context of precise geoid determination.

One of the most interesting methods of gravimetric reduction is the Rudzki inversion scheme, developed by the Polish scientist Rudzki in 1905 (Rudzki, 1905; Heiskanen and Meinesz, 1958; Heiskanen and Moritz, 1967). He postulated his theory of gravimetric reduction in such a way that the potential of topographical masses above the geoid is equal to that of inverted topographical masses inside the geoid. Besides Rudzki's own original work on this reduction scheme, it had neither been used in the past nor is it used at the present for geoid determination. However, the emphasis on using this gravimetric scheme had been given by Lambert (1930). This reduction method is purely mathematical and has no associated geophysical meaning, which is not as important in geoid determination as in geophysics.

The study of terrain aliasing effects on geoid determination is very important for every terrain reduction technique. There are different resolutions of digital terrain model (DTM)

available these days throughout the world. Since a small grid spacing in modern DTMs can represent the local features of rugged terrain very precisely, such high-resolution DTMs should be used (if available) in the numerical computation of different mass modeling techniques for geoid determination and gravity densification; this has been shown in previous studies (see, e.g., Kotsakis and Sideris, 1997; Kotsakis and Sideris, 1999).

The knowledge of actual crust density is required in each gravity reduction method (including the terrain correction) in order to effectively and rigorously remove all the masses above the geoid. Constant density is often used in practice instead of actual crust density because of lack of actual bedrock density information. However, two-dimensional digital density models (DDMs) are becoming available these days in some countries though a three-dimensional model is required to represent a real topographical density distribution. These density models should be incorporated in the terrain correction (TC) computation. This has been studied by Tziavos et al. (1996), Huang et al. (2000), and Tziavos and Featherstone (2000). The study of the effects on gravity and geoid using actual density information in different mass reduction techniques will show us the significance of using variable density instead of using constant crust density for precise geoid determination.

Molodensky's solution is the other fundamental solution to the geodetic boundary value problem. This approach considers the Earth's surface as the boundary reference surface. This solution overcomes the problem of removing all the topographical masses above the geoid, which is strictly required by Stokes's approach. Molodensky formulated the integrals in the form of series, which consist of gravity anomalies and the topographical heights. Molodensky's theory requires both gravity anomalies and the topographical heights be available at the same points but does not require the knowledge on the crust density information. This modern solution gives the quasigeoid but not a level surface (geoid) as in Stokes's solution. Brovar's and Pellinen's solutions to this modern geodetic boundary problem have been extensively discussed in Moritz (1980). The importance of

gravimetrtic mass reduction in quaisigeoid determination was first introduced by Pellinen (1962).

Gravity interpolation is one of the important aspects in Helmert geoid determination. The gravity anomalies based on Helmert's second method of condensation are very rough. The Free-air (FA) anomalies computed directly can not be used in practice for precise Helmert geoid determination and thus the Bouguer gravimetric terrain reduction is most commonly used for interpolation to obtain smoother FA anomalies. The study of using different gravimetric terrain reductions for interpolating FA anomalies in addition to the Bouguer reduction is very important in precise geoid determination using Helmert's second method of condensation.

1.2 Objectives

The main objectives of the research are the following:

(i) The first and primary objective of this research is to study gravimetric geoid solutions in planar approximation using different gravimetric reduction schemes in the context of precise geoid determination. The gravimetric geoid solutions based on the Rudzki inversion scheme, Helmert's second method of condensation, RTM method, and Airy-Heiskanen (AH) and Pratt-Hayford (PH) topographic-isostatic methods will be studied and they will be critically compared in terms of their usefulness in precise geoid determination.

(ii) The second objective is to investigate two important aspects of precise geoid determination using Helmert's second method of condensation, which is commonly used in practice. The first one is to study the importance of using actual crust density information instead of using constant density. A two dimensional digital density model will be incorporated not only in the TC computation, but also in all steps of Helmert's geoid computational process.

The next one is to study the effect of different gravimetric terrain reductions on gravity interpolation and on Helmert geoid determination.

(iii) The third and final objective is to investigate the importance of using various grid resolution levels of DTM for different mass reduction schemes within the context of precise geoid determination. The terrain aliasing effects on geoid determination using the Rudzki inversion scheme, Helmert's second method of condensation, the RTM model, and Pratt-Hayford model will be studied.

1.3 Thesis outline

This thesis consists of six chapters. Each chapter from chapter 2 to chapter 6 is structured in such a way that it will focus on each objective described above followed by the results from numerical investigations carried out in the test area.

Chapter 2 describes the concepts of geoid and quasigeoid, briefly explains each gravimetric reduction scheme and presents computational formulas required to compute indirect effects and geoid undulations using each gravimetric reduction scheme.

Chapter 3 presents all mathematical formulations required to study the direct topographical effects on gravity for every mass reduction scheme.

Chapter 4 presents the numerical investigation of different types of topographic and topographic-isostatic gravity anomalies in the test area along with their critical comparisons. The results of indirect effects, gravimetric geoid solutions using different reductions, their differences with GPS-levelling geoid of the test area, and their comparison are shown in this chapter.

Chapter 5 shows numerical results of two important aspects of precise Helmert geoid determination. First, it shows results of the effects that different gravimetric reductions schemes have on gravity interpolation and precise Helmert geoid determination. Second, it shows results illustrating the importance of using actual density information instead of using constant density in the context of precise Helmert geoid determination.

Chapter 6 presents the results of the terrain aliasing effects in two parts. First, it shows the results of aliasing effects on TC computation. Second, it shows the terrain aliasing effects on geoid determination using the Rudzki inversion scheme, Helmert's second method of condensation, the RTM model, and the Pratt-Hayford topographic-isostatic method.

In chapter 7, conclusions are drawn from the investigations of the research carried out in this thesis, and some recommendations are presented based on these investigations.

Chapter 2
Gravimetric Geoid Determination

2.1 Geoid and quasigeoid

Precise geoid determination is one of the most important tasks in physical geodesy. The geoid is a vertical datum for orthometric heights. The orthometric height is the height above sea level. The ellipsoidal height is the height above reference ellipsoid. The recent advances of GPS techniques made it possible to determine the ellipsoidal heights with an accuracy of millimetre/centimetre depending on the observation and processing techniques. The combination of GPS and a precise gravimetric geoid is an alternative tool to the orthometric height determination using spirt levelling (and/or trigonometric levelling).

This modern approach of determining orthometric height can be more effective in both cost and time compared to the conventional spirit (and/or trigonometric) levelling. The precise geoid is important not only in geodetic applications, but also in geophysical and oceanographic applications. The accurate geoid determination possesses more demand these days than ever before because of the latest developments in GPS technology which let us obtain the ellipsoidal height with high accuracy.

The geoid is defined as an equipotential surface (a surface of constant potential), a level surface, which approximates the mean sea surface of the earth; it represents the mathematical formulation of a “horizontal” surface at sea level (Heiskanen and Moritz, 1967). Geoid determination is carried out using Stokes’s approach, which is regarded as a classical solution to the geodetic boundary value problem. Figure 2.1 illustrates the geometrical principle of the geoid. The geoid undulation is the vertical separation between the geoid and the ellipsoid. The ellipsoidal height h_e can be obtained from the orthometric height, h and the geoid undulation, N, as follows:

orthometric height (P_oP): h

ellipsoidal height (Q_oP): h_e

geoidal undulation (P_oQ_o): N

normal height ($P'P = Q_oQ$): h_n

height anomaly ($QoP' = PQ$): ζ

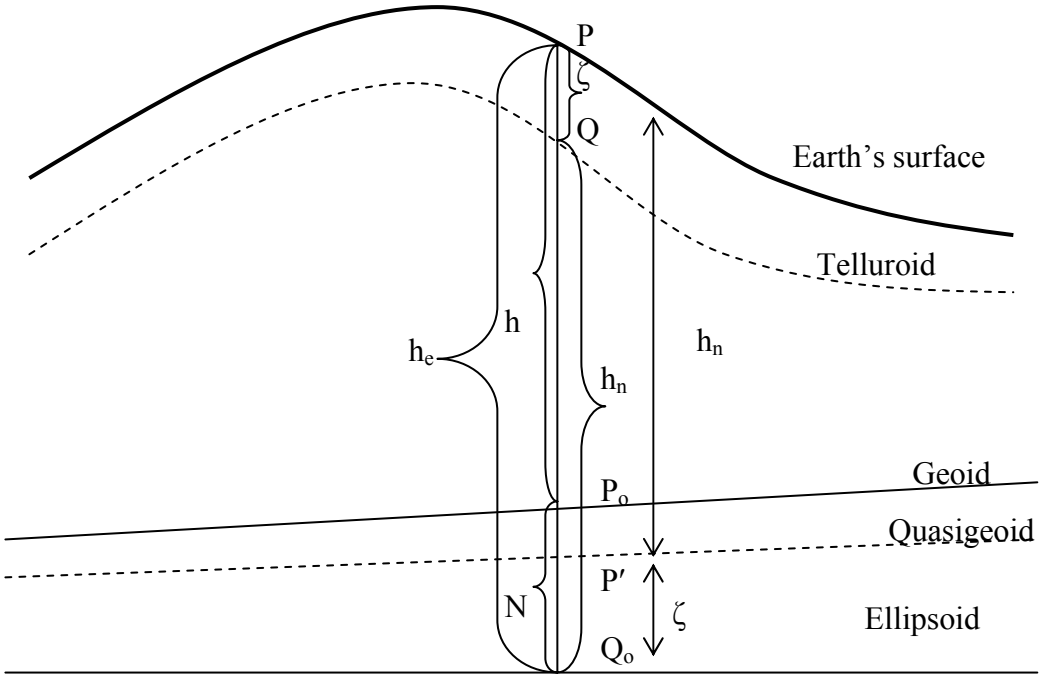

Fig. 2.1 Geoid and quasigeoid

$$h_e = h + N \qquad (2.1)$$

Geoid determination using the classical Stokes approach requires the knowledge of the actual crust density above the geoid. The topographical masses above the geoid should be completely removed and the gravity anomalies should refer to the geoid surface in Stokes's gravimetric solution.

Molodensky, on the other hand, introduced a new approach to solve the geodetic boundary value problem. His theory does not require the knowledge of crust density. The gravity anomalies according to his boundary value problem solution refer to the ground.

The geometrical principle of the quasigeoid is shown in Figure 2.1. The surface, whose normal potential at every point Q is equal to the actual potential at the corresponding point P on the Earth's surface with the points P and Q on the same ellipsoidal normal, is termed as the telluroid by Molodensky. The vertical separation between the telluroid and the physical surface of the Earth, is called height anomaly. The quasigeoid is the surface obtained by plotting the height anomalies above the ellipsoid. It is not a level surface and does not have any geophysical meaning. The vertical distance between the ellipsoid and the telluroid, which is equal to the vertical distance between quasigeoid to the Earth's surface, is the normal height. The ellipsoidal height according to this modern boundary value problem solution can be expressed as

$$h_e = h_n + \zeta \qquad (2.2)$$

where h_n is the normal height which replaces the orthometric height and ζ is the height anomaly instead of the geoid undulation of equation (2.1) in the case of geoid determination. The height anomaly is also equal to vertical separation between the quasigeoid and ellipsoid.

2.2 Gravimetric terrain reductions

There are various gravimetric reduction techniques in physical geodesy to remove topographical masses above the geoid in the classical solution of the geodetic boundary value problem using Stokes's formula. The Bouguer and residual terrain model (RTM) topographic mass reductions, Airy-Heiskanen, Pratt-Hayford, and Vening Meinesz topographic-isostatic reductions, Helmert's first and second methods of condensation, and the inversion method of Rudzki are mostly described and used in practice both in geodesy and geophysics.

In this thesis, the Bouguer and the RTM topographic reductions, the Pratt-Hayford and Airy-Heiskanen topographic isostatic reductions, Helmert's second method of

condensation, and the Rudzki inversion method are used. The brief description of each of these reductions is presented in this section with illustrations. The details of mathematical formulations using each of these gravimetric schemes are presented in Chapter 3.

The Bouguer reduction is one of the most common gravimetric reduction schemes used both in geodesy and geophysics. In geodesy, it is used for gravity interpolation, but not for geoid determination. This reduction removes all the masses above the geoid using a Bouguer plate. TC, which represents the effect of the topography deviating from the Bouguer plate should be considered to remove rigorously all topographic masses above the geoid surface. The Bouguer reduction, which includes TC in its reduction process is called the refined Bouguer reduction. Figure 2.2 shows the Bouguer reduction. The Bouguer plate of thickness h_p, which is equal to the height of a point P removes all the topographical masses above the geoid except TC.

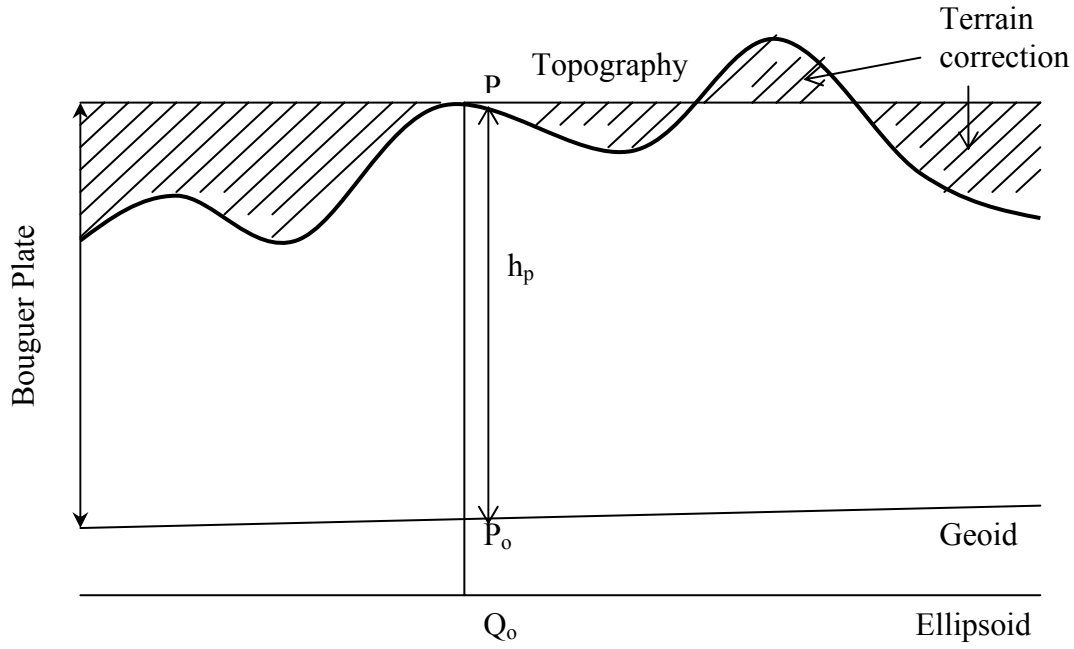

Fig. 2.2 Bouguer reduction

The Residual Terrain Model (RTM) is one of the most common terrain reduction methods used in geoid determination. This reduction scheme was introduced by Forsberg (1984). A reference surface (a mean elevation surface), which is defined by low pass filtering of local terrain heights, is used in this terrain reduction. The topographical masses above this reference surface are removed and masses are filled up below this surface. The RTM reduction is illustrated by Figure 2.3. A quasigeoid is obtained using this mass reduction model.

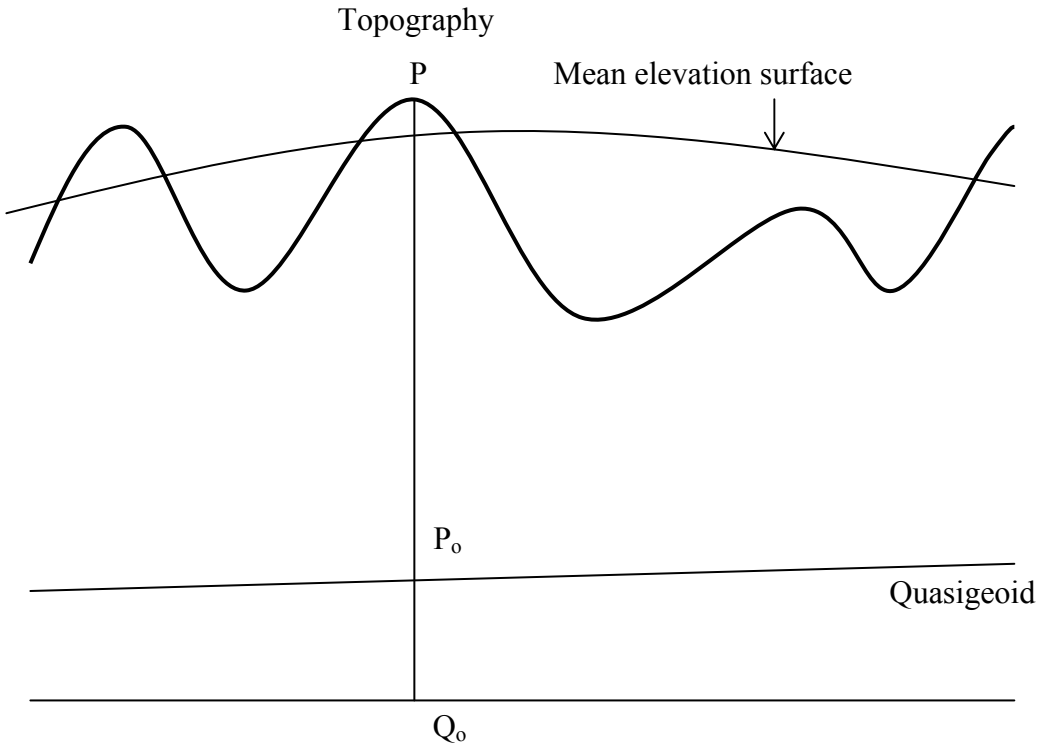

Fig. 2.3 Residual terrain model

The Rudzki inversion is the only gravimetric reduction scheme which, by definition, does not change the equipotential surface and thus introduces zero indirect effect in geoid computation. The topographical masses above the geoid are inverted into its interior in

this scheme. The inverted masses are also called mirrored masses. Figure 2.4 illustrates the geometry of the Rudzki reduction.

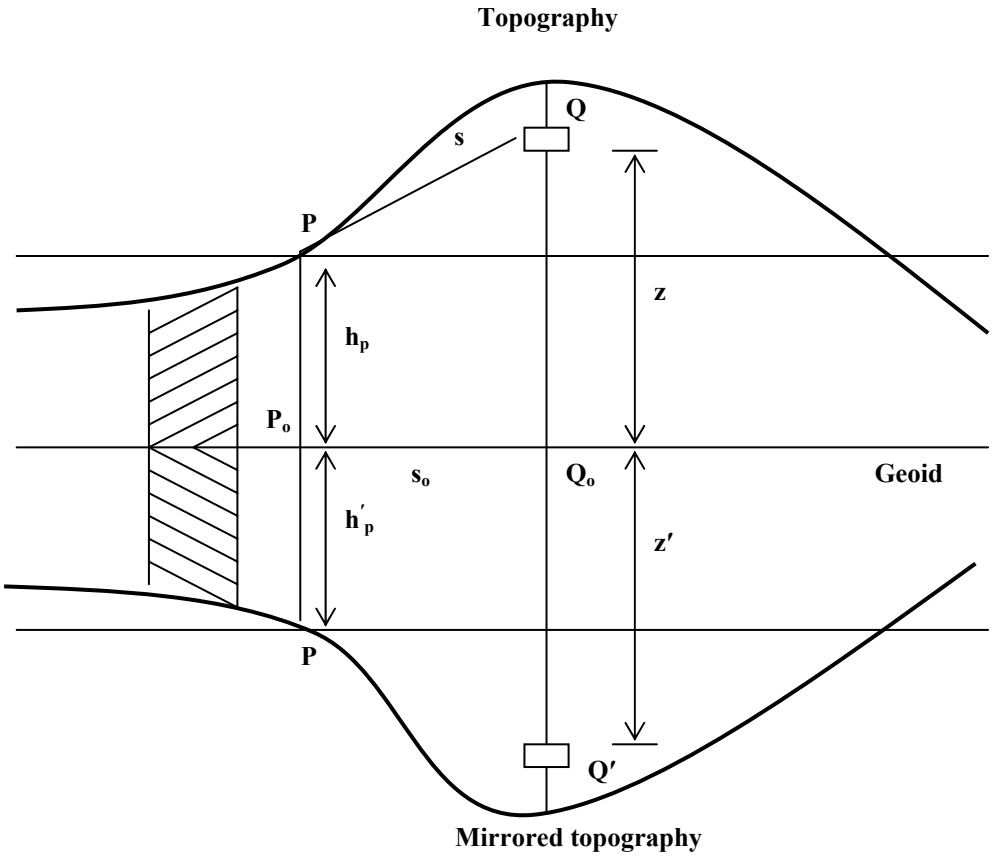

Fig. 2.4 Geometry of Rudzki reduction in planar approximation

Helmert's second method of condensation is one of the most common gravimetric reduction schemes used in practical geoid determination. In this scheme, the topographical masses are condensed on the geoid surface as a surface layer. Helmert defined this condensation scheme in two ways depending on the location of this infinitesimally thin condensation layer. In his first method of condensation, the topographical masses are condensed on a surface parallel to the geoid located 21 km (this value represents the difference between semi-major axis and semi-minor axis of a reference ellipsoid) below the geoid, whereas these masses are condensed on the geoid

surface in his second method (Heiskanen and Moritz, 1967; Heck, 1993; Heck 2003). His first method has not been used in geoid determination and has been recently suggested by Heck (2003). This reduction scheme is shown in Figure 2.5.

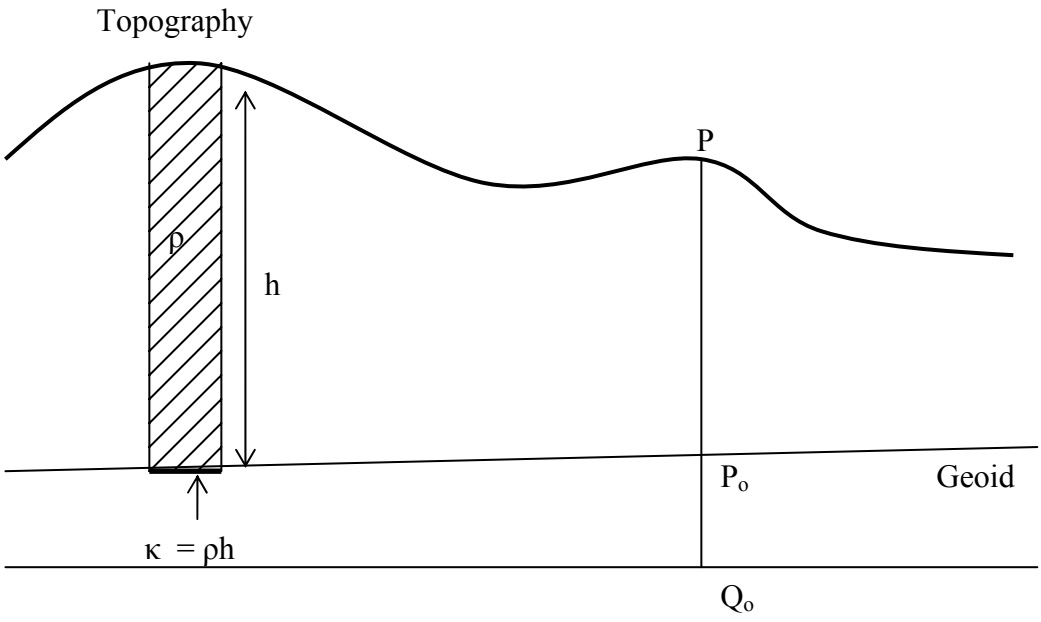

Fig. 2.5 Helmert's second method of condensation

The Pratt-Hayford reduction scheme is one of the topographic-isostatic mass reduction techniques used in physical geodesy. The topographic masses above the geoid are distributed between the level of compensation and the sea level. This reduction principle is illustrated by the Figure 2.6

The density is uniform underneath the level of compensation, whereas the mass of each column of cross section is equal above this level of compensation. The topography is removed together with its isostatic compensation yielding a homogenous crust of constant density and constant depth of compensation.

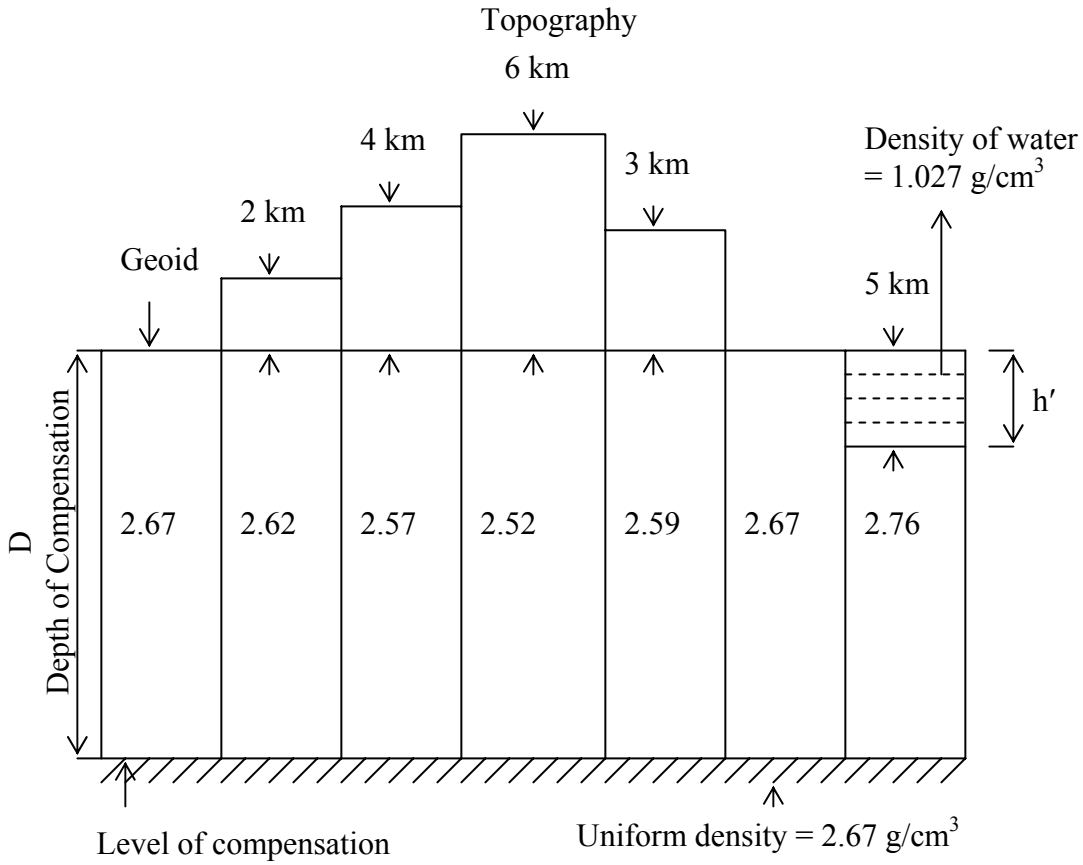

Fig. 2.6 Pratt-Hayford model

The Airy-Heiskanen model is another topographic isostatic reduction scheme commonly used in geodesy and geophysics. In this topographic-isostatic scheme, the topographical masses are removed to fill roots of the continents bringing the density from its constant value to that of upper mantle.

The masses above the geoid surface are removed together with their isostatic compensation according to the Airy-Heiskanen theory yielding a homogenous crust of constant density and constant normal crust thickness. The principle of this theory is illustrated by Figure 2.7. Airy stated that the higher mountains sink deeper than moderate lands and are floating on material of higher density.

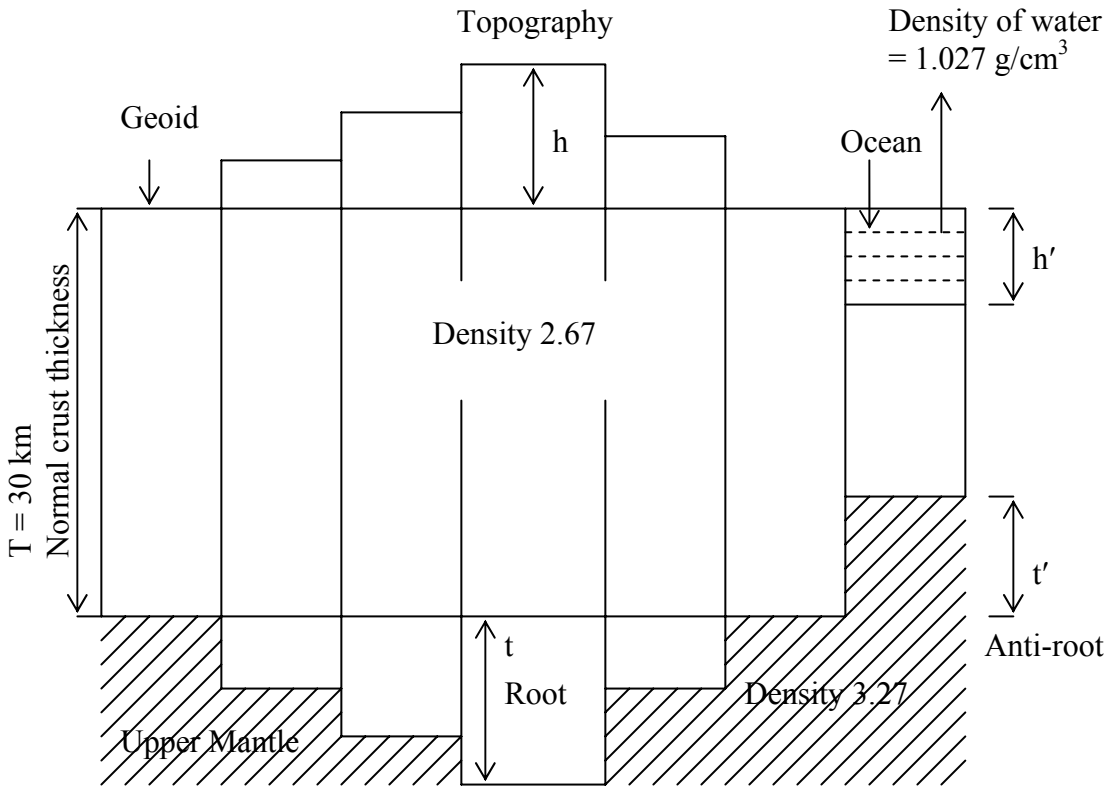

Fig. 2.7 Airy-Heiskanen model

2.3 Computational formulas for geoid determination

Global geopotential model, local gravity information and digital terrain model represent the low, medium and high frequency part of the gravity signal, respectively. Gravimetric geoid solution is carried out using the remove-restore technique in this thesis for all gravity reduction methods in planar approximation. Each method treats the topography in a different way as described in the earlier section. First, the gravity anomalies are reduced in a remove step using a mass reduction scheme to formulate boundary values on the geoid, which can be expressed as:

$$\Delta g_r = \Delta g_F - \Delta g_T - \Delta g_{GM} \tag{2.3}$$

where Δg_F is the Free-air anomalies, Δg_T is the direct topographical effect on gravity in each reduction method used as formulated in Chapter 3, and Δg_{GM} is the reference gravity anomaly from a geopotential model.

The surface computed by Stokes's formula without considering the indirect effect on geoid is called the cogeoid, which is not the geoid. This surface is also called the regularized geoid since it is obtained by regularizing the external masses above the geoid surface as Stokes's approach requires (Heiskanen and Moritz, 1967). Figure 2.8 shows the relation between geoid and the co-geoid. The vertical distance between geoid and co-geoid caused by the change in potential due to the gravimetric reduction process is called the indirect effect on geoid.

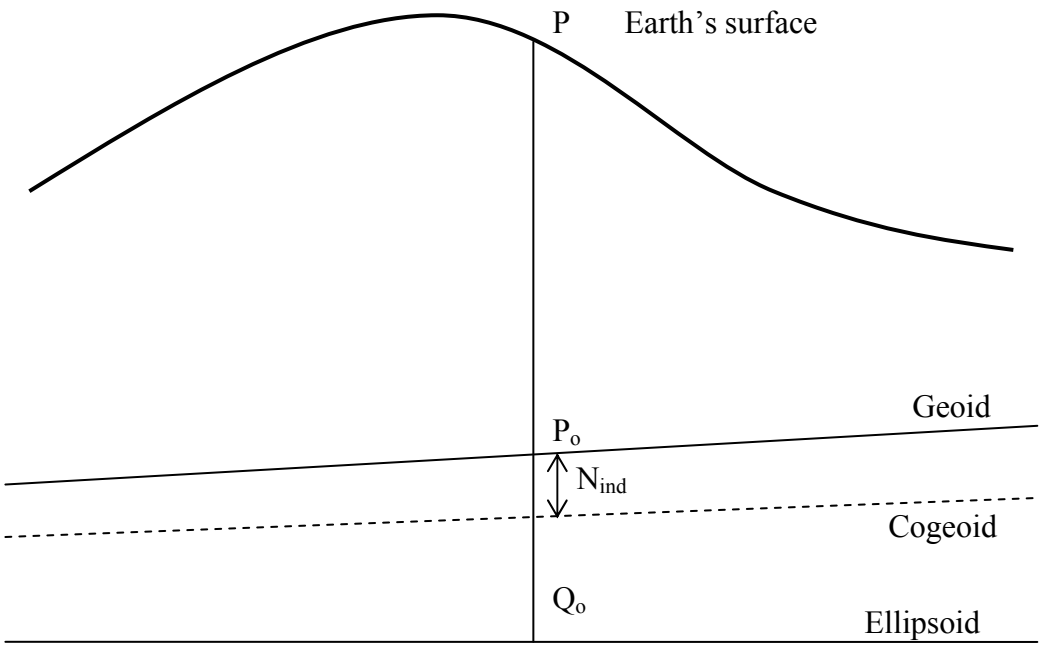

Fig. 2.8 Geoid and cogeoid

The indirect effect on gravity, which reduces gravity anomaly from the co-geoid to the geoid, should be added in equation (2.3) for Helmert's second method of condensation and the topographic-isostatic mass reduction schemes, and can be expressed using the simple free-air gradient (Heiskanen and Moritz, 1967):

$$\delta g = 0.3086 N_{ind} \text{ mGal} \tag{2.4}$$

The direct topographical effect on gravity Δg_T in equation (2.3) for each mass reduction scheme can be expressed as:

$$\Delta g_T = A - A_{(Inv,Cond,Comp,Ref)} \tag{2.5}$$

where A is the attraction of all topographic masses above the geoid and A ($_{Inv\ ,Cond,\ Comp,\ Ref)}$ represents the attraction of either inverted topographical masses, or the condensed masses, or the compensated masses, or the reference topographic masses for the Rudzki, Helmert, AH or PH, and RTM reduction schemes, respectively.

In spherical approximation, the reference gravity anomaly at latitude φ_p and longitude λ_p is expressed by (Heiskanen and Moritz, 1967)

$$\Delta g_{GM} = \frac{GM}{R^2} \sum_{n=2}^{nmax} (n-1) \sum_{m=0}^{n} [\bar{C}_{nm} \cos m\lambda_p + \bar{S}_{nm} \sin m\lambda_p] P_{nm}(\sin \varphi_P) \tag{2.6}$$

where R is the mean radius of the Earth, $\bar{C}_{nm}$ and $\bar{S}_{nm}$ are the fully normalized spherical harmonic coefficients of the anomalous potential, and P_{nm} is the fully normalized associated Legendre function.

The total geoid obtained as the result of the restore step can be expressed as:

$$N = N_{GM} + N_{\Delta g} + N_{ind} \tag{2.7}$$

where N_{GM} denotes the long wavelength part of the geoid obtained from a geopotential model, $N_{\Delta g}$ represents residual geoid obtained by using Δg_r from equation (2.3) in Stokes's formula, and N_{ind} is the indirect effect on the geoid, which depends on the mass reduction scheme used. The reference geoid undulation N_{GM} from a geopotential model can be expressed as (Heiskanen and Moritz, 1967)

$$N_{GM} = R \sum_{n=2}^{nmax} \sum_{m=0}^{n} [\bar{C}_{nm} \cos m\lambda_p + \bar{S}_{nm} \sin m\lambda_p] \bar{P}_{nm}(\sin\varphi_p) \tag{2.8}$$

Stokes's formula for the classical solution of the geodetic BVP is given by (Heiskanen and Moritz, 1967)

$$N = \frac{R}{4\pi\gamma} \iint_{\sigma} \Delta g \, S(\psi) \, d\sigma \tag{2.9}$$

The above formula using gridded gravity anomalies can be formulated as (Li and Sideris, 1994)

$$N_{\Delta g} = \frac{\Delta\varphi \Delta\lambda R}{4\pi\gamma} \sum_{n=0}^{N-1} \sum_{m=0}^{M-1} \Delta g_r(\varphi_n, \lambda_m) \cos\varphi_n S(\varphi_P, \lambda_P, \varphi_n, \lambda_m) \tag{2.10}$$

where Δg_r is the reduced gravity anomaly given by equation (2.3) and S (φ_p, λ_p, φ_n, λ_m) is the spherical Stokes kernel function defined by

$$S(\varphi_p,\lambda_P,\varphi,\lambda) = 1/s - 6s + 1 - 5(1-2s^2) - 3(1-2s^2)\ln(s+s^2)$$

$$s^2 = \sin^2\frac{\varphi_p-\varphi}{2} + \sin^2\frac{\lambda_P-\lambda}{2}\cos\varphi_P\sin\varphi \qquad (2.11)$$

Equation (2.10) can be expressed as a convolution in the East-West direction considering that spherical Stokes's kernel is constant for all points on one parallel but different for points at different latitudes (Haagmans et al., 1993)

$$N_{\Delta g} = \frac{\Delta\varphi\Delta\lambda R}{4\pi\gamma}\sum_{n=0}^{N-1}\mathbf{F}_1^{-1}\{\mathbf{F}_1\{\Delta g(\varphi_n)\cos\varphi_n\}\mathbf{F}_1\{S(\varphi_P,\varphi_n,\delta\lambda)\}\} \qquad (2.12)$$

where $\mathbf{F_1}$ and $\mathbf{F_1}^{-1}$ denote the one-dimensional Fourier and inverse Fourier transform operators.

The indirect effect on the geoid, in equation (2.7), can be computed from Bruns's formula, as follows:

$$N_{ind} = \frac{\Delta T}{\gamma} \qquad (2.13)$$

where γ is the normal gravity and ΔT is the change in the potential at the geoid, which depends on the reduction method used and can be expressed as follows:

$$\Delta T = T - T_{(Inv,Cond,comp,Ref)} \qquad (2.14)$$

where T is the gravitational potential of the actual topographical masses and $T_{(Inv,\ Cond,\ Comp,\ Ref)}$ represents the potential of the inverted, condensed, compensated, and reference masses for the Rudzki, Helmert, AH or PH reduction schemes, and RTM reduction,

respectively. The topographical masses between the geoid surface and the reference surface in the RTM reduction are called the reference masses. ΔT in the equation (2.14) is zero for the Rudzki inversion scheme since the potential of the topography is equal to that of the inverted topography as given by the equation (3.40). The potentials of the topographical masses and the compensating masses can be given as:

$$T = G\rho \iiint_{E\ 0}^{h} \frac{1}{s(x_p - x, y_p - y, h_p - z)} dxdydz$$

$$T_{Comp(Airy)} = G\Delta\rho \iiint_{E\ -T-t}^{-T} \frac{1}{s(x_p - x, y_p - y, h_p - z)} dxdydz$$

$$T_{Comp(Prratt)} = G\Delta\rho \iiint_{E\ -D}^{0} \frac{1}{s(x_p - x, y_p - y, h_p - z)} dxdydz$$

$$T_{RTM} = G\rho \iiint_{E\ h_{Ref}}^{0} \frac{1}{s(x_p - x, y_p - y, h_p - z)} dxdydz \qquad (2.15)$$

where ρ is topographical density and $\Delta\rho$ is the density defect in topographical isostatic reduction schemes.

The integrals in equation (2.15) can be numerically integrated using rectangular prisms with the computation point coinciding with the origin of the coordinate system (Nagy, 1966):

$$T = G\rho \,|||\, xy \ln(z + r) + xz \ln(y + z) + yz(x + r)$$
$$- \frac{x^2}{2} \tan^{-1}\left(\frac{yz}{xr}\right) - \frac{y^2}{2} \tan^{-1}\left(\frac{xz}{yr}\right) - \frac{z^2}{2} \tan^{-1}\left(\frac{xy}{zr}\right) \Big|_{x_1}^{x_2} \Big|_{y_1}^{y_2} \Big|_{z_1}^{z_2} \qquad (2.16)$$

Figure 2.9 shows the notations used for the definition of a prism. The prism is bounded by planes parallel to the coordinate planes. The prism is defined by the coordinates x_1, x_2, y_1, y_2, z_1 and z_2. Point P is the computation point. Equation (2.15) of the prism serves as the

basic formula for the computation of the potential for different mass reduction schemes in this thesis.

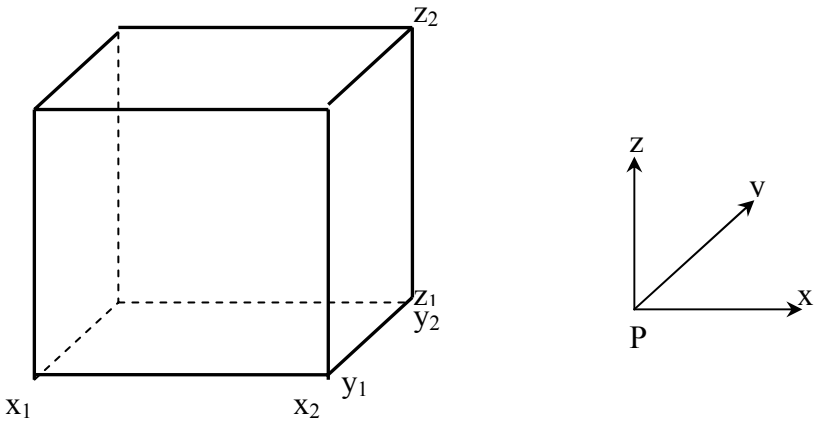

Fig. 2.9 Notations used for the definition of a prism

The indirect effect for Helmert's second method of condensation can be obtained in planar approximation as (Wichiencharoen, 1982)

$$N_{ind} = -\frac{\pi G\rho}{\gamma} h_P^2 - \frac{G\rho}{6\gamma} \iint_E \frac{h^3 - h_P^3}{s^3} dxdy \qquad (2.17)$$

The RTM reduction method gives the quasigeoid. Equation (2.7) for the RTM reduction scheme gives the height anomaly, which is also known as the quasigeoid height. Similarly, the gravimetric quantity, N_{ind}, in equation (2.7) represents the indirect effect on quasigeoid for this reduction, which is also known as the restored terrain effect on the quasigeoid. This gravimetric quantity in RTM reduction is also equal to the distance between the original telluroid and the changed telluroid, which is illustrated in figure 2.10. Equation (2.7) for quasigeoid determination can be formulated as

$$\zeta = \zeta_{GM} + \zeta_{\Delta g} + \zeta_{ind} \qquad (2.18)$$

The separation between quasigeoid and geoid, which is required to obtain the geoid from the quasigeoid in the RTM method, can be computed from (Heiskanen and Moritz, 1967)

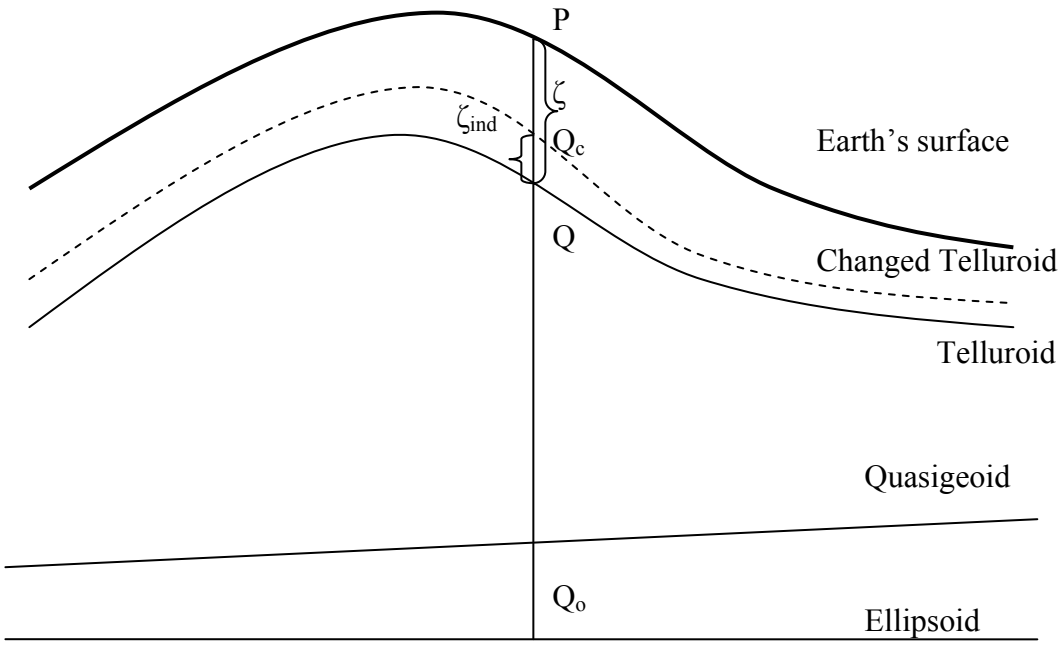

Fig. 2.10 Telluroid and changed telluroid

$$\zeta - N = -\frac{\bar{g} - \bar{\gamma}}{\bar{\gamma}} h \approx \frac{\Delta g_B}{\bar{\gamma}} h \qquad (2.19)$$

where $\bar{g}, \bar{\gamma}$, and Δg_B represent the mean (along the plumb line) gravity, normal gravity, and Bouguer anomaly, respectively.

Chapter 3
Direct Topographical Effects on Gravity

3.1 Refined Bouguer Reduction

The refined Bouguer reduction removes all the topographical masses above the geoid as already described in Chapter 2, which includes not only the removal of topographical masses contained in the Bouguer plate but also the rough part of the topography deviating from the Bouguer plate, which is called terrain correction. The following steps are required to compute Bouguer (refined Bouguer) anomalies:

1. Measure gravity at a point P on the Earth's surface.
2. Remove all the masses above the geoidal surface with the Bouguer plate (including TC for refined Bouguer). Subtract this direct effect on gravity due to Bouguer reduction from the observed gravity value.
3. Bring the gravity station down to the geoidal surface with the Free-air reduction.
4. Compute the normal gravity at corresponding point Q_o on the reference ellipsoid and subtract it from the reduced gravity.

The topographic potential at a surface point P (see figure 2.2) can be expressed by Newton's integral

$$T = G\iiint_{v}\frac{\rho}{s}dv \qquad (3.1)$$

where ρ is the density of the topographic masses, G is Newton's gravitational constant, dv is a volume element, and s is the distance between the mass element dm = ρ dv and the attracted point P. Introducing rectangular coordinates in equation (3.1), we have

$$T = T^1 + T^2 = G\rho \iint_E \int_0^{h_p} \frac{1}{s} dE dz + G\rho \iint_E \int_{h_p}^{h} \frac{1}{s} dE dz \qquad (3.2)$$

where $s = \sqrt{(x - x_P)^2 + (y - y_P)^2 + (z - h_p)^2}$, $dE = dxdy$, and ρ is assumed constant and taken out of the integral. The integral of equation (3.1) is separated into two integrals in equation (3.2). The first term, T^1 represents the potential of a Bouguer plate of thickness h_p and the second one, T^2 represents the potential of the irregular topography deviating from the Bouguer plate. The potential T^1 of the Bouguer plate of radius a and thickness b at a point P of height h_p (Figure 3.1) can be expressed as follows (Heiskanen and Moritz, 1967):

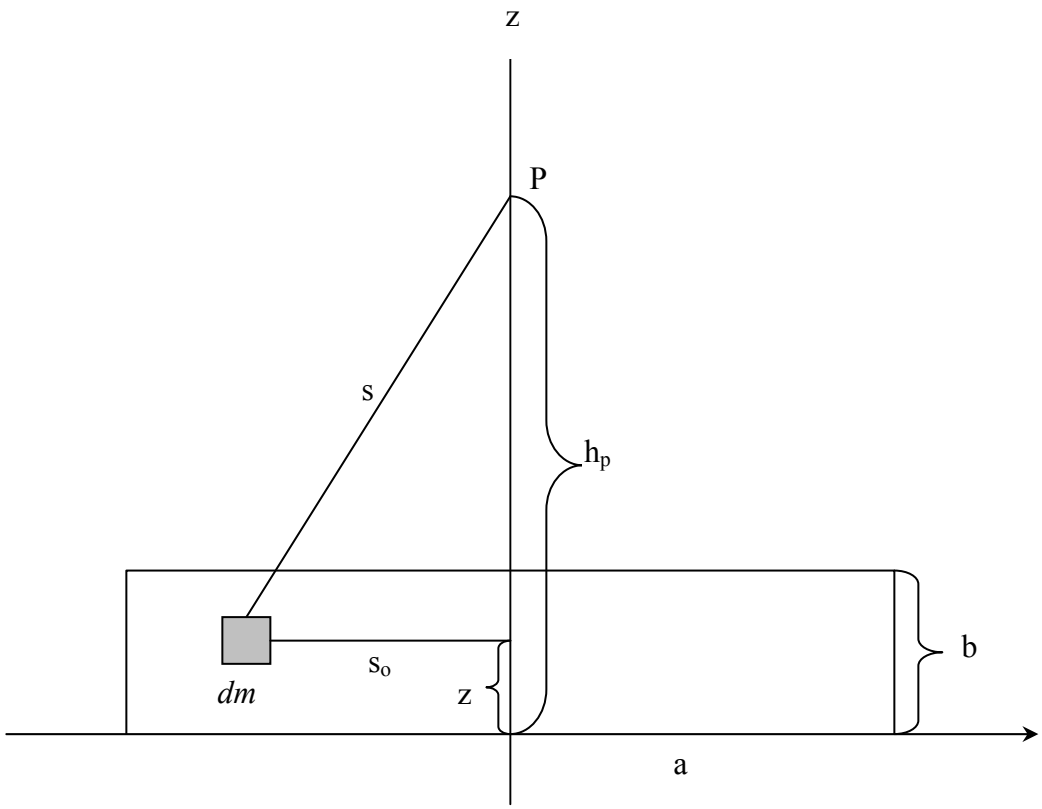

Fig. 3.1 The homogeneous cylinder

$$T^1 = \pi G\rho[(h_p - b)^2 - h_p{}^2 - (h_p - b)\sqrt{a^2 + (h_p - b)^2} + h_p\sqrt{a^2 + h_p^2} \\ - a^2 \ln(h_p - b + \sqrt{a^2 + (h_p - b)^2}) + a^2 \ln(h_p + \sqrt{a^2 + h_p^2})] \quad (3.3)$$

The vertical attraction, A^1, of the Bouguer plate at P can be expressed as

$$A^1 = -\frac{\partial T^1}{\partial h_p} = 2\pi G\rho[b + \sqrt{a^2 + (h_p - b)^2} - \sqrt{a^2 + h_p^2}] \quad (3.4)$$

The potential of equation (3.3) and the vertical attraction of equation (3.4) for the computation point P on the cylinder ($h_p = b$, which means the computation point is on the earth's topography) can be expressed as

$$T^1 = \pi G\rho[-h_p^2 + h_p\sqrt{a^2 + h_p^2} + a^2 \ln\frac{h_p + \sqrt{a^2 + h_p^2}}{a}] \quad (3.5)$$

$$A^1 = -\frac{\partial T^1}{\partial h_p} = 2\pi G\rho[h_p + a - \sqrt{a^2 + h_p^2}] \quad (3.6)$$

The attraction of the Bouguer plate with an infinite radius, $a \to \infty$, is given by the following equation:

$$A^1 = 2\pi G\rho h_p \quad (3.7)$$

This attraction is called "direct topographical effect" (Heiskanen and Moritz, 1967) of Bouguer reduction on gravity. The term "direct topographical effect" will be used in the following sections for the attraction of either the topographical masses above the geoid or the topographical effect of compensated, condensed, or inverted masses for AH and PH topographic-isostatic models, Helmert's second method of condensation, and the Rudzki

inversion scheme, respectively. This gravimetric quantity is also called the "attraction change effect" (Wichiencharoen, 1982), or the "topographical attraction effect" (Vanicek and Kleusberg, 1987). The gravity anomalies for the Bouguer reduction scheme can be expressed as

$$\Delta g_B = g_P - \gamma_{Q_o} + F - A^1 \tag{3.8}$$

The attraction for the complete Bouguer reduction can be expressed as

$$A_B = 2\pi G\rho h_p - c \tag{3.9}$$

and the refined Bouguer anomalies can be expressed by the following formula:

$$\Delta g_B = g_P - \gamma_{Q_o} + F - A_B \tag{3.10}$$

where g is the measured gravity value on Earth's surface at point P, γ_{Qo} is the normal gravity computed on the reference ellipsoid at a point Q_o, F is the Free-air reduction, A_B is the direct topographical effect on gravity for the complete Bouguer reduction, and c is the TC, the details of which are described in the next section.

Normal gravity in this thesis is based on Geodetic Reference System 1980 (GRS80), which was adopted at the XVII General Assembly of the IUGG in Canberra, December 1979. The rigorous formula for the computation of normal gravity on the ellipsoid given by Somigliana's formula (Heiskanen and Moritz, 1967)

$$\gamma = \frac{a\gamma_a \cos^2\varphi + b\gamma_b \sin^2\varphi}{\sqrt{a^2\cos^2\varphi + b^2\sin^2\varphi}} \tag{3.11}$$

where γ_a and γ_b represent the normal gravity at the equator and the pole, respectively, and φ is the geodetic latitude of the gravity station.

The free-air reduction is not a topographic reduction, but only a part of the topographic reduction procedure. This reduction process brings the gravity stations measured on the Earth's topography down to the geoidal surface. It is a requirement in the classical solution of boundary value problem using Stokes's formula. In other words, the gravity at point P (Figure 2.2) is transferred to P_o on the geoid by means of the Free-air reduction. The change of gravity due to the Free-air reduction is given by

$$F = -\frac{dg}{dh}h \tag{3.12}$$

In practice, the normal gradient of gravity is used to replace the vertical gradient of gravity as follows (Heiskanen and Moritz, 1967):

$$F = -\frac{d\gamma}{dh}h = 0.3086h \tag{3.13}$$

Free-air anomalies are referred to the geoidal surface in the classical geoid solution using Stokes's approach, while they are referred to the topographical surface in the modern boundary value problem of Molodensky approach and can be given by

$$\Delta g = g_P - \gamma_Q \tag{3.14}$$

where g_p is the same as in equation (3.8) but γ_Q represents the normal gravity not on the ellipsoid but on the telluroid. It can be computed from the normal gravity on the ellipsoid γ_{Qo} applying the free-air gradient in the upward direction (Heiskanen and Moritz, 1967):

$$\gamma_Q = \gamma_{Q_o} + \frac{\partial \gamma}{\partial h_e} h_n + \frac{1}{2!} \frac{\partial^2 \gamma}{\partial h_e^2} h_n^2 + \ldots\ldots\ldots \quad (3.15)$$

where h_n is the normal height of the station at P. It is obvious that conventional Free-air anomalies are different from those based on modern boundary value problem of Molodensky and should not be interchanged with each other. Free-air anomalies also should not be confused and interchanged with Helmert (or Faye) anomalies. They can only be regarded as an approximation to Helmert (or Faye) anomalies on the condition that gravity stations are measured on the sea surface or in moderate terrains. The TC in these areas is negligible. The negative of TC is the difference between the attraction of all topographical masses and their condensation on the geoid according to Helmert's second method of condensation as will be described in the following sections.

3.1.1 Terrain Correction

The TC is a key auxiliary quantity in gravity reductions, which are used in solving the geodetic boundary value problem of physical geodesy and in geophysics. It contains the high frequency part of the gravity signal representing the irregular part of the topography, which deviates from the Bouguer plate. Helmert's second method of condensation is mostly used in practice as the mass reduction technique in the classical solution of the geodetic boundary value problem. Helmert anomaly (or Faye anomaly), which consists of free-air anomaly plus TC, represents the boundary values in the Helmert Stokes approach since TC alone is the difference between the attraction of the topography and the attraction of the condensed topography in planar approximation; see Moritz (1968), Wichiencharoen (1982) and Sideris (1990). In Molodensky's problem, TC can replace the g_1 term under the assumption that the gravity anomalies are linearly dependent on the heights (Moritz, 1980).

The TC integral at a point P which is the negative derivative of the second potential integral, T^2, in formula (3.2) is given by (Heiskanen and Moritz, 1967)

$$c_p = G\iint_E \int_{h_p}^{h} \frac{\rho(x,y,z)(h_p - z)}{s^3(x_p - x, y_p - y, h_p - z)}\,dxdydz \qquad (3.16)$$

where ρ (x, y, z) is the topographical density at the running point, h_p and h are the computation and running point, respectively, and E denotes the integration area.

Various computational approaches have been developed based on conventional methods, which usually evaluate the TC integral of equation (3.16) using a model of rectangular prisms with flat tops (Nagy, 1966) or even with inclined tops (Blais and Ferland, 1984). TC computation based on these formulas is very time-consuming but rigorous. Recently, Biagi et al. (2001) have given a new formulation for residual TC (RTC) and Strykowski et al. (2001) have introduced a polynomial model for TC computation. The TC computation can be performed very fast in the frequency domain by means of fast ForFFT, having the TC convolution integral expanded in the form of Taylor series; see for example, Sideris (1984), Forsberg (1984), Tziavos et al. (1988), Harrison and Dickinson (1989), Sideris (1990), Li and Sideris (1994), Li et al. (2000), Sideris and Quanwei (2002).

Integrating equation (3.16) with respect to z gives

$$c = G\rho\iint_E \left(\frac{1}{s_o}\left[1 - \left[1 + \left(\frac{\Delta h}{s_o} \right)^2 \right]^{-1/2} \right] \right) dxdy \qquad (3.17)$$

where $s_o^2 = (x_p - x)^2 + (y_p - y)^2$ and $\Delta h = h_P - h$.

The term $\left[1 + \left(\frac{\Delta h}{s_o} \right)^2 \right]^{-1/2}$ with the condition $\left(\frac{\Delta h}{s_o} \right)^2 \le 1$, can be expanded into a series as follows:

$$\left[1+\left(\frac{\Delta h}{s_o}\right)^2\right]^{-1/2}=1-\frac{1}{2}\left(\frac{\Delta h}{s_o}\right)^2+\frac{1\cdot 3}{2\cdot 4}\left(\frac{\Delta h}{s_o}\right)^4-\frac{1\cdot 3\cdot 5}{2\cdot 4\cdot 6}\left(\frac{\Delta h}{s_o}\right)^6+\ldots\ldots\ldots\ldots \quad (3.18)$$

Inserting equation (3.18) into equation (3.17) and keeping only up to two terms in the binomial series expansion, the following formula is obtained:

$$c=G\iint_E\left(\rho\left\{\frac{\Delta h^2}{2s_o^3}-\frac{3\Delta h^4}{8s_o^5}\right\}\right)dxdy \quad (3.19)$$

The closed analytical expressions for the potential and its derivatives using rectangular prisms have been extensively used since the early eighties in gravity field modelling for flat-Earth approximation (Nagy, 1966; Forsberg 1984). The closed formula (which is similar to the equation (2.15) given for the gravitational potential in chapter 2) for the equation (3.16) using right rectangular prisms for the computation of TC at a computational point can be expressed as follows (Nagy,1966):

$$c=G\rho\,|||\, x\ln(y+r)+y\ln(x+r)-z\arctan\frac{xy}{zr}\,|_{x_1}^{x_2}\,|_{y_1}^{y_2}\,|_{z_1}^{z_2} \quad (3.20)$$

3.1.1.1 Mass prism topographic model

A prism with a mean height of the topography represents the height within each cell in mass prism (MP) topographic representation. The two dimensional convolution formulas for each term in equation (3.19) for the TC integral using the MP algorithm with variable density can be evaluated by means of fast Fourier transform (FFT) as Tziavos et al. (1996) provided that the grid size DTM and the DDM is the same:

$$c_1(i,j)=\frac{G}{2}[(h_{ij}^2-\alpha^2)\mathbf{F}^{-1}\{PF_1\}-2h_{ij}\mathbf{F}^{-1}\{PH_1F_1)+\mathbf{F}^{-1}\{PH_2F_1\}] \quad (3.21)$$

$$c_2(i,j) = -\frac{G}{8}[(h_{ij}^2 - \alpha^2)^2 \mathbf{F}^{-1}\{PF_2\} - 4h_{ij}(h_{ij}^2 - \alpha^2)\mathbf{F}^{-1}\{PH_1F_2\} + (6h_{ij}^2 - 2\alpha^2)\mathbf{F}^{-1}\{PH_2F_2\} - 4h_{ij}\mathbf{F}^{-1}\{PH_3F_2\} + \mathbf{F}^{-1}\{PH_4F_2\}] \quad (3.22)$$

where $P = \mathbf{F}\{\rho\}, PH_1 = \mathbf{F}\{\rho h_{nm}\}, PH_2 = \mathbf{F}\{\rho h_{nm}^2\}, PH_3 = \mathbf{F}\{\rho h_{nm}^3\}, PH_4 = \mathbf{F}\{\rho h_{nm}^4\}$

$$H_k = \mathbf{F}\{h^k\}, \qquad k = 1,2,3,4,5,6 \quad (3.23)$$

$$F_1 = \mathbf{F}\{f_{11}(x,y,\alpha) + f_{11}(y,x,\alpha) - f_{12}(x,y,\alpha)\} \quad (3.24)$$

$$F_2 = \mathbf{F}\{f_{21}(x,y,\alpha) + f_{21}(y,x,\alpha) - f_{22}(x,y,\alpha)\} \quad (3.25)$$

$$f_{11}(x,y,\alpha) = \frac{-x}{(y + r(x,y,\alpha))r(x,y,\alpha)} \Bigg|_{x_n - \frac{\Delta x}{2}}^{x_n + \frac{\Delta x}{2}} \Bigg|_{y_n - \frac{\Delta y}{2}}^{y_n + \frac{\Delta y}{2}} \quad (3.26)$$

$$f_{22}(x,y,\alpha) = \frac{xy}{3(x^2y^2 + \alpha^2 r^2)r}\left[\frac{2(r^2 + \alpha^2)^2}{(x^2y^2 + \alpha^2 r^2)} - \frac{r^2}{\alpha^2} + \frac{\alpha^2}{r^2} - 4\right] - \frac{1}{3\alpha^3}\arctan\frac{xy}{\alpha r} \Bigg|_{x_n - \frac{\Delta x}{2}}^{x_n + \frac{\Delta x}{2}} \Bigg|_{y_n - \frac{\Delta y}{2}}^{y_n + \frac{\Delta y}{2}} \quad (3.27)$$

where **F** and $\mathbf{F}^{-1}$ are fast Fourier transform and inverse Fourier transform. α is a parameter used to speed up the convergence of the series; the optimal value for this parameter is given by the standard deviation of the heights divided by the square root of two (Li and Sideris, 1994). The formulas in the frequency domain considering lateral density variation need some additional computation of Fourier transform of density function compared to those considering constant density.

$$\alpha = \sigma_h / \sqrt{2}\,. \quad (3.28)$$

The density function can be taken outside the integral in equation (3.19) when the DDM is not available. The modified TC formula using constant crust density and mass prism algorithm can be obtained by modifying equations (3.21) and (3.22) as given by Li (1993) and Li and Sideris (1994):

$$c_1(i,j) = \frac{G}{2}[(h_{ij}^2 - \alpha^2)\mathbf{F}^{-1}\{H_0F_1\} - 2h_{ij}\mathbf{F}^{-1}\{H_1F_1) + \mathbf{F}^{-1}\{H_2F_1\}] \tag{3.29}$$

$$\begin{aligned} c_2(i,j) = -\frac{G}{8}[(h_{ij}^2 - \alpha^2)^2\mathbf{F}^{-1}\{H_0F_2\} - 4h_{ij}(h_{ij}^2 - \alpha^2)\mathbf{F}^{-1}\{H_1F_2) + (6h_{ij}^2 - 2\alpha^2)\mathbf{F}^{-1}\{H_2F_2\} \\ - 4h_{ij}\mathbf{F}^{-1}\{H_3F_2) + \mathbf{F}^{-1}\{H_4F_2\}] \end{aligned} \tag{3.30}$$

3.1.1.2 Mass line topographic model

The mass of the prism is concentrated along its vertical axis of symmetry representing the topography as a line mass in the mass line (ML) model. In this case, the TC integral in the form of 2-D convolutions using mass line algorithm and using variable density can be formulated for up to two terms in binomial series expansion as (Tziavos et al., 1996; Li, 1993; Li and Sideris,1994)

$$c_1(i,j) = \frac{G}{2}[h_{ij}^2\mathbf{F}^{-1}\{PR_1\} - 2h_{ij}\mathbf{F}^{-1}\{PH_1R_1) + \mathbf{F}^{-1}\{PH_2R_1\}] \tag{3.31}$$

$$\begin{aligned} c_2(i,j) = -\frac{3G}{8}[\{(h_{ij}^2 - \alpha^2)^2 - \alpha^4\}\mathbf{F}^{-1}\{PR_2\} - 4h_{ij}(h_{ij}^2 - \alpha^2)\mathbf{F}^{-1}\{PH_1R_2) \\ + (6h_{ij}^2 - 2\alpha^2)\mathbf{F}^{-1}\{PH_2R_2\} - 4h_{ij}\mathbf{F}^{-1}\{PH_3R_2) + \mathbf{F}^{-1}\{PH_4R_2\}] \end{aligned} \tag{3.32}$$

where R_k is given by

$$R_k = \mathbf{F}\left\{\frac{1}{(x^2 + y^2 + \alpha^2)^{2k+1}}\right\}, \qquad k = 1,2 \tag{3.33}$$

Equations (3.31) and (3.32) can be modified to use constant density in a similar way as in the mass prism algorithm. The unified two dimensional convolution formulas for equation (3.19) using MP and ML algorithms can be evaluated by means of FFT (Li et al., 2000)

There are different resolutions of DTM available these days throughout the world. TC computation using FFT technique is one of the most efficient tools to handle the large amounts of height data efficiently. The convergence condition, that the slope of the topography be less than 45^o, can be regarded as a major problem in the application of FFT to the series expansion of the TC integral, especially in rugged areas. Divergence of the series has been observed with densely sampled height data in rough terrain; for example see Martinec et al. (1996) and Tziavos et al. (1996). A combined method, based on the evaluation of the numerical integration method in the intermediate zone around the computation point and the use of FFT in the rest of area, has been used to tackle the convergence problem by Tsoulis (1998) and Tziavos et al. (1998).

3.2 Rudzki inversion gravimetric scheme

Rudzki reduction is not a gravimetric reduction scheme that has been widely used for geoid determination. Although by definition the potential of the topography is equal to that of the inverted masses, and thus there is no indirect effect on geoid using this mass reduction scheme, the attractions of the topography and the inverted topography are not equal.

In potential theory, a point Q' (see figure 3.2) can be regarded as the inversion of a point Q on a sphere of radius R, if both points are on the same ray from the center of the sphere and if the radius of the sphere is the geometric mean of their distances r and r' from the

center (Kellog, 1929). Hence the term *inversion* is used in Rudzki's gravimetric method. The point Q' is also known as the mirror image of the point Q. The geoid is approximated by the sphere of radius R. Not only single points can be inverted (or mirrored) into the geoid using this inversion theory, but also the whole topographical masses as shown in Figure 3.2. The condition of the inversion on the sphere can be expressed as (Macmillan, 1958)

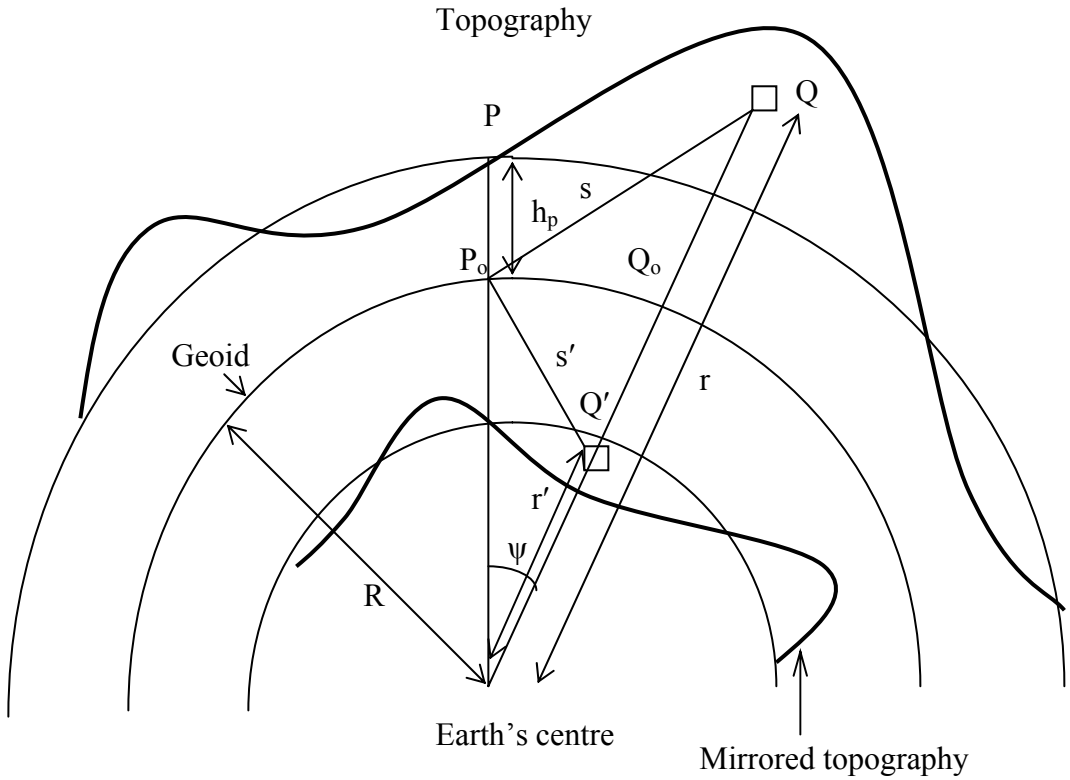

Fig. 3.2 Geometry of Rudzki reduction in spherical approximation

$$\frac{r}{R} = \frac{R}{r'} \; ; \quad dr = \frac{R^2}{r'^2} dr' \tag{3.34}$$

An algebraic negative sign in the second part of the above equation is eliminated for convenience, assuming that when r changes to r+dr, the corresponding r' will move to r'-

dr' to make both dr and dr' of the same sign.

The main condition in Rudzki's inversion method is that the indirect effect on the geoid is zero. The gravitational potential at point P_o on the geoid (and for any points on the geoidal surface) due to mass element dm at point Q is equal to that of the inverted mass element dm' at point Q', which can be expressed as

$$\Delta T = T - T' = 0; \quad T = T' \tag{3.35}$$

where ΔT is the difference in the gravitational potential T of the topographical masses and the one of the inverted topographical masses, T'. The differential potential dT at point P_o on the geoidal surface due to the topographic mass element dm and the differential potential dT' at the same point due to the mirrored topographical mass element dm' can be expressed as

$$dT = G\frac{dm}{s} = \frac{G\rho r^2 \cos\varphi dr d\lambda d\varphi}{\sqrt{(r^2 + R^2 - 2rR\cos\psi)}}; \qquad dT' = G\frac{dm'}{s'} = \frac{G\rho' r'^2 \cos\varphi dr' d\lambda d\varphi}{\sqrt{(r'^2 + R^2 - 2r'R\cos\psi)}} \tag{3.36}$$

where G is the universal gravitational constant, (r, φ, λ) and (r', φ, λ) are the spherical coordinates of the topographical mass element of density ρ and the mirrored topographical mass element of density ρ', respectively, s and s' are the radial distances between point P_o and the mass elements, and ψ is the angle formed by the radius vectors pointing from the Earth's geocenter to point P_o and the mass elements. Applying the condition of the inversion on the sphere from equation (3.34) and the condition of Rudzki's scheme from equation (3.35) to equation (3.36), the following equation can be obtained:

$$\rho' = \left(\frac{r}{R}\right)^5 \rho = \left(1 + \frac{z}{R}\right)^5 \rho \qquad (3.37)$$

where $z = r - R$ is the height Q_oQ of topographical mass element. This equation provides the fundamental relationship between the topographical crust density and the density of mirrored topographical masses below the geoid in Rudzki's gravimetric scheme. It shows that the ratio of the densities of the topography and mirrored masses is proportional to the fifth power of the ratio of the radial distance of the topographical mass to the radius of the Earth. If we take the mass element at the top of Mt. Everest, the density of the mirrored topographical mass element will change by 0.7% of the standard Earth's crust density of 2.67 g/cm^3.

Similarly, from equations (3.34), (3.35) and (3.36), the following formula can be obtained:

$$dm' = \frac{R}{r} dm \qquad (3.38)$$

This condition shows us that the shifting of topographical masses into the geoid by mirrored masses introduces a slight mass change. The inverted topographical masses are slightly smaller than the topographical masses. It is obvious from equation (3.38) that if the mass element is near the geoidal surface, these two types of masses are nearly equal and the height of the topographical mass element will be nearly equal to the depth of the inverted masses below the geoid. For the planar approximation (see figure 2.4), we can obtain the following conditions:

$$\rho' = \rho; \quad dm' = dm; \quad h'_P = h_P; \quad z' = z \qquad (3.39)$$

The gravitational potential T_p of all topographical masses outside the geoid at a point P on the topographical surface can be expressed by the following expression introducing the

equation (3.5) into the equation (3.2):

$$T_p = \pi G\rho[-h_p^{\,2} + h_p\sqrt{a^2 + h_p^{\,2}} + a^2\frac{\ln(h_p + \sqrt{a^2 + h_p^{\,2}})}{a} + G\rho\iint_E\int_{h_p}^{h}\frac{1}{s}dEdZ \qquad (3.40)$$

This equation represents the potential of the regular (Bouguer plate of thickness h_p) and irregular part (TC) of the topography.

The gravitational attraction of all topographical masses above the geoid at a point P is equal to the negative derivative of equation (3.40). It can be represented by equation (3.9). The following expression is obtained introducing equation (3.17) into equation (3.9).

$$A_p = 2\pi G\rho h_p - G\rho\iint_E\left(\frac{1}{s_0} - \frac{1}{\left[s_0^2 + (h - h_p)^2\right]^{1/2}}\right)dE \qquad (3.41)$$

This formula represents the gravitational attraction due to all the topographical masses above the geoid, which is a sum of the attractions of the regular and irregular parts of the topography. This equation is common in all gravimetric reductions since the topographical masses above the geoid should be removed completely before applying their compensation (condensation or inversion) below the geoid.

The expression for the gravitational attraction at a point P on the topographical surface due to the mirrored topographical masses can also be expressed as a sum of the gravitational attraction due to regular and irregular parts of the inverted topography as follows:

$$A_P^{'} = 2\pi G\rho^{'}h_P^{'} - G\rho^{'}\iint_E\left(\frac{1}{\left[s_0^2 + (h_P + h^{'})^2\right]^{1/2}} - \frac{1}{\left[s_0^2 + (h_P + h_P^{'})\right]^{1/2}}\right)dE \qquad (3.42)$$

The expression for the direct topographical effect on gravity, which is equal to the difference between the gravitational attraction due to all topographical masses above the geoid and that due to the mirrored topographical masses inside the geoid in Rudzki's scheme, can be obtained from equations (3.39), (3.41) and (3.42) as follows:

$$\delta A_{\text{Rudzki}} = A_p - A_P^{'} = G\rho \iint_E \left(\frac{1}{s_0} - \frac{1}{\left[s_0^2 + (h - h_p)^2 \right]^{1/2}} + \frac{1}{\left[s_0^2 + (h_P + h)^2 \right]^{1/2}} - \frac{1}{\left[s_0^2 + (2h_P)^2 \right]^{1/2}} \right) dE \tag{3.43}$$

In this formula, it is obvious that the attractions due to the regular parts of the topographical and mirrored topographical masses are equal and cancel out. The direct topographical effect on gravity in this Rudzki reduction scheme is the difference of the attraction due to the irregular part of the topography and mirrored topography evaluated at a point P on the surface of the Earth.

Rudzki anomalies can be given by the following formula:

$$\Delta g_{\text{Rudzki}} = g_P - \gamma_{Q_o} + F - \delta A_{\text{Rudzki}} \tag{3.44}$$

3.3 Residual Terrain Model

The topographical masses above the reference surface (see figure 2.3), which is defined by low pass filtering of local terrain heights, are removed and masses are filled up below this surface in the RTM gravimetric reduction scheme. The direct topographical effect on gravity for this reduction method can be expressed as (Forsberg, 1984)

$$\delta A_{\text{RTM}} = G\rho \iint_E \int_{h_{Ref}}^{h} \frac{(h_p - z)}{s^3(x_p - x, y_p - y, h_p - z)} dx dy dz \tag{3.45}$$

where h_{ref} and h represent the height of reference surface and the topographic heights, respectively. Using rectangular prisms for the computation of the direct RTM topographical effect at a computational point a closed expression can be obtained as follows:

$$\delta A_{RTM} = G\rho \,|||\, x \ln(y+r) + y \ln(x+r) + y \ln(x+r) - z \arctan\frac{xy}{zr} \,|_{x_1}^{x_2} |_{y_1}^{y_2} |_{h_{Ref}}^{h_p} \qquad (3.46)$$

The RTM reduction is also approximated by the following formula when the mean elevation computed is adequate enough to represent the long wavelength surface (Forsberg, 1984):

$$\delta A_{RTM} = 2\pi G\rho(h - h_{ref}) - c \qquad (3.47)$$

The first term in the above formula is the difference between two Bouguer plates, the first one computed with the thickness of the height of the computation point and the second one with the height of the reference surface. In other words, the topographical masses above the geoid are removed with the complete Bouguer reduction and then are restored with the reference Bouguer plate. This formula also exhibits the importance of the TC in the RTM method. The RTM gravity anomalies can be expressed as

$$\Delta g_{RTM} = g_P - \gamma_{Q_o} - \delta A_{RTM} \qquad (3.48)$$

A quasigeoid is obtained using this mass reduction technique instead of the geoid. A correction term should be applied to convert from quasigeoid to geoid.

Though RTM gravity anomalies have been compared with topographic-isostatic gravity anomalies (Forsberg 1984), the RTM reduction has no geophysical or mathematical relations with isostatic compensation, or with condensation, and thus does not possess any geophysical meaning. The integration for the computation of the direct RTM terrain

effect on gravity needs to be carried out only up to an appropriate radius. The density anomalies oscillate between positive and negative values depending on the position of the gravity points from the reference surface and the effect of distant topography on gravity thus cancels out (Forsberg 1984).

The measured gravity stations above the reference surface after applying the RTM method lie in the air while those below that surface remain inside the topographic mass since we remove the topographical masses above this surface and fill up the masses in the valleys below this reference surface. The potential below this surface is not a harmonic function and therefore imposes a great theoretical problem in this method.

3.4 Helmert's second method of condensation

Helmert's second method of condensation is one of most common gravimetric reduction schemes used in practical geoid determination in addition to the RTM method described in the previous chapter. Studies on direct topographical effect on gravity using this scheme are available in the geodetic literature (Heiskanen and Moritz, 1967; Wichiencharoen, 1982; Vanicek and Kleusberg, 1987; Wang and Rapp,1990; Sideris, 1990; Martinec and Vanicek, 1993; Martinec et al., 1993; Heck, 1993; and Heck, 2003). Helmert postulates that the topographical masses above the geoid can be shifted onto a condensation layer (see Figure 2.4), the surface density of which is equal to the product of topographical density and the height. This condition can be mathematically expressed as

$$\kappa = \rho h \tag{3.49}$$

where κ, ρ and h are surface density of the condensation layer, the density of the Earth's crust, and topographical height, respectively.

The potential of the condensed masses can be expressed as (Heiskanen and Moritz,1967):

$$T_{Cond} = G\iint_{E}\frac{\kappa}{s}dE \tag{3.50}$$

The following expression for the attraction due to the regular part of the condensed topography can be obtained by letting b→ 0 in the equation (3.4)

$$A_{Cond}^{Reg} = 2\pi G\rho h_P\left(1-\frac{h_p}{\sqrt{a^2+h_p^2}}\right) \tag{3.51}$$

For a Bouguer plate of an infinite radius (a→∞) it becomes

$$A_{Cond}^{Reg} = 2\pi G\rho h_P \tag{3.52}$$

The expression for the attraction due to the irregular part of the condensed masses computed on the geoid is given by (Sideris, 1990; Wang and Rapp, 1990 and Heck, 1993):

$$A_{Cond}^{Irreg} = -\left[\frac{\partial}{\partial h_p}G\rho\iint_{E}\frac{h-h_P}{s}dE\right]_{h_p=0} = 0 \tag{3.53}$$

The following expression for the attraction of the condensed masses (both regular and irregular) computed on the geoid can be obtained by combining equations (3.52) and (3.53)

$$A_{Cond} = \frac{\partial T_c}{\partial h_P}\Big|_{hp=0} = A_{Cond}^{Reg} + A_{Cond}^{Irreg} = 2\pi G\rho h_P \tag{3.54}$$

The direct topographical effect on gravity can then be computed using equations (3.9) and (3.54) as follows:

$$\delta A_{\text{Helmert}} = A - A_{\text{Cond}} = -c \tag{3.55}$$

This quantity, which represents the high frequency of gravitational signal, is an important gravimetric quantity in solving not only classical problem of BVP using Stokes scheme, but also modern BVP using Molodensky approach.

Helmert (or Faye) anomalies can be expressed by the following formula:

$$\Delta g_{\text{Helmert(Faye)}} = g_P - \gamma_{Q_o} + F + c \tag{3.56}$$

3.5 Pratt-Hayford topographic isostatic reduction

The PH reduction method is one of the topographic-isostatic reduction schemes used in physical geodesy. Although this method was used as a mass reduction technique in the past, it has not been used since the late seventies for geoid determination. Pratt studied first the geodetic evidence for isostatic equilibrium of topographical masses from the geodetic and astro-geodetic measurements carried out in the triangulation stations of the Himalayas in India. The big difference in the deflections of the vertical between two stations 375 miles apart made him conclude that the attraction of the Himalayas on these stations must be compensated by mass deficiencies located under the mountains. According to him, the mountains had risen from the base like fermenting dough and the density underneath the mountains would be less than that in the lowland.

Hayford, of U.S. Coast and Geodetic Survey, carried out a new study on Pratt's hypothesis of isostatic equilibrium in 1910 for geodetic purpose. This method has been named the Pratt Hayford method since then. This scheme can be formulated as follows:

1. The density underneath high mountains is uniformly smaller than that under moderate lands. Isostatic compensation is uniform.
2. The compensation starts from directly under the mountains.

3. The compensation reaches down to a compensation depth D, where isostatic equilibrium exists.
4. The relation between the density ρ_o of the compensating masses in a column of height D and the density ρ of a column with height equal to sum of the height of the topography and the compensation depth is then (see Figure 2.6)

$$\rho = \frac{D}{D+h}\rho_o \tag{3.57}$$

where h is the height of the topography. The compensation depth D is assumed equal to 100 km. The normal or standard density value ρ_o is taken equal to 2.67 g/cm^3. It is obvious from formula (3.57) that the actual density is smaller than the standard value, which implies that there is mass deficiency given by

$$\Delta\rho = \rho_o - \rho = \frac{h}{D+h}\rho_o \tag{3.58}$$

Similarly, in the ocean, the density of ρ of the column D-h′ can be given by

$$\rho = \frac{D\rho_o - h'\rho_w}{D-h'} \tag{3.59}$$

where h′ and ρ_w are the depth of the ocean and the density of the water, respectively. There is a mass surplus in the ocean given by

$$\Delta\rho = \rho - \rho_o = \frac{h'}{D-h'}(\rho_o - \rho_w) \tag{3.60}$$

The isostasy is defined as a hydrostatic equilibrium that prevails at a depth of compensation in such a way that every unit area at the compensation depth is under the

same pressure everywhere under mountain or ocean. The condition of equality of pressure for a unit column is given by the equation

$$\int_{-D}^{H} \rho g dz = \text{Const.} \tag{3.61}$$

The condition of equality of mass can be expressed as

$$\int_{-D}^{H} \rho \left(1 + \frac{z}{R}\right)^2 dz = \text{Const.} \tag{3.62}$$

where R is the Earth's radius and z is the vertical coordinate. The PH hypothesis agrees neither with the condition of pressure nor with that of mass. The difference of mass computed using these two conditions shows that the equal pressure hypothesis of compensation is four times closer than equal mass hypothesis (Heiskanen and Vening Meinesz, 1958). The equality of topographical masses and their compensation can thus be regarded as an approximation to the equality of pressure since the latter depends not only on mass but also on gravity.

The direct topographical effect in the PH model can be regarded as the attraction change due to the topographical masses above the geoid and compensated masses below the geoid, which lie within the depth of compensation. The direct topographical effect at a point P for this reduction method can be expressed as follows:

$$\delta A_{PH} = A - A_{Comp} \tag{3.63}$$

where A and A_{Comp} represent the attraction of the topographical masses and the compensated masses, respectively, and they can be expressed by the following integrals:

$$A = G\iiint_{E\ 0}^{h} \frac{\rho(x,y,z)(h_p - z)}{s^3(x_p - x, y_p - y, h_p - z)}dxdydz \tag{3.64}$$

$$A_{Comp} = G\iint_{E} \int_{-D-h_p}^{-h_p} \frac{\Delta\rho(x,y,z)(h_p - z)}{s^3(x_p - x, y_p - y, h_p - z)}dxdydz \tag{3.65}$$

Equations (3.64) and (3.65) can be numerically integrated using rectangular prisms as follows (Nagy, 1966):

$$A = G\rho \,|||\, x\ln(y+r) + y\ln(x+r) + y\ln(x+r) - z\arctan\frac{xy}{zr}\,|_{x_1}^{x_2}\,|_{y_1}^{y_2}\,|_{0}^{h(x,y)} \tag{3.66}$$

$$A_{Comp} = G\rho \,|||\, x\ln(y+r) + y\ln(x+r) + y\ln(x+r) - z\arctan\frac{xy}{zr}\,|_{x_1}^{x_2}\,|_{y_1}^{y_2}\,|_{-D}^{-D-h(x,y)} \tag{3.67}$$

The following steps are required to compute PH anomalies:

1. Measure gravity at a point P on the Earth's surface.
2. Compute the effect on gravity due to the complete removal of the topography above the geoid using formula (3.66).
3. Compute the effect on gravity due to the compensating masses using the formula (3.67).
4. Compute the direct topographical effect on gravity for this PH reduction scheme using formula (3.63).
5. Bring the gravity station down to the geoid surface with the Free-air reduction.
6. Compute the normal gravity of the reference ellipsoid at the corresponding point Q_o on the reference ellipsoid.

The PH topographic-isostatic anomalies can be given by the following formula:

$$\Delta g_{Pratt-Hayford} = g_P - \gamma_{Q_o} + F - \delta A_{Pratt-Hayford} \quad (3.68)$$

3.6 Airy-Heiskanen topographic-isostatic reduction

The AH model is based on the principle that mountains are floating on material of higher density forming roots under mountains and anti-roots under the oceans. A British astronomer, G. B. Airy, came to the same conclusion as did J. H. Pratt from the geodetic-astronomical observations in the triangulation chains of India, that the masses of mountains are compensated in some way but postulated his hypothesis of isostatic equilibrium in a different way compared to that postulated by Pratt. The theory that the gravitational attraction of the masses of the mountains is compensated either due to compensating masses of lesser density underneath the mountains according to Pratt or due to root formation according to Airy is an important similarity between these two theories. According to the "mountain-root theory" proposed by Airy, mountains can be pictured as Earth's crust floating in a magma-like layer, the density of which is higher than that of the Earth's crust (see Figure 2.7).

W. A. Heiskanen formulated Airy's hypothesis more precisely for the computation of topographic-isostatic anomalies for geodetic purposes, and made the following assumptions (Heiskanen and Vening Meinesz, 1958):

1. The isostatic compensation is complete.
2. The compensation is local, which means the compensating masses lie directly under mountains.
3. The density of the Earth's crust is constant and is assumed to be 2.67 gm/cm^3.
4. The density of the upper mantle is also constant but 0.6 gm/cm^3 higher than that of the Earth's crust.
5. The normal crust thickness is assumed to be 30 km.
6. The condition of floating equilibrium for the continents can be formulated as

$$t = \frac{h}{\Delta\rho}\rho_o \tag{3.69}$$

where t represents the thickness of root and $\Delta\rho$ is density contrast between the normal crust thickness, ρ_o and the upper mantle, ρ_1 , which is equal to 0.6 g/cm^3. It is obvious from the equation (3.69) that the smaller the difference in density between the normal crust thickness and the upper mantle, the greater the thickness of the mountain root. Similarly, the thickness of the antiroot in the ocean can be expressed as

$$t' = \frac{\rho_o - \rho_w}{\rho_1 - \rho_o} h' \tag{3.70}$$

where h′ and ρ_w are the depth of the ocean and the density of the water, respectively. The density contrast for the case of ocean is given by

$$\Delta\rho = \rho_1 - \rho_o = \frac{\rho_o - \rho_w}{t'} h' \tag{3.71}$$

The direct topographical effect due to this AH topographic isostatic scheme is the difference in the attraction between topographical masses and their compensating masses within the depth of the root. It can be represented by the equation (3.63), where the second term A_{Comp} stands for the attraction due to compensated masses according to AH gravimetric scheme. The first term which shows the gravitational attraction of the topographical masses is evaluated by the equations (3.64) and (3.66). The second term can be expressed as

$$A_{Comp} = G\iint_E \int_{-D-t-h_p}^{-D-h_p} \frac{\Delta\rho(x,y,z)(h_p - z)}{s^3(x_p - x, y_p - y, h_p - z)} dxdydz \tag{3.72}$$

where t is the thickness of root and D is the normal crust thickness. The attraction of the compensating masses can be given in the same way as in equation (3.67):

$$A_{Comp} = G\rho \,|||\, x\ln(y+r) + y\ln(x+r) - z\arctan\frac{xy}{zr}\Big|_{x_1}^{x_2}\Big|_{y_1}^{y_2}\Big|_{-D-h(x,y)}^{-D-t-h(x,y)} \quad (3.73)$$

AH topographic-isostatic anomalies can be computed by the following steps:

1. Measure gravity at a point P on the Earth's surface.
2. Compute the effect on gravity due to the complete removal of the topography above the geoid using formula (3.66).
3. Compute the effect on gravity due to the compensation of masses according to AH model using formula (3.73).
4. Compute the direct topographical effect on gravity for this AH reduction scheme using the formula (3.63).
5. Bring the gravity station down to the geoid surface with the Free-air reduction.
6. Compute the normal gravity of the reference ellipsoid at the corresponding point Q_o on the reference ellipsoid.

AH topographic-isostatic anomalies can be given by the following formula:

$$\Delta g_{Airy-Heiskanen} = g_P - \gamma_{Q_o} + F - \delta A_{Airy-Heiskanen} \quad (3.74)$$

Table 3.1 shows three criteria of each reduction method used in this investigation.

Table 3.1 Characters of gravimetric reduction methods

Reduction scheme	Indirect effects	Smoothness	Geophysical meaning
Bouguer	Very large indirect effects	smooth	It has geophysical meaning
Helmert (Faye)	Very small indirect effects	rough	It has no geophysical meaning
Airy Heiskanen	Small indirect effects (larger than Helmert's)	smooth	It has geophysical meaning
Pratt Hayford	Small indirect effects (larger than Helmert's)	smooth	It has geophysical meaning
Residual Terrain model	very small restored terrain effect	smooth	It has no geophysical meaning
Rudzki	zero indirect effect	rough	It has no geophysical meaning

Chapter 4

Numerical Tests

4.1 Gravimetric reductions

One of the most rugged areas in the Canadian Rockies bounded by latitude between 49ºN and 54ºN and longitude between 124º W and 114ºW is selected to compute direct topographical effects on gravity using the different gravity reductions presented in the previous chapters. They include the Rudzki inversion method, Helmert's second method of condensation, the refined Bouguer and RTM topographic reduction schemes, and the AH and PH topographic-isostatic reduction methods. A total of 9477 measured gravity values are used for this test, the distribution of which is given in Figure 4.1. The maximum and minimum values of measured gravity are 981219 mGal and 980226 mGal with a standard deviation 179 mGal. The normal gradient of 0.3086 mGal/m is

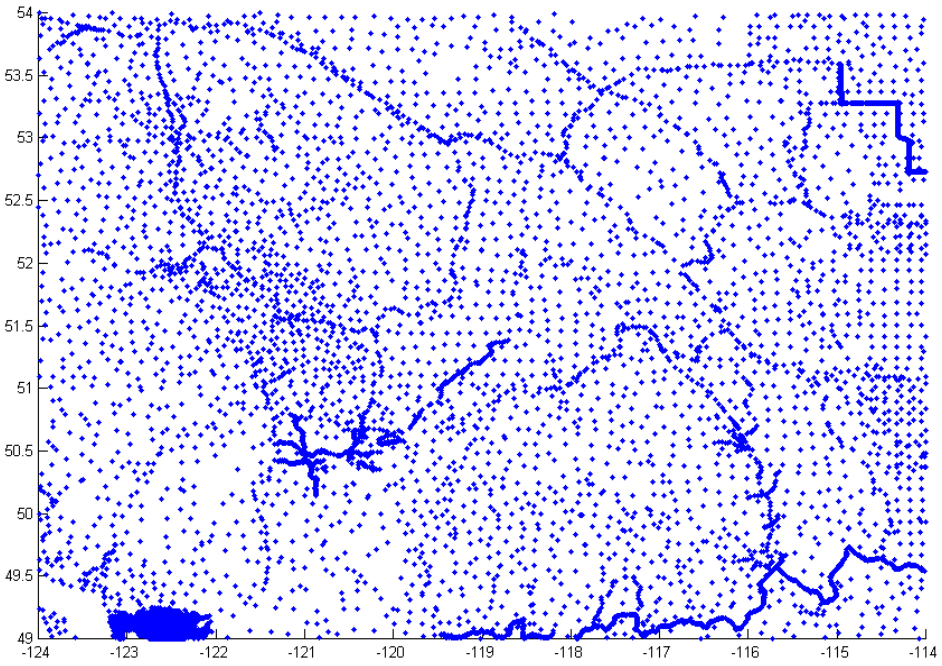

Fig. 4.1 The distribution of gravity points in the test area of Canadian Rockies

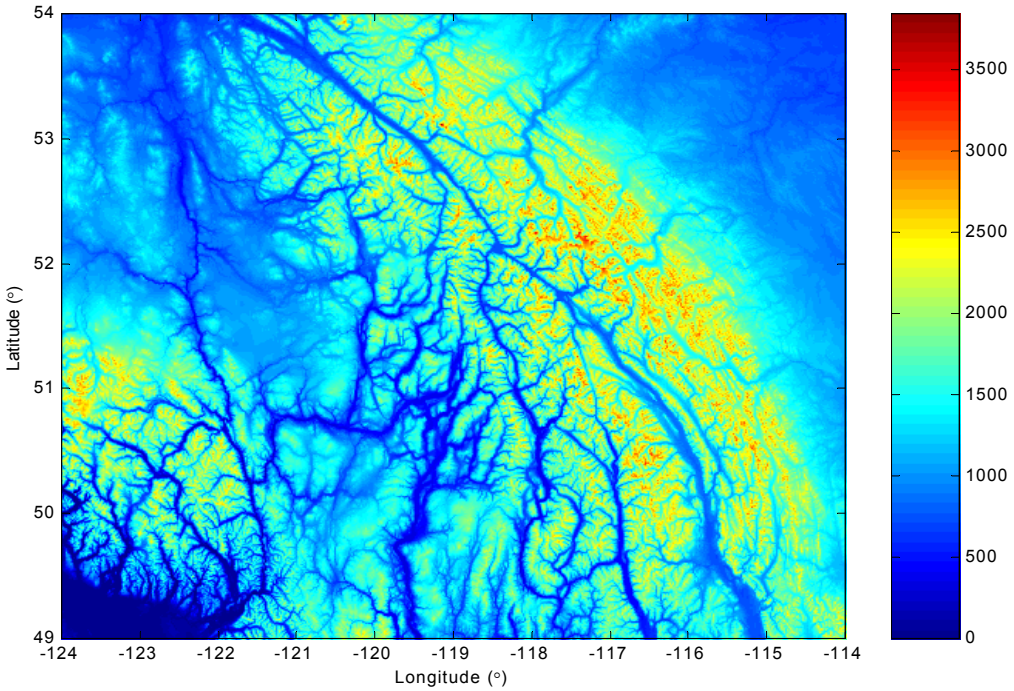

Fig. 4.2 The digital terrain model of Canadian Rockies (m)

used for the computation of Free-air anomalies. The standard constant density of 2.67 g/cm^3 is assumed. A digital terrain model with 6″ (0.12 km in East West and 0.18 km in North South directions) grid resolution is used in the computations. The attraction of the topography, the attraction of the compensating masses, and the attraction of the inverted masses are computed integrating a radius of 300 km around the computation point. There is a maximum elevation of 3937 m with a standard deviation of 420 m in the test area. Figure 4.2 shows the digital terrain model of the test area. The grid resolution used for gravity anomalies for each reduction method is 5′ × 5′.

Figures 4.3 and 4.4 show the refined Bouguer anomalies (computed using formula 3.10) and their correlation with the topography, respectively. The statistics of the refined

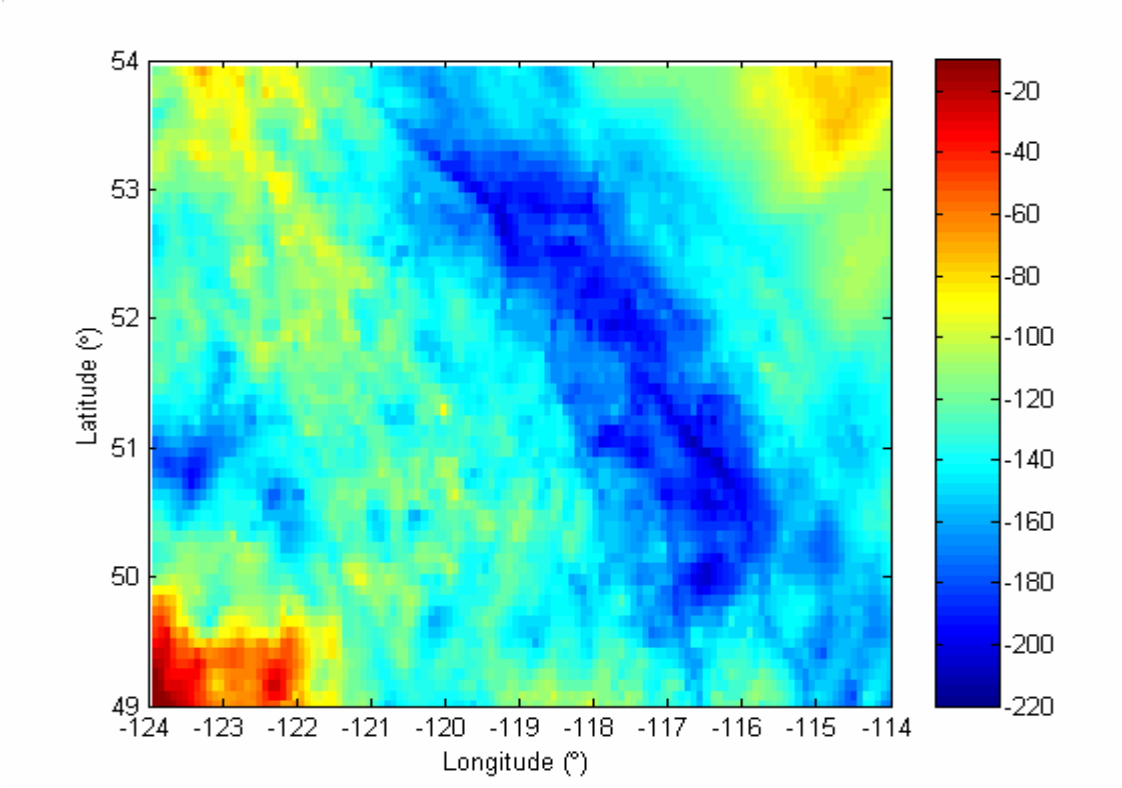

Fig. 4.3 The refined Bouguer anomalies (mGal)

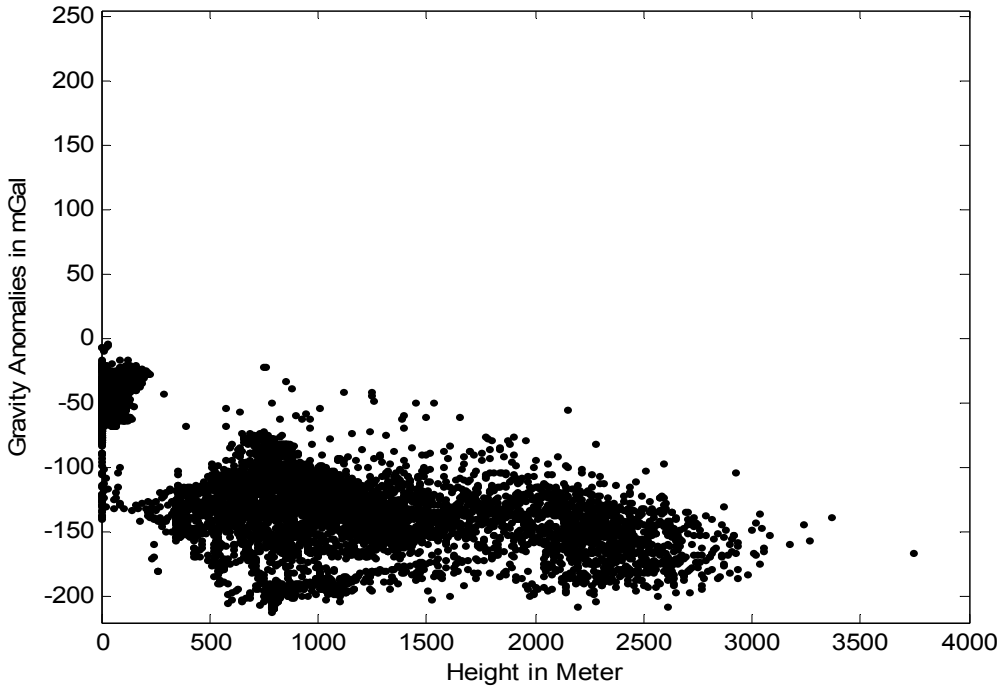

Fig. 4.4 The correlation between refined Bouguer anomalies and topography

Bouguer anomalies have a maximum value of –6 mGal, a minimum value of –213 mGal, a mean value of -110 mGal, and a standard deviation of 44 mGal. The higher the mountains in the test area, the more negative the value of the anomalies. These large negative values suggest that the topographic masses of the Rocky Mountains are compensated according to some models of topographic-isostatic hypothesis. It is obvious from the formula (3.7) of an infinite Bouguer plate that Bouguer anomalies are linearly dependent on the elevation.

In the modern context of geoid or quasigeoid determination, Helmert or Faye anomalies (see formula 3.55) can be regarded as an important type of gravity anomalies. This is because, on one hand, geoid determination using Helmert's second method of condensation is most commonly used in practice throughout the world and, on the other hand, the Molodensky correction term, in planar approximation, is equal to the TC (under

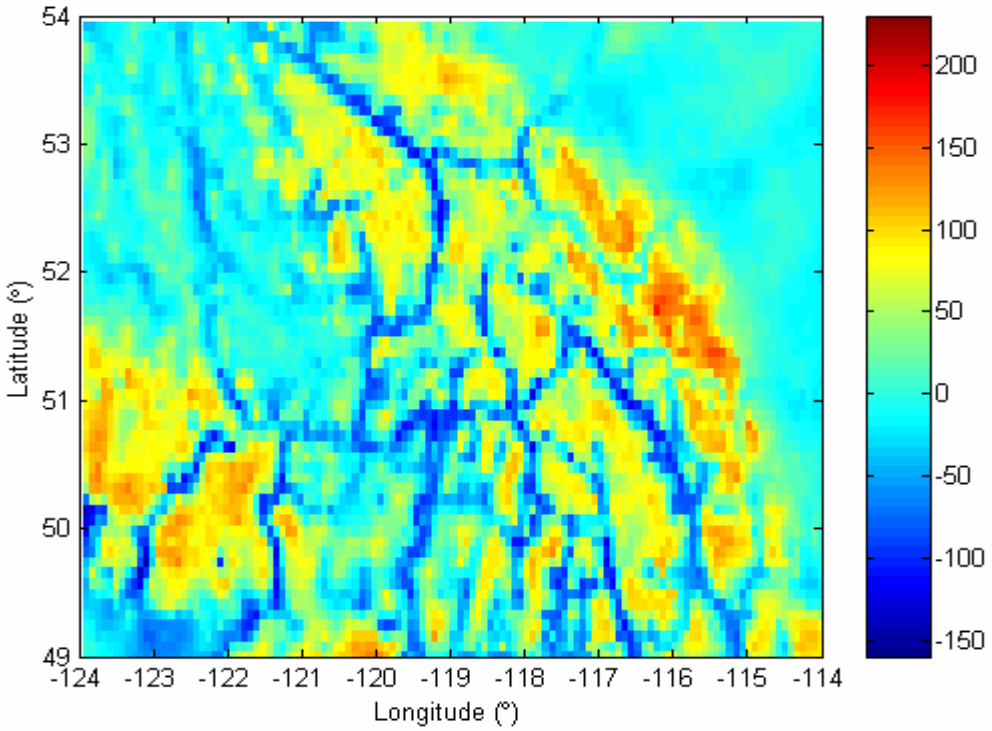

Fig. 4.5 Helmert (Faye) anomalies (mGal)

the assumption that the free air anomalies are linearly correlated with the height) which when added to Free-air anomaly gives us the Helmert or Faye anomaly. Though their physical meanings are different, they are approximately equal numerically. Also, Free-air anomalies can replace Helmert anomalies in the ocean areas where there is negligible effect of TC.

Figures 4.5 and 4.6 show the Helmert anomalies (computed using formula 3.56) and the correlation between Helmert anomalies with the topography. Helmert anomalies fluctuate between positive and negative values, with a maximum value of 252 mGal and a minimum value of -153 mGal. The maximum and minimum values are seen in high mountains and low valley stations, respectively. The correlation with height is bigger than that of the refined Bouguer anomalies.

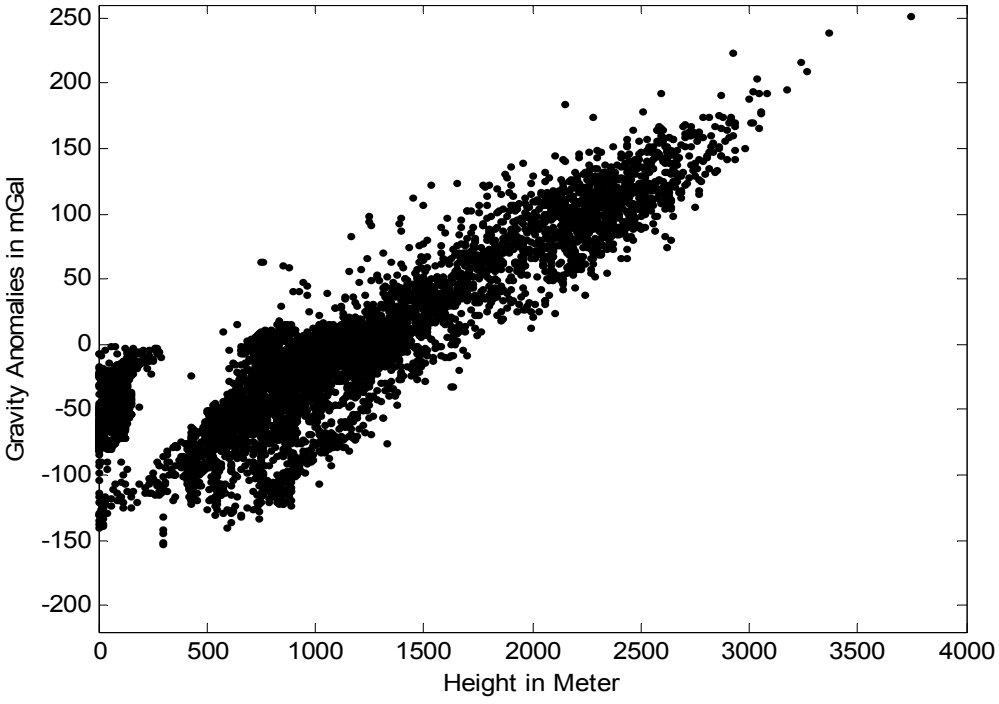

Fig. 4.6 The correlation between Helmert anomalies and topography

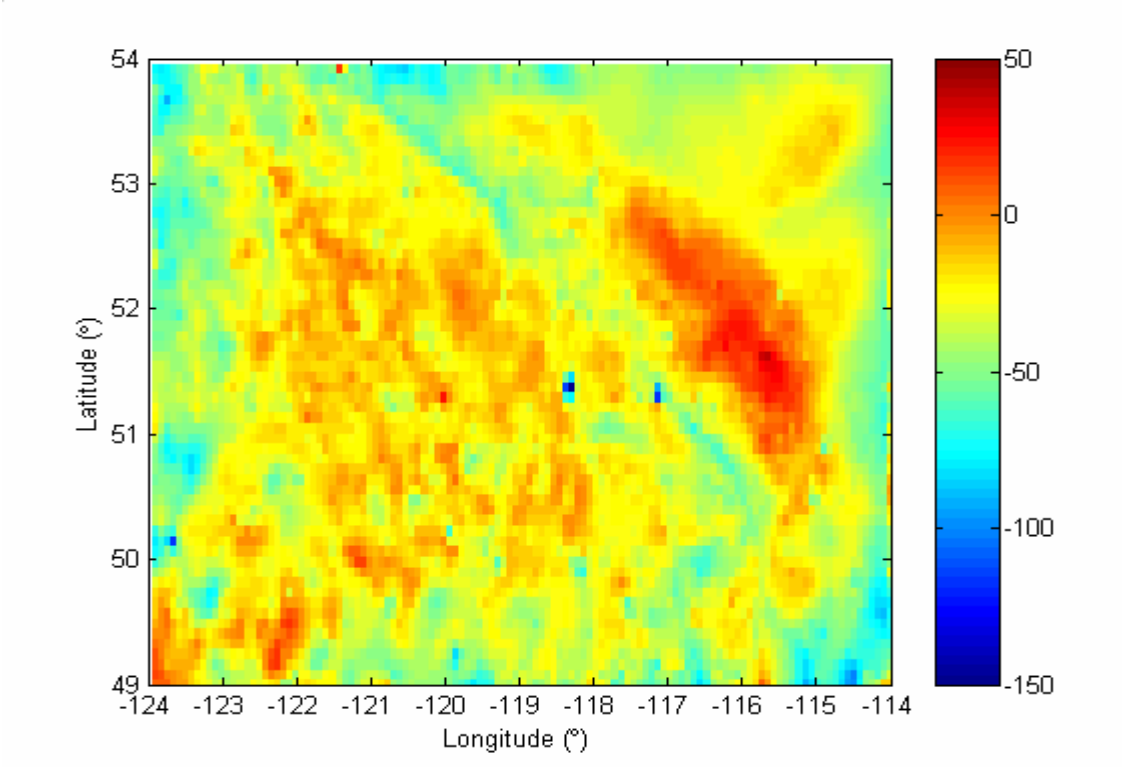

Fig 4.7 PH topographic-isostatic anomalies (mGal)

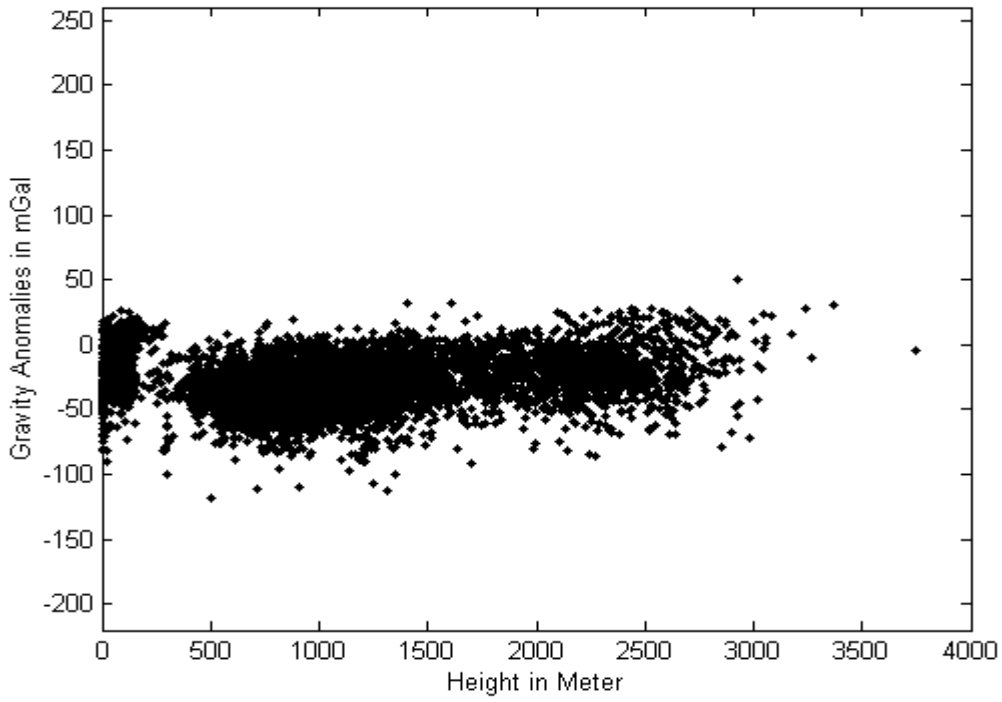

Fig. 4.8 The correlation between PH topographic-isostatic anomalies and topography

Figures 4.7 and 4.8 represent the Pratt Hayford topographic isostatic anomalies (computed using formula 3.68) and their correlation with the topography. The compensation depth for this mass reduction scheme is assumed to be equal to 100 km for the computation of PH anomalies. The maximum and minimum values vary from -108 mGal to 50 mGal. The range of the difference between maximum and minimum values is approximately two and half times smaller than that of Helmert anomalies and also smaller than that of the refined Bouguer anomalies by 60 mGal. The standard deviation is 18 mGal, which is much smaller than that of the Bouguer, Free-air, and Helmert (Faye) anomalies.

Figures 4.9 and 4.10 show the Airy Heiskanen topographic-isostatic anomalies (computed using 3.74) and their correlation with the topography, respectively. The normal crust thickness is assumed to be equal to 30 km and the density contrast between the normal crust thickness and the upper mantle is assumed to be 0.6 gm/cm^3 in the computational process for this mass reduction scheme. The statistics of AH anomalies are similar to those of PH model. The small difference in the statistics between these two sets of topographic-isostatic anomalies indicates that the attraction of compensating masses using AH and PH models is nearly equal.

The correlation of AH and PH anomalies with topography is much smaller than that of Free-air, Bouguer, and Helmert (or Faye) anomalies. The removal of topographical masses along with compensated masses according to Pratt Hayford and Airy Heiskanen topographic isostatic hypothesis prove better on eliminating the strong correlation of gravity anomalies with the height as seen with Bouguer and Helmert anomalies. The maximum value is observed in the highest mountains. The range of the difference between maximum and minimum values is much smaller (almost two and a half times) compared to that of Helmert anomalies and also smaller than that of refined Bouguer anomalies by 51 mGal.

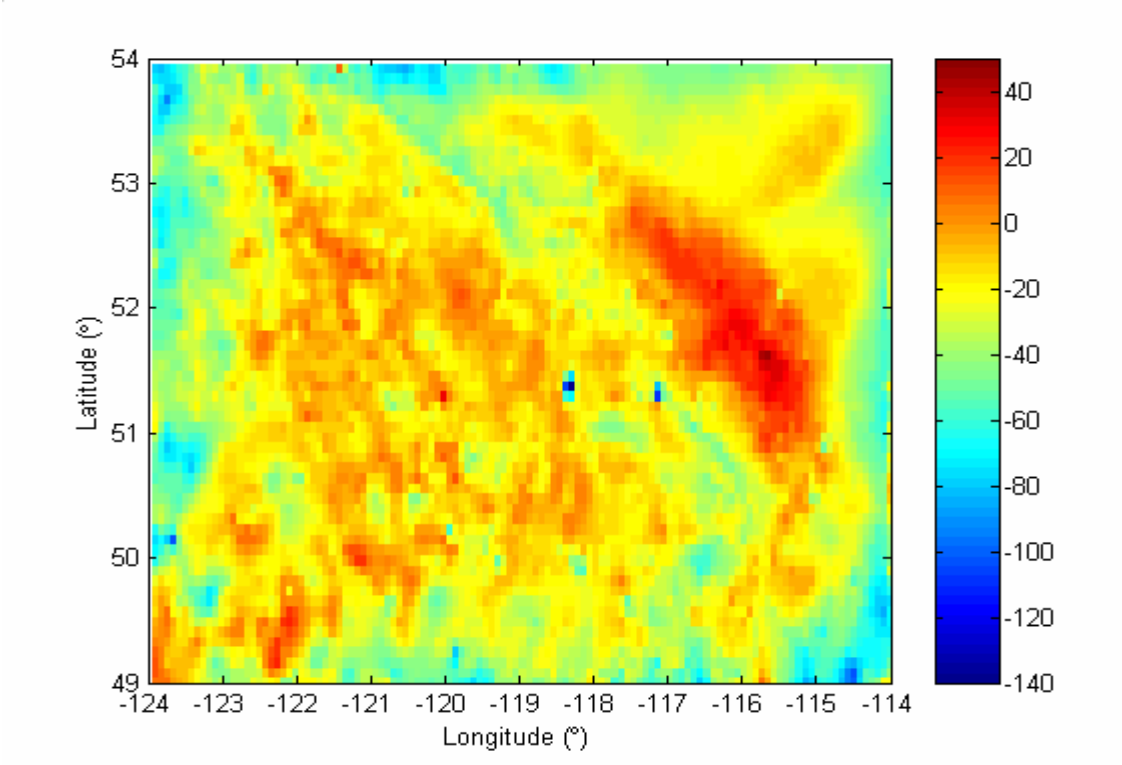

Fig. 4.9 AH topographic-isostatic anomalies (mGal)

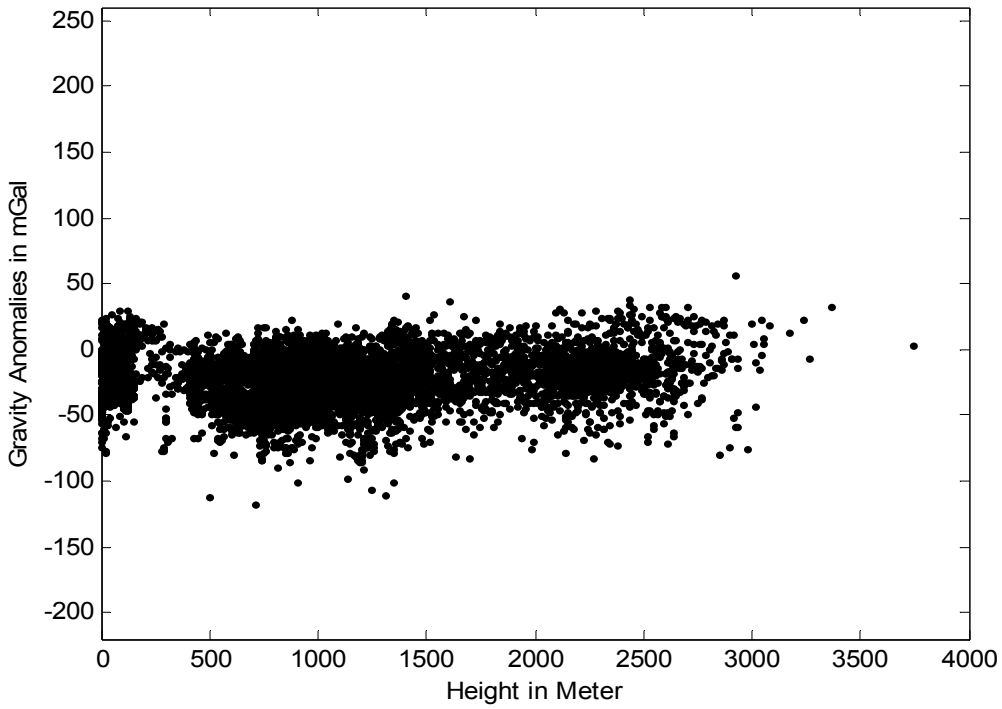

Fig. 4.10 The correlation between AH anomalies and topography

The statistics of Rudzki anomalies (computed using the formula 3.44) show that they fluctuate between a maximum value of 124 mGal and a minimum value of –123 mGal. When we compare Rudzki anomalies with Helmert, they show similar statistics. However, the range between maximum and minimum values is smaller (more than one and a half times) than that of Helmert and Free-air anomalies. The standard deviation of Rudzki anomalies is 36 mGal, which is much smaller than those of Helmert and Free air anomalies (58 mGal and 51 mGal, respectively) but bigger than those of both the AH and the PH topographic isostatic anomalies.

Figures 4.11 and 4.12 show the Rudzki anomalies and their correlation with the topography, respectively. Their correlation with the topography is less than that of

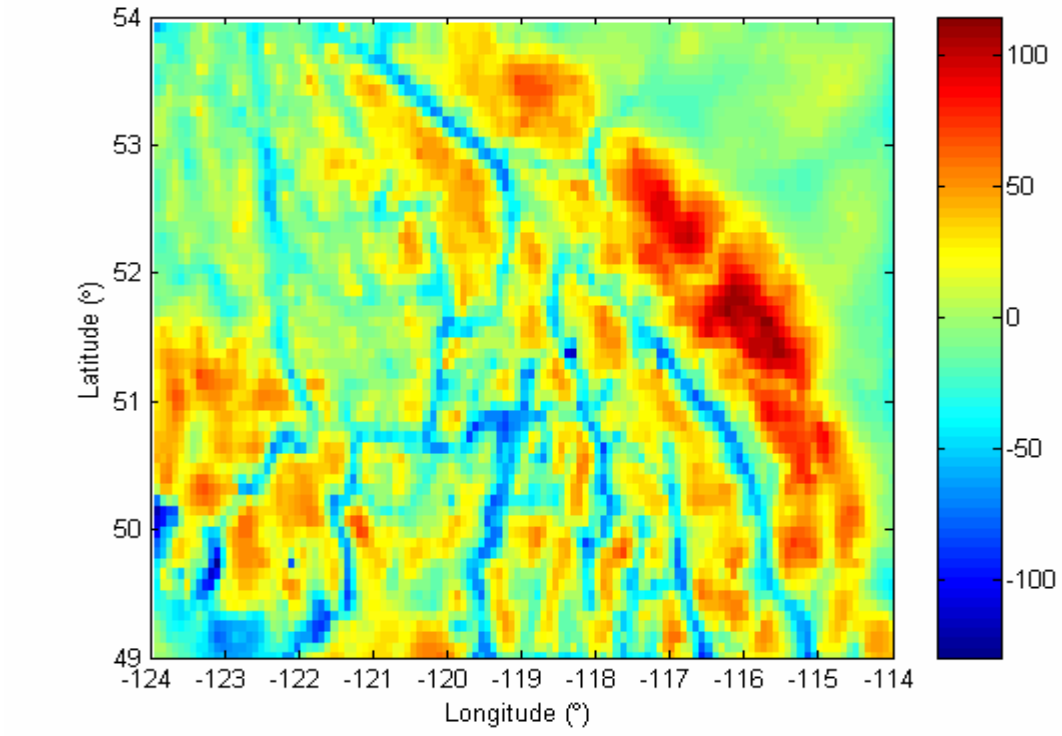

Fig. 4.11 Rudzki anomalies (mGal)

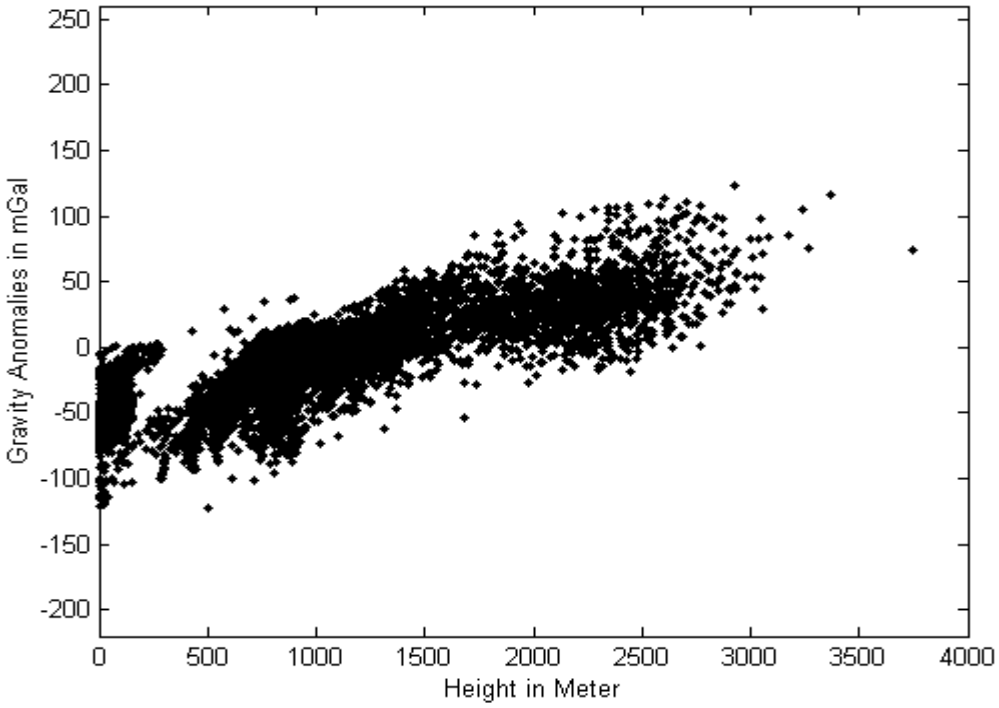

Fig. 4.12 The correlation between Rudzki anomalies and topography

Helmert anomalies. However, the removal of topography with inverted masses could not remove the strong correlation of Rudzki anomalies with height as significantly as topographic isostatic mass reduction schemes. The maximum and minimum values are seen at stations in mountains and low valleys, respectively.

The RTM anomalies are not used in geophysics. They were merely developed for geoid determination. Figures 4.13 and 4.14 show the RTM gravity anomalies (computed using formula 3.48) and their correlation with the topography. The statistics of the RTM anomalies are similar to those of topographic isostatic anomalies using the PH and AH reduction schemes, though the RTM reduction scheme is not a topographic isostatic reduction scheme.

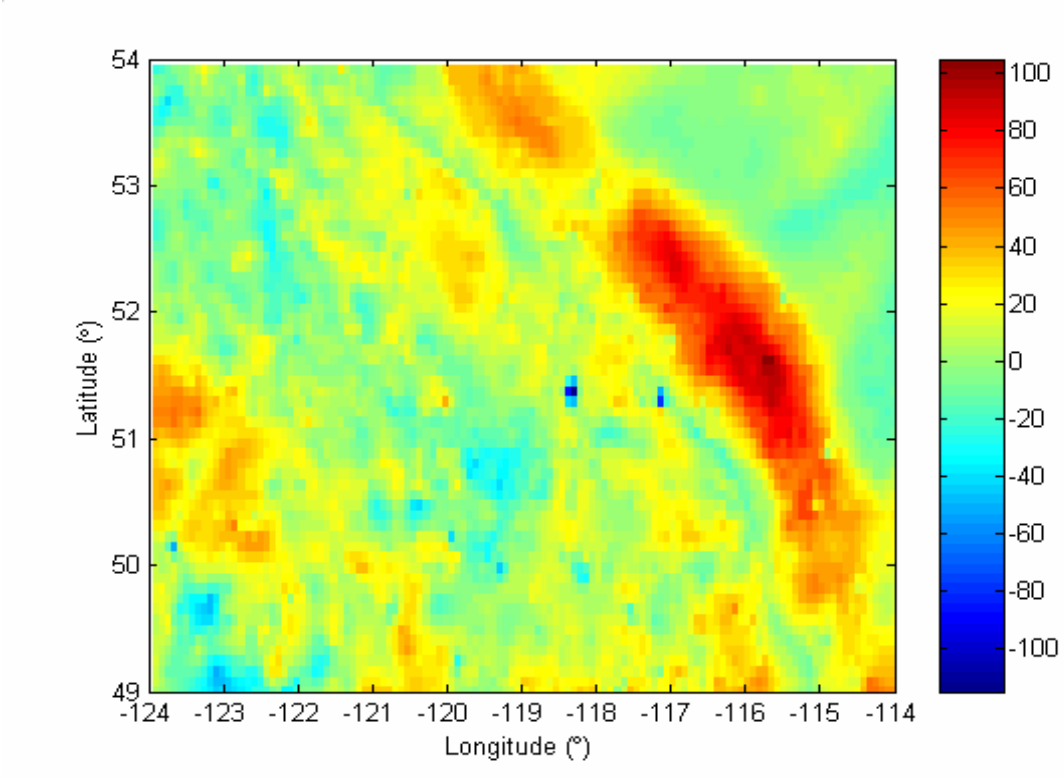

Fig. 4.13 RTM anomalies (mGal)

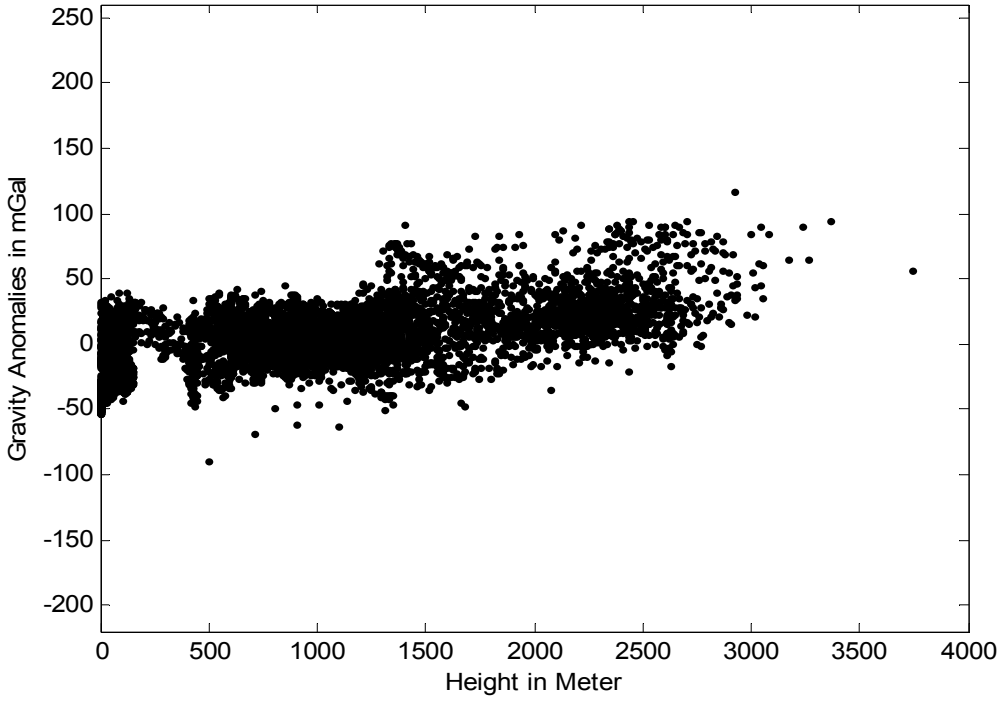

Fig. 4.14 The correlation between RTM anomalies and topography

The RTM anomalies were also less correlated with the topography, like the PH and AH topographic isostatic anomalies. They have a maximum value of 116 mGal and a minimum value of –90 mGal with a mean value of –1 mGal. The standard deviation is 23 mGal, which is closer to those of topographic isostatic schemes and smaller compared to that of Free-air, Bouguer, Helmert, and Rudzki anomalies. The maximum value of RTM anomalies is seen in mountains and the minimum in moderate lands.

The statistics of gravity anomalies for different gravimetric mass reduction schemes are presented in Table 4.1. The AH and PH topographic isostatic gravity anomalies result in the smoothest gravity field in terms of standard deviation among all mass reduction techniques used in this investigation. Their range is the smallest compared to those of all other methods. Helmert anomalies yield the roughest gravity field for the test area. The Free-air and Helmert anomalies show similar statistics. The statistics of Rudzki anomalies are better than those of Helmert and Free air anomalies in terms of both the range and the standard deviation. RTM anomalies, though they do not belong to any topographic isostatic reduction scheme and have some theoretical problems as described in the earlier chapter, show statistics similar to topographic isostatic anomalies, which is a main reason why they are favored for geoid determination and are being widely used throughout the world these days. Figures 4.15 and 4.16 present all gravity anomalies and their correlation

Table 4.1 The statistics of gravity anomalies (mGal)

Reduction scheme	Max	Min	Mean	Std
Free-air	166.38	-183.58	-22.39	50.71
Refined Bouguer	-5.52	-212.87	-110.08	43.62
Helmert (Faye)	251.56	-152.67	-15.06	58.22
AH	49.86	-118.83	-25.14	18.54
PH	49.86	-107.58	-29.78	18.05
RTM	115.45	-89.91	-0.57	23.49
Rudzki	123.69	-122.34	-17.38	35.85

with the topography once again in single pages for the purpose of easy comparisons. The maximum and minimum values of gravity anomalies are held fixed in Figure 4.15.

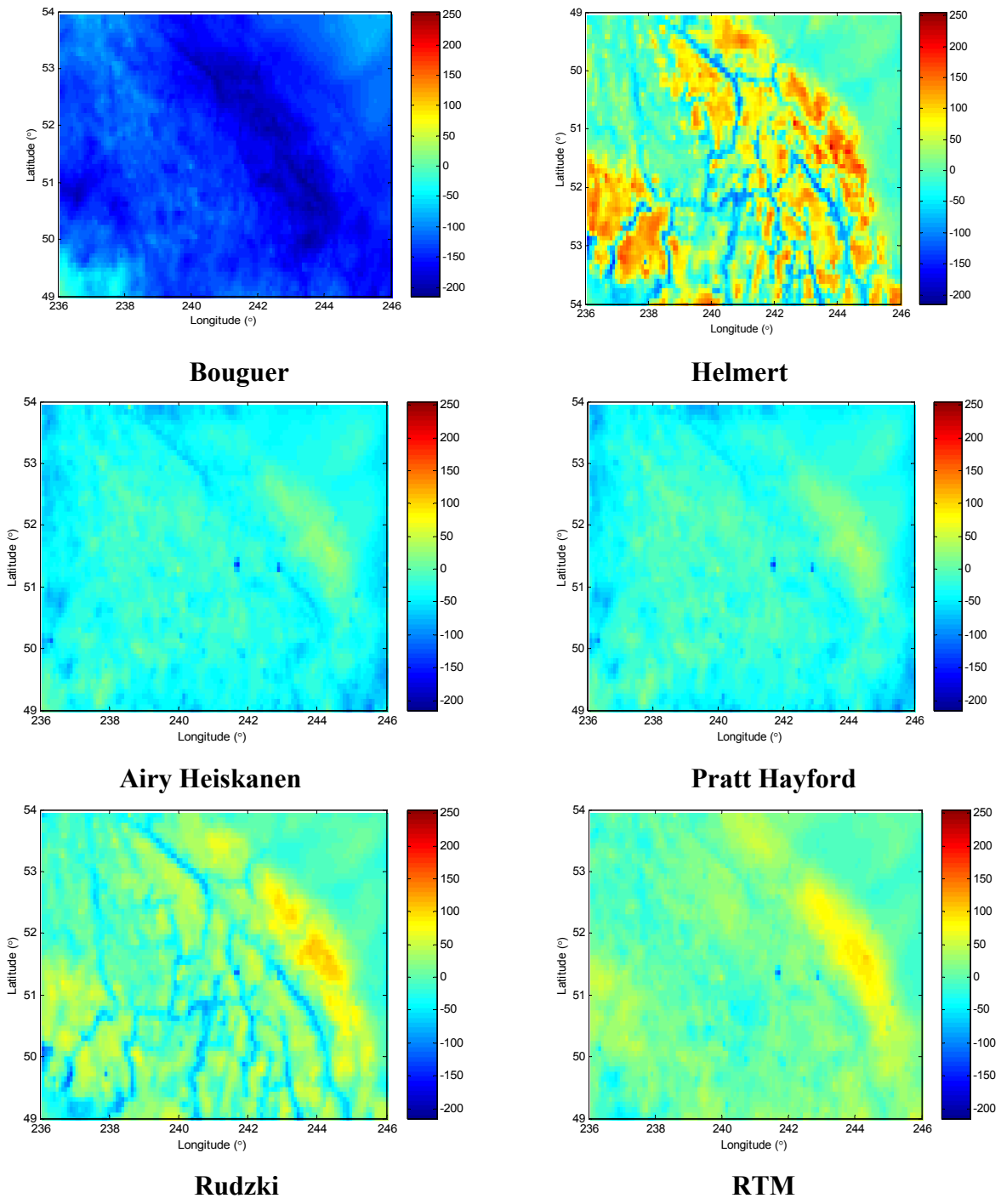

Fig. 4.15 Gravity anomalies

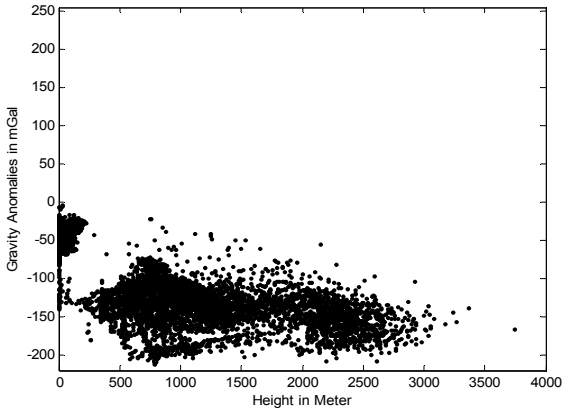

Bouguer

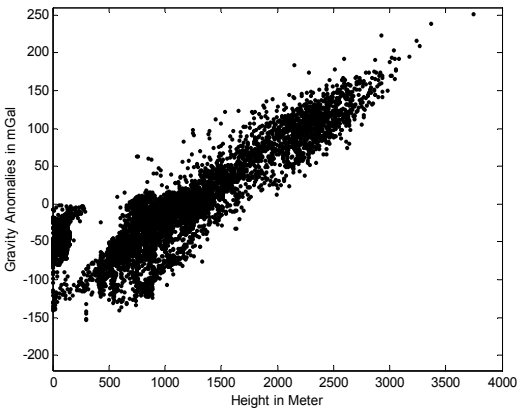

Helmert

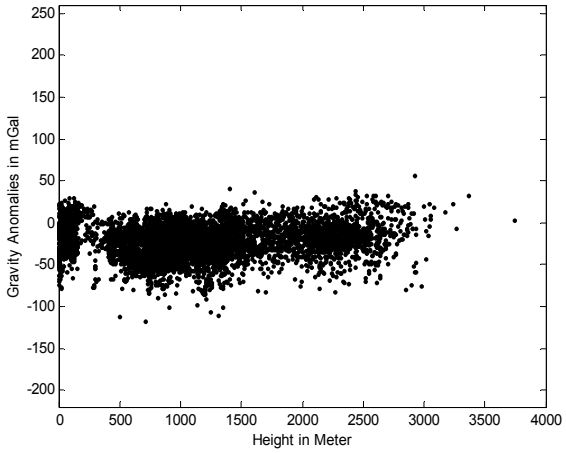

Airy Heiskanen

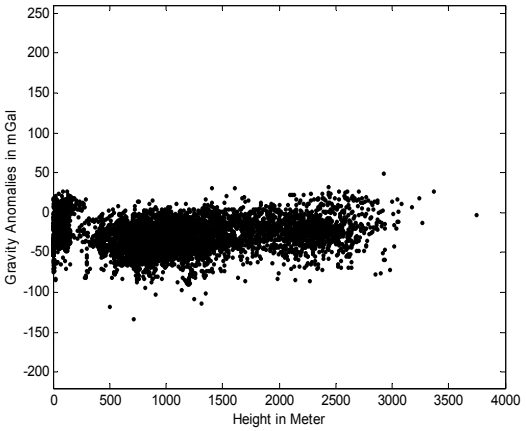

Pratt Hayford

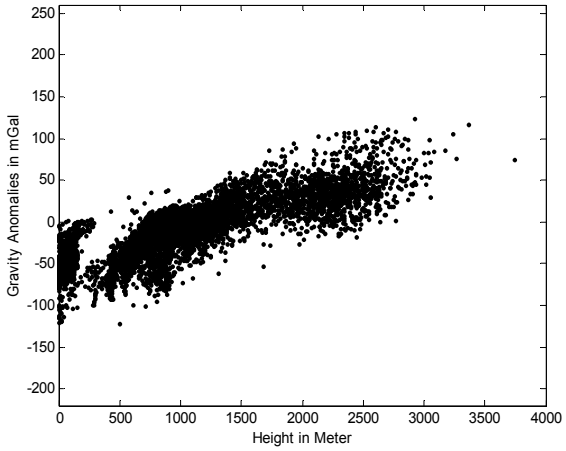

Rudzki

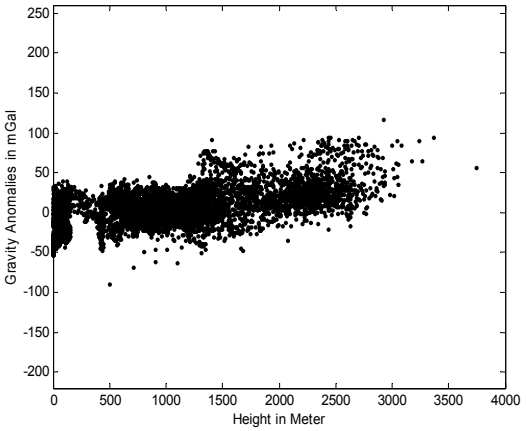

RTM

Fig. 4.16 The correlation of gravity anomalies with topography

4.2 Gravimetric geoid determination

The terrain-reduced gravity anomalies are further reduced with a geopotential model to extract the long wavelength component of the gravity signal prior to the solution of the geodetic boundary value problem using the classical Stokes formula. It is restored again in the computational process to compute the total geoid. This procedure is regarded as the "remove restore" technique in geoid determination.

The geopotential model EGM96 is used as a reference model for all mass reduction schemes used in this investigation. Comparing the statistics of reduced gravity anomalies (see equation 2.3) in Table 4.2 to those in Table 4.1 we see that the removal of the global reference field does improve the statistics of the reduced gravity anomalies for Free-air, Helmert, Rudzki, and RTM schemes but not for the refined Bouguer, AH and PH topographic-isostatic methods in terms of standard deviation and range. The standard deviation and the range get bigger for refined Bouguer, AH and PH models, exhibiting a disagreement of these reduction schemes with the geopotential model.

Table 4.2 The statistics of reduced gravity anomalies (mGal)

Reduction scheme	Max	Min	Mean	Std
Free-air	125.47	-185.77	-16.53	44.03
Refined Bouguer	26.61	-261.30	-104.23	64.21
Helmert(Faye)	214.65	-155.74	-9.20	50.15
Airy-Heiskanen	65.38	-136.98	-19.29	28.41
Pratt-Hayford	62.80	-144.13	-23.93	29.59
RTM	67.59	-78.29	5.20	15.29
Rudzki	77.04	-118.16	-11.54	24.22

It is theoretically not correct to use the EGM96 geopotential model, which is based on FA anomalies, to extract the long-wavelength component for all gravimetric reduction

schemes. The EGM96 geopotential model is based on FA anomalies and therefore either a geopotential model corresponding to each reduction scheme should be used or the corresponding correction for each reduction method should be applied to FA coefficients (also see Kuhn, 2000). However, it will be very difficult in practice to create geopotential models based on each reduction scheme.

The 258 GPS benchmarks available in the test area of Canadian Rockies are used as control for estimating the accuracy of the gravimetric geoid solutions; their distribution is given in Figure 4.17. There are no GPS leveling points above the elevation of 2000 m.

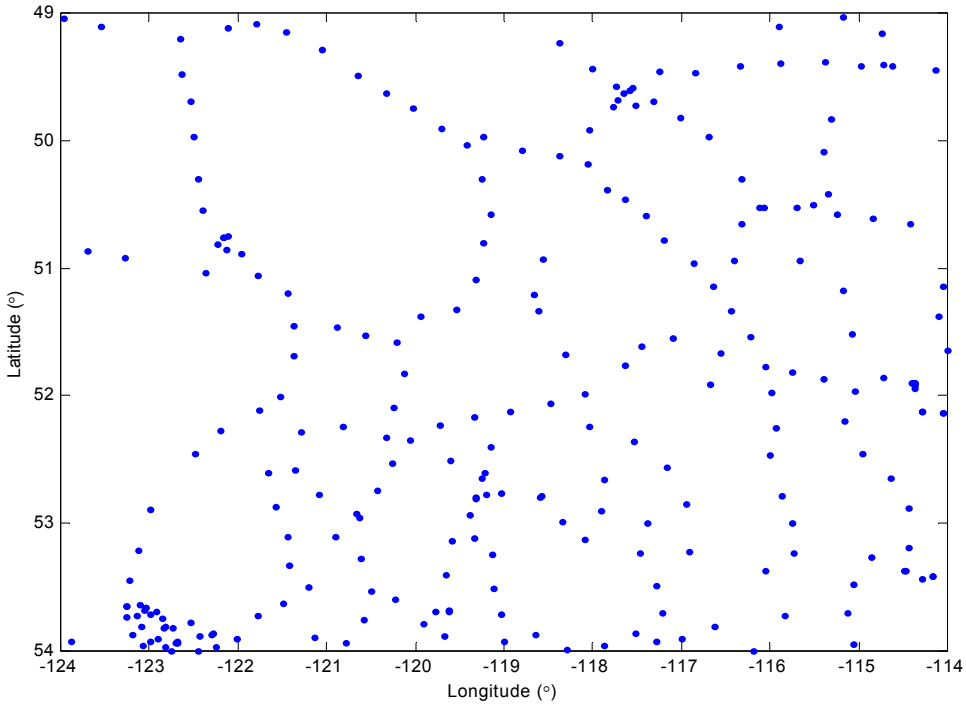

Fig 4.17 The distribution of GPS leveling points in the test area

The indirect effect on gravity for Helmert, AH, and PH models is considered before applying Stokes's formula for these reductions. The statistics of the indirect effects on gravity and the geoid are given in Table 4.3. The indirect effect on gravity for Helmert's method is very small, while that of the PH topographic-isostatic reduction reaches a

maximum of 3 mGal. The indirect effect on geoid undulations for the PH isostatic reduction changes the geoid by nearly 10 m, while that for Helmert's method changes the geoid by only 47 cm. The indirect effect for Helmert's second method is computed using FFT method (based on Formula 2.17) in 6″ × 6″ grid. The indirect effects on geoid for

Table 4.3 Indirect effects on gravity (mGal) and on geoid undulation (m)

Geoid Model	Indirect Effect	Max	Min	Mean	STD
Helmert	gravity	0.26	0.00	0.04	0.03
	geoid	0.01	-0.47	-0.12	0.08
Airy Heiskanen	gravity	2.61	0.09	1.04	0.64
	geoid	8.46	0.31	3.36	2.06
Pratt Hayford	gravity	3.08	0.18	1.35	0.75
	geoid	9.97	0.59	4.36	2.41
RTM (restored terrain effect)	quasigeoid	1.07	-1.03	-0.33	0.46

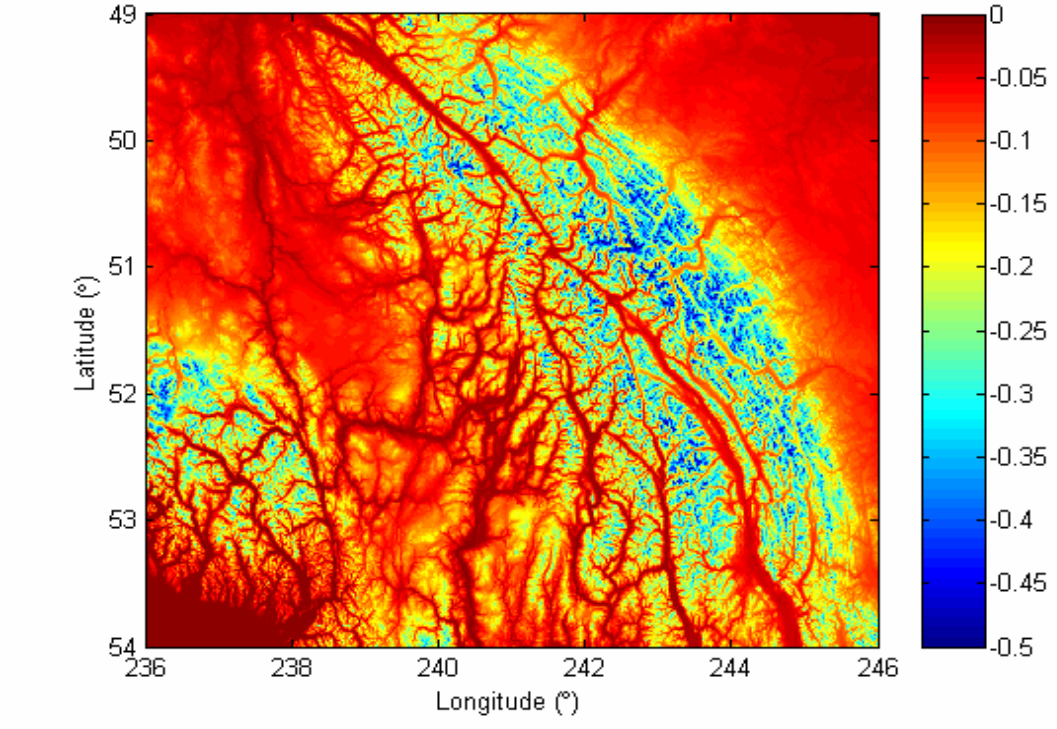

Fig 4.18 The indirect effect on geoid for Helmert scheme (m)

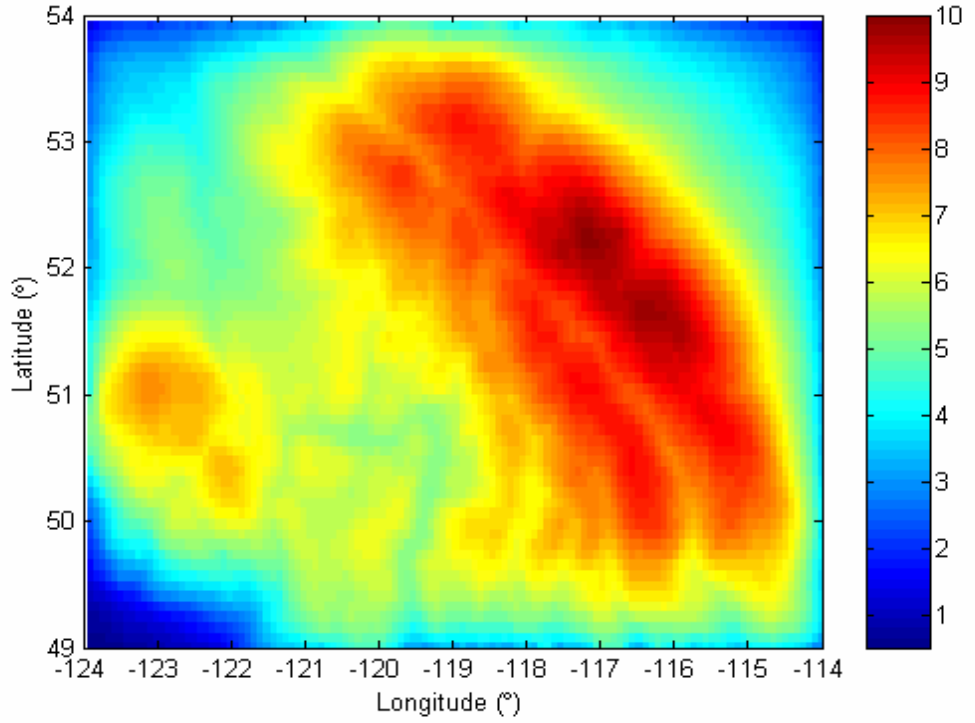

Fig 4.19 The indirect effect on the geoid for the PH reduction (m)

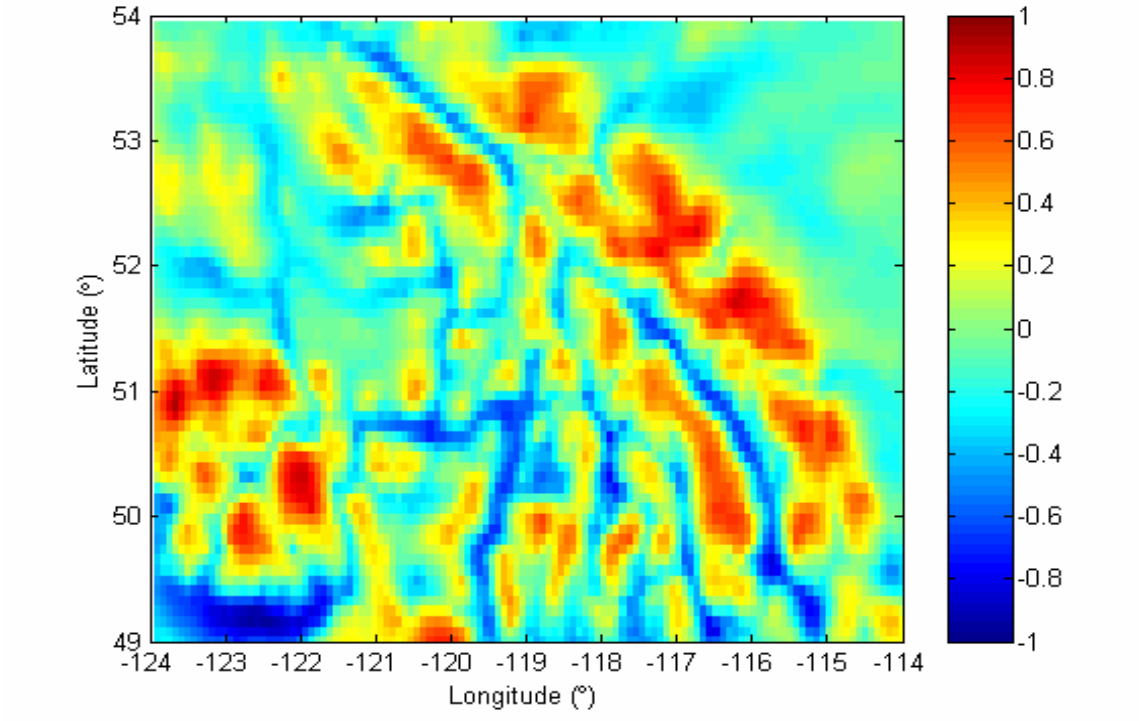

Fig 4.20 Restored terrain effect on the quasigeoid for the RTM reduction (m)

AH and PH models and restored terrain effect on quasigeoid for RTM method are computed using the numerical integration of rectangular prisms given by Formula 2.16. The results are then gridded to $5' \times 5'$ resolution.

The indirect effects on gravity and geoid for the AH and PH models have similar statistics. Figures 4.18 and 4.19 show the indirect effect on geoid for Helmert's second method of condensation and the PH model. The maximum indirect effect for all reduction schemes is seen in mountains. The restore terrain effect on the quasigeoid for the RTM model reaches nearly a metre and is shown in figure 4.20.

A four-parameter trend surface is applied to fit the gravimetric geoid solutions to GPS-leveling. The statistics of the difference of gravimetric geoid undulations with GPS-leveling before and after the fit are given in table 4.4.

The gravimetric geoid solution based on Rudzki's inversion reduction shows almost the same differences as the RTM and Helmert methods in terms of standard deviation and range after the fit. The absolute magnitudes of maximum, minimum, and mean values of the differences between the Rudzki gravimetric solution with GPS-levelling before fit are the smallest, and those based on the topographic-isostatic gravimetric solutions of AH and PH models are the largest. As mentioned in the earlier paragraph, the main reason for this large bias is the use of the global geopotential model EGM96, which is based on FA coefficients.

These biases are removed by the fit to GPS levelling geoid and the range of maximum and minimum values for these models becomes nearly the same as for the Rudzki, Helmert, and RTM methods. However, their standard deviation is 6 cm bigger than other methods. The figure of absolute geoid using every reduction scheme looks nearly the same as that of the Rudzki geoid shown in figure 4.21.

Table 4.4 Statistics of different gravimetric geoid solutions compared with GPS leveling geoid (m)
(values in the parentheses are before fit)

Reduction scheme	Max	Min	Mean	Std
Helmert	0.62	-0.59	0.00	0.19
	(1.97)	(0.65)	(1.33)	(0.23)
Airy-Heiskanen	0.59	-0.86	0.00	0.26
	(-4.85)	(-6.64)	(-5.64)	(0.35)
Pratt-Hayford	0.54	-0.81	0.00	0.25
	(-5.18)	(-6.81)	(-5.77)	(0.34)
RTM	0.76	-0.55	0.00	0.19
	(1.46)	(0.31)	(0.77)	(0.21)
Rudzki	0.76	-0.56	0.00	0.19
	(0.12)	(-1.37)	(-0.67)	(0.35)

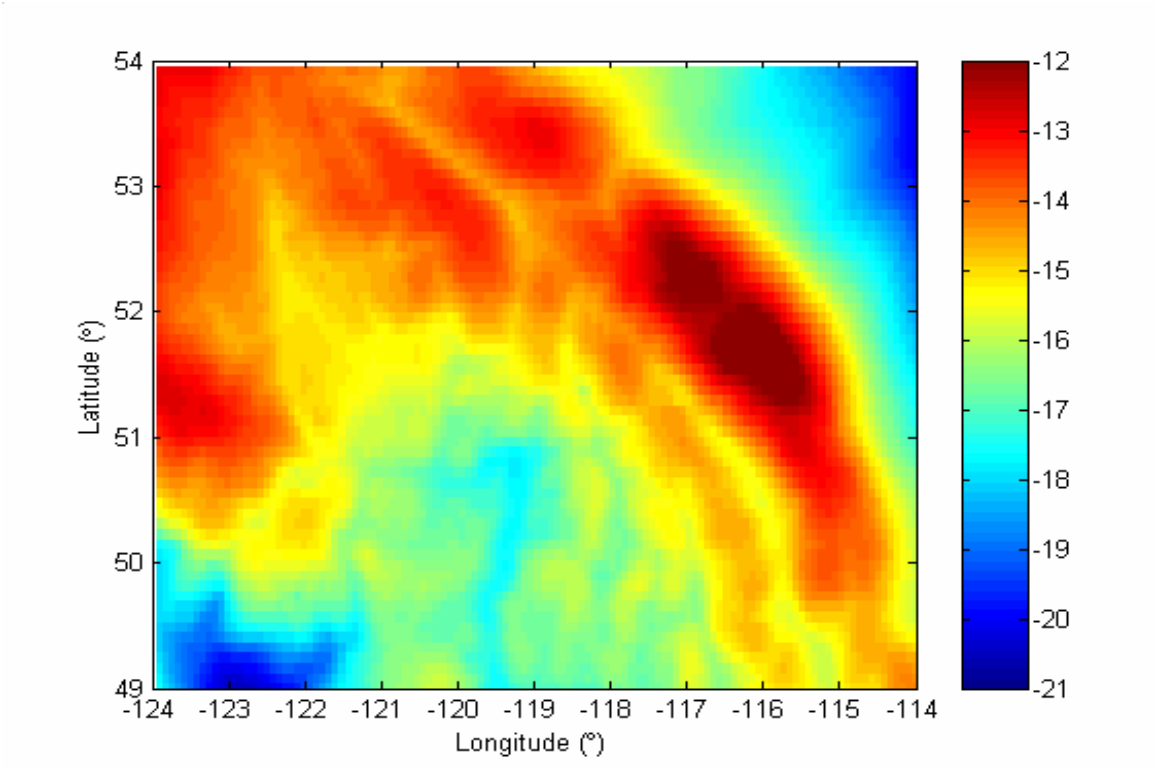

Fig. 4.21 The Rudzki geoid (m)

4.3 Summary of results

A numerical investigation was carried out to explore different gravimetric reduction schemes in addition to the usual Helmert's second method of condensation and the RTM method, in the context of precise geoid determination. The Rudzki geoid, which had never been used in the past for geoid determination, proves to be as good as the Helmert and RTM geoids, and better than the AH and PH geoids, compared to GPS-levelling after fit. Also, it has the smallest bias among all other reduction schemes. The main advantage of using this method is that one does not have to compute the indirect effect on the geoid required for all other reduction schemes. Therefore, it can become an alternative tool for gravimetric geoid determination in the future.

The AH and PH topographic-isostatic anomalies are the smoothest among all in terms of range and standard deviation. Rudzki anomalies have smaller standard deviation and range than Helmert anomalies, which yield the roughest gravity field in the test area. However, Rudzki, RTM, and Helmert anomalies seem to be in better agreement with EGM96 (which is based on FA coefficients) than the AH and PH anomalies, and thus are the best anomalies for geoid determination using a geopotential model like EGM96. The large bias in the topographic-isostatic geoid solutions indicates that one should use a corresponding topographic-isostatic geopotential model to extract the low frequency part of the gravity signal.

The indirect effect of Helmert's second condensation method is very small (47 cm), while that of the topographic-isostatic reductions is as big as 10 metres. The maximum restored terrain effect on the quasigeoid for the RTM reduction is nearly a metre. The Bouguer correction term to transform from quasigeoid to geoid is as big as 59 cm.

Chapter 5

Density and Gravity Interpolation Effects on Helmert Geoid Determination

5.1 Gravity Interpolation Effects on Helmert Geoid Determination

The importance of Helmert's second method of condensation as a common gravimetric tool to handle the topography for Stokes's boundary value problem solution has been already described in previous chapters. Because the Helmert anomalies based on this method are very rough, gravity interpolation is one of the very important aspects to be cautiously treated for precise geoid determination using this mass reduction technique. The Bouguer reduction is generally used in practice to remove all the topographical masses above the geoid before gridding Free-air anomalies and then the corresponding Bouguer effect is added back to the gridded gravity values.

The main purpose of the investigation in this section is to study the effects that different gravimetric reductions have on gravity interpolation and Helmert geoid determination, in addition to the commonly used Bouguer scheme. As described earlier, the main principle of using a gravimetric terrain reduction for the interpolation of free-air anomalies is that the topography is first removed either completely with the refined Bouguer reduction or removed with compensating or inverted masses depending on the reduction method used before gridding, and these corresponding masses are added back again to the gridded gravity anomalies producing free-air anomalies.

This section will illustrate via a numerical test in the Canadian Rockies the effect different gravity reduction schemes have on gravity interpolation and on Helmert geoid determination. The Bouguer and residual terrain modelling (RTM) topographic reductions, the Rudzki inversion scheme, and the topographic-isostatic reduction of PH

are used to remove terrain effects before gridding reduced FA anomalies, and then their corresponding topographic or topographic-isostatic or inverted masses are restored to produce FA anomalies. The procedure for interpolation using different gravimetric reduction schemes is shown in figure 5.1.

This investigation is carried out in the same area of the Canadian Rockies used in the previous investigations. The data sets of gravity points and GPS-levelling points are the ones used in the numerical investigation for gravimetric geoid determination in chapter 4.

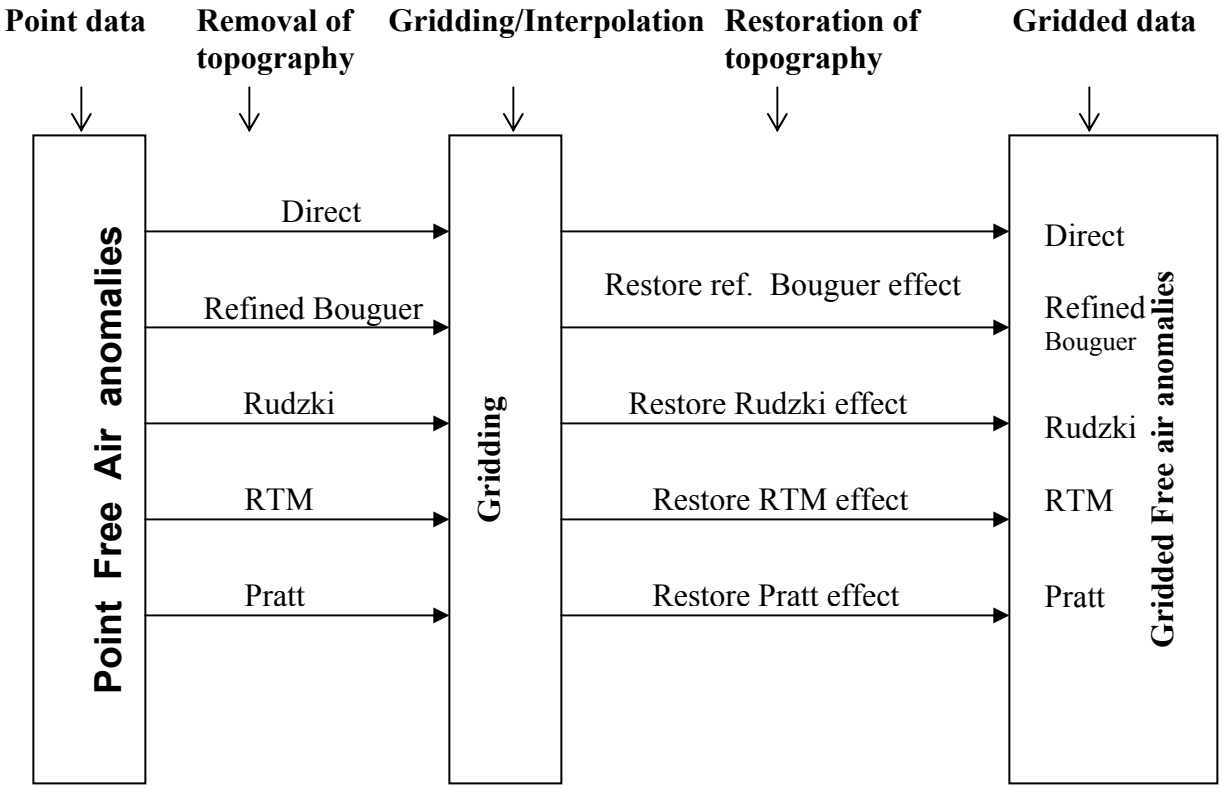

Fig. 5.1 Procedure for gravity interpolation

A digital terrain model of 15″ grid resolution is used for this test. The assumptions made on the density, density contrast, compensation depth, and normal crust thickness for topographic and topographic-isostatic reductions are the same as those in the previous tests. The main difference in the data sets used for this part of research is the OSU91A

geopotential model. This model is used in this test instead of EGM96, and the gravity observations are referenced to GRS67.

The procedure for computing the Helmert geoid is the same one applied in chapter 4. The results presented in this section come from the difference of using different gravimetric reduction methods for gridding free-air anomalies instead of using just a simple Bouguer scheme used in chapter 4.

First, the Helmert gravity anomalies are computed using the same formula (3.55) used in chapter 4. The different sets of Free-air anomalies are obtained using different mass reduction schemes for gridding. Their statistics, shown in table 5.1, show that Helmert anomalies using any gravimetric reduction for interpolating FA anomalies become smoother in terms of standard deviation and range than those using directly computed FA anomalies. The standard deviation of Helmert anomalies decreases by at least 10 mGal using any gravimetric reduction scheme for FA interpolation. The Pratt Hayford and RTM reductions prove to be the best among all reduction schemes used in this test for gravity interpolation.

Table 5.1 The statistics of Helmert anomalies using different mass reduction schemes for interpolating free-air anomalies (mGal)

Reduction Scheme Used for Gridding	Max	Min	Mean	Std
Direct (Free-air)	225.84	-145.98	27.84	58.36
Refined Bouguer	190.18	-138.90	15.42	49.73
Pratt-Hayford	179.24	-134.52	12.61	48.62
RTM	178.49	-133.76	11.57	48.56
Rudzki	178.09	-143.00	11.46	48.82

Second, the difference between directly interpolated Free-air anomalies and those obtained from using different reduction schemes is computed. They are presented in table

5.2. The difference is very big and reaches a maximum of 229 mGal, with a standard deviation of 43 mGal using the Pratt Hayford method.

Table 5.2 Difference between FA anomalies directly interpolated and after applying different mass reduction schemes for interpolation (mGal)

Reduction scheme	Max	Min	Mean	Std
Direct-Refined Bouguer	228.18	-198.86	12.44	42.43
Direct-Pratt	223.02	-207.88	16.29	42.61
Direct-RTM	228.58	-210.47	15.25	42.84
Direct-Rudzki	180.22	-150.96	16.83	36.92

Table 5.3 The statistics of difference of Helmert geoids using different mass reduction schemes for interpolation (m)

Reduction scheme	Max	Min	Mean	Std
Direct-Refined Bouguer	8.77	2.00	4.30	1.25
Direct-Pratt	9.84	2.92	5.55	1.33
Direct-RTM	9.68	2.49	5.26	1.36
Direct-Rudzki	9.62	2.71	5.83	1.41

Third, the Helmert geoids using different gravimetric reduction techniques for gridding FA anomalies are computed. In this thesis, the Helmert geoids obtained from using the Bouguer, Rudzki, RTM, and Pratt Hayford gravimetric reductions for gravity interpolation will be named Bouguer-Helmert, Rudzki-Helmert, RTM-Helmert, and PH-Helmert, respectively, and the one obtained from directly interpolated FA anomalies is termed direct-Helmert. The differences between the direct-Helmert geoid and the other Helmert geoids are given in table 5.3. The difference is as high as 9.8 m for the PH

topographic isostatic method. The standard deviation and the range of the differences are greater than a metre and 10 metres, respectively. These results suggest that one should not use directly interpolated FA anomalies for Helmert geoid determination.

Table 5.4. The statistics of difference between different Helmert geoids and GPS-levelling geoid solution (m)

Helmert geoid	Max	Min	Mean	Std
Direct-Helmert	5.93	2.29	4.68	1.00
	(6.89)	(1.98)	(4.21)	(0.95)
Bouguer-Helmert	-0.23	-1.62	-0.72	0.34
	(0.55)	(-0.83)	(0.00)	(0.22)
PH-Helmert	0.18	-1.27	-0.49	0.28
	(0.76)	(-0.76)	(0.00)	(0.22)
RTM-Helmert	0.47	-1.06	-0.22	0.29
	(0.73)	(-0.62)	(0.00)	(0.20)
Rudzki-Helmert	0.13	-1.84	-0.82	0.38
	(0.57)	(-0.97)	(0.00)	(0.22)

The statistics of the differences between different Helmert geoids (applying different mass reduction schemes for gravity interpolation) and the GPS-levelling geoid solution are given in table 5.4. The results show that the RTM-Helmert and PH-Helmert geoids demonstrate better fit with GPS-levelling geoid of the test area before fit than the Bouguer–Helmert and Rudzki-Helmert geoids. However, the standard deviation after fit becomes nearly the same for all Helmert geoids (except for direct-Helmert) but the range of the RTM-Helmert and Pratt-Helmert geoids is still smaller compared to that of Bouguer-Helmert and Rudzki-Helmert geoids.

We can draw a very important conclusion from the results obtained in this test, namely, that the use of a proper gravimetric terrain reduction scheme for the interpolation of free-air gravity anomalies plays a key role in precise Helmert geoid computation, especially in areas of rugged topography. The commonly used Bouguer reduction scheme should be replaced by the topographic-isostatic gravimetric reduction schemes like the PH model, or by the RTM topographic reduction method for gravity interpolation in the context of precise Helmert geoid determination.

5.2 Helmert Geoid Determination Using Lateral Density Variation

This study will show the importance of using actual crust density information on Helmert geoid determination. The information on density, which is available as a two-dimensional digital density model for the test area, is incorporated in all steps of the geoid

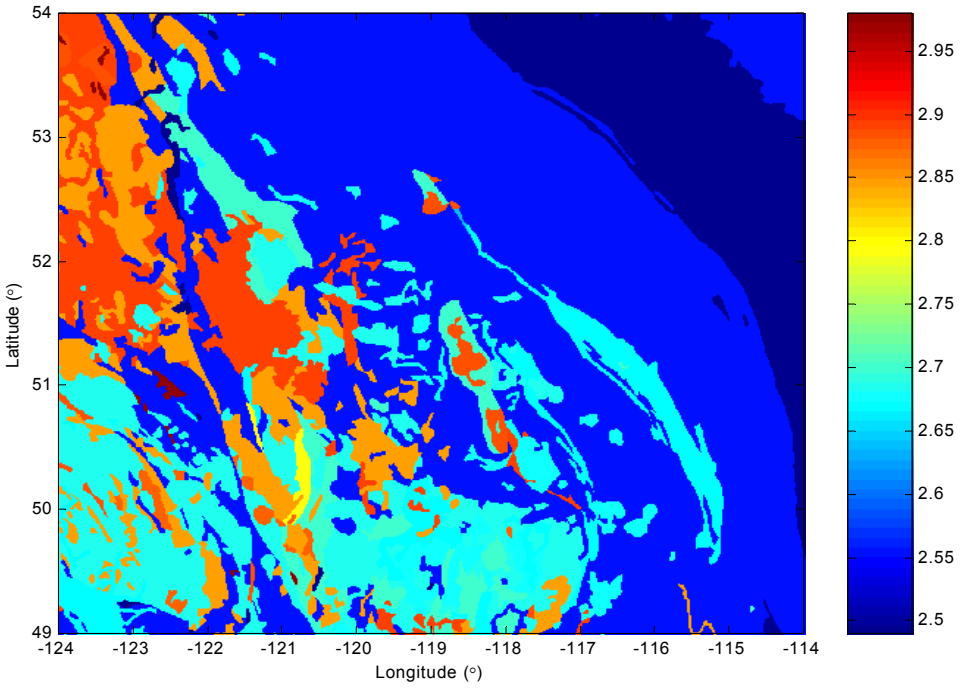

Fig 5.2 The density model in the Canadian Rockies (g/cm^3)

computational process. The actual density information is used in the computation of refined Bouguer anomalies, which is used for the interpolation of free-air anomalies, in the computation of terrain correction (which is the direct topographical effect on gravity for Helmert's second method of condensation scheme as described in chapter 3), and in the computation of the indirect effect on geoid for this mass reduction scheme.

The numerical test is carried out in the same area of the Canadian Rockies as for the other investigations. The computational methodology and all data sets required for geoid determination in this test are the same as those applied in the previous investigation of geoid determination, except for the DTM grid resolution. Since the DDM grid resolution available for this test is 30″, a 30″ grid spacing of DTM and DDM is used for this test. Figure 5.2 shows large contrasts in the topographic density of the Canadian Rockies, with maximum and minimum values of 2.98 g/cm^3 and 2.63 g/cm^3, respectively.

Table 5.5 The statistics of TC using constant and variable density (mGal)

Density	Max	Min	Mean	RMS	Std
Constant	100.07	0.05	6.97	9.77	6.86
Variable	95.98	0.05	6.86	9.62	6.75
Difference	10.87	-4.91	0.13	0.38	0.36

Table 5.6 The statistics of direct topographical effect on geoid using constant and variable density (m)

Density	Max	Min	Mean	RMS	Std
Constant	3.779	1.179	2.482	2.556	0.612
Variable	3.703	1.152	2.436	2.509	0.600
Difference	0.105	-0.011	0.046	0.052	0.024

The TC computation is carried out using the MP model for up to the second term in the Taylor series expansion using constant and variable density. The kernel function is computed over the whole area and 100% zero padding is performed around the matrices of heights in order to remove circular convolution effects.

Figure 5.3 shows the difference in terrain correction using constant and variable density information. The difference is as much as 10.9 mGal with the standard deviation of 0.4 mGal and is correlated with the topography. The maximum value is observed at the top of the mountains. Their effect on geoid undulation is shown in the Figure 5.4 and their statistics are given in the Table 5.6. There is a maximum effect of 10 cm with an RMS of 5.2 cm on geoid undulation using constant and lateral density variation in Canadian Rockies.

Table 5.7 presents the statistics of refined Bouguer anomalies using constant and variable density. There is a difference of 29 mGal in maximum value and 5 mGal in standard deviation using constant and lateral density variation in the computation of refined Bouguer anomalies.

Table 5.8 shows the statistics of Helmert anomalies using constant and variable density not only for terrain correction computation but also for interpolation of free-air anomalies using the Bouguer reduction scheme. The difference of Helmert anomalies using constant and variable density reaches up to 33 mGal with the standard deviation of 7 mGal.

Table 5.7 The statistics of Bouguer anomalies using constant and variable density (mGal)

Density	Max	Min	Mean	Std
Constant	-4.77	-297.07	-117.41	50.77
Variable	-5.11	-268.80	-113.37	47.59
Difference	29.08	-28.27	-4.05	5.54

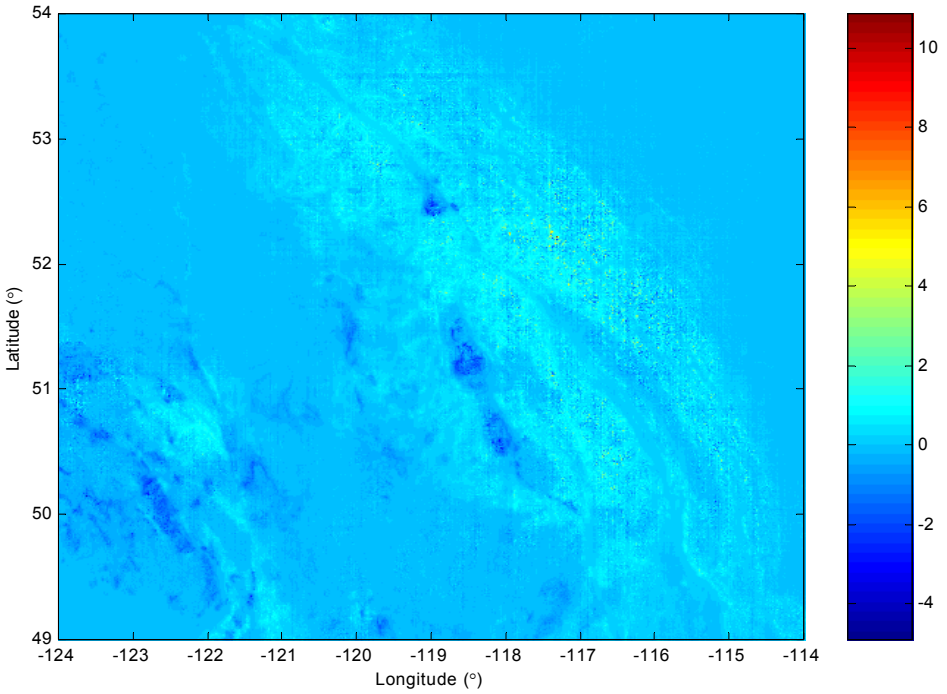

Fig 5.3 Difference in TC using constant and variable density (mGal)

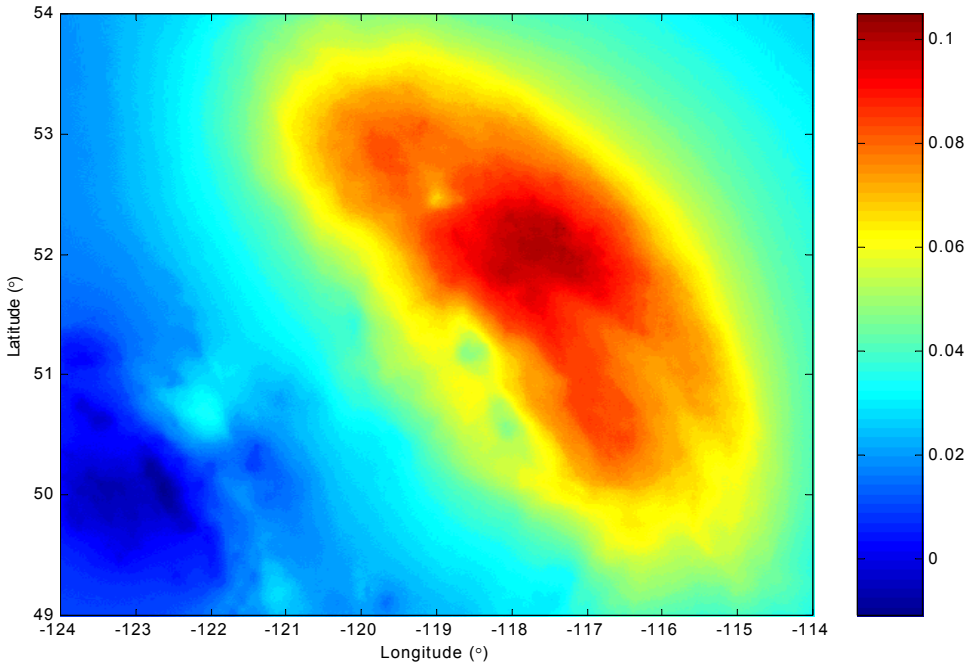

Fig. 5.4 Difference of direct topographical effect on geoid undulation using constant and variable density (m)

Table 5.8 The statistics of Helmert anomalies using constant and variable density for terrain correction computation and interpolation of Free-air anomalies (mGal)

Density	Max	Min	Mean	Std
Constant	193.57	-151.16	4.71	45.98
Variable	188.72	-151.66	8.72	47.04
Difference	32.75	-41.91	-4.01	7.24

The statistics of indirect effects on Helmert geoid using constant and variable density is given in the Table 5.9. These results suggest that the difference in using constant density instead of using actual density information for the computation of indirect effects can alter the geoid as much as 5 cm.

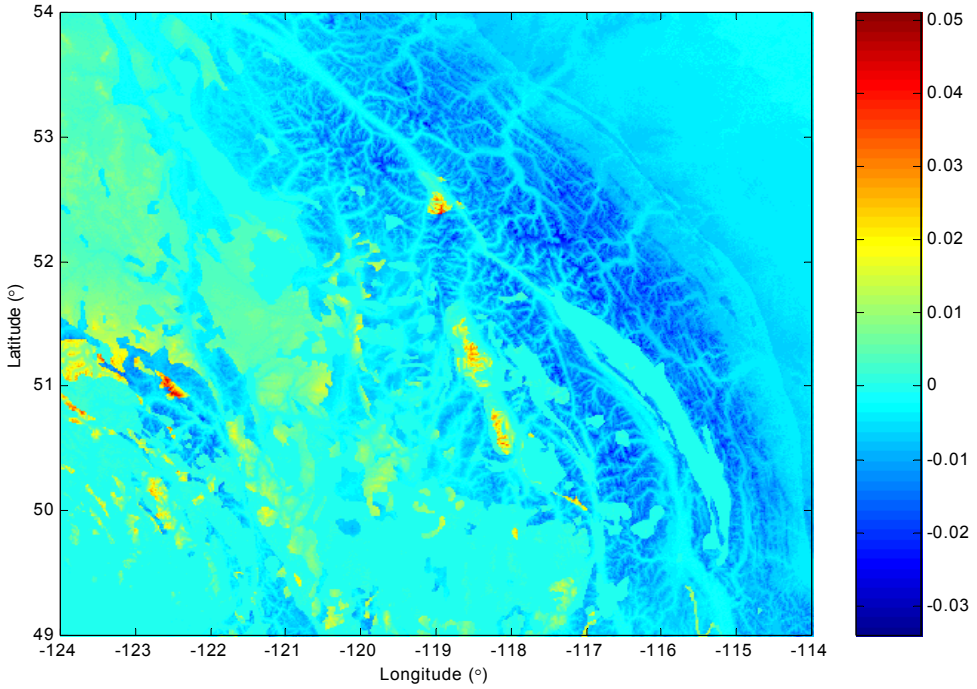

Fig 5.5 Difference of indirect effects on Helmert geoid using constant and variable density (m)

Table 5.9 The statistics of indirect effects on Helmert geoid using constant and variable density (m)

Density	Max	Min	Mean	Std
Constant	0.000	-0.818	-0.122	0.152
Variable	0.000	-0.784	-0.119	0.148
Difference	0.051	-0.034	-0.002	0.006

Table 5.10 The statistics of total terrain effects on Helmert geoid using constant and variable density (m)

Density	Max	Min	Mean	Std
Constant	3.745	1.148	2.360	0.579
Variable	3.669	1.116	2.317	0.570

The statistics of the total terrain effects (direct and indirect effects) on Helmert geoid is given in Table 5.10. The statistics of the differences between Helmert gravimetric geoid solutions using constant and variable density with the GPS-levelling geoid is shown in table 5.11. The results demonstrate that Helmert geoid determination incorporating actual Earth crust density information in all steps of its computational process shows better fit with the GPS-levelling geoid of the test area in terms of standard deviation (34 cm) than when using constant density (56 cm) before fit.

5.3 Summary of results

This chapter investigated two important aspects of precise Helmert geoid determination. From the results of the first investigation, the topographic-isostatic reduction schemes like Pratt-Hayford or the RTM reduction should be used for smooth gravity interpolation rather than a simple Bouguer reduction scheme, which is most commonly used in practice. The difference between direct-Helmert geoid and other Helmert geoids can be as

Table 5.11 The statistics of difference between Helmert gravimetric geoid solutions using constant and variable density with GPS-levelling geoid (before and after fit) (m)

Density	Max	Min	Mean	Std
Constant (before fit)	-0.28	-3.04	-1.61	0.56
Variable (before fit)	0.55	-1.70	-0.15	0.34
Constant (after fit)	0.54	-1.27	0.00	0.25
Variable (after fit)	0.69	-0.77	-0.00	0.25

large as 10 metres with the standard deviation of more than a metre. Therefore the direct Helmert geoid can not be used for Helmert geoid determination, even when we are after an accuracy of several metres. The Pratt-Helmert and RTM-Helmert geoids demonstrate better fit with the GPS-levelling geoid of the test area before fit than the Bouguer–Helmert and Rudzki-Helmert geoids do. Also, their range is the smallest compared to other ones.

The second investigation in this chapter has illustrated the importance of using actual crust density information (if available) in all steps of Helmert geoid determination; (i) TC computation; (ii) gravity interpolation and (iii) the computation of indirect effects. The results show that Helmert geoid determination incorporating actual Earth crust density information in all steps of its computational process shows better results compared to the GPS-levelling geoid of the test area in terms of standard deviation (34 cm) than using constant density (56) cm before fit.

The difference in terrain correction using constant and variable density information can alter the geoid as much as 10 cm with an RMS of 5.2 cm in the test area. The difference in using constant density instead of using actual density information for the computation of indirect effects can alter the geoid as much as 5 cm.

The real density information of the topographical masses above the geoid, which is required by Stokes's boundary value problem, produces smoother terrain reduced and interpolated gravity anomalies.

Chapter 6

Terrain-Aliasing Effects on Geoid Determination

This chapter focuses on investigating the importance of using various DTM resolutions for different mass reduction schemes within the context of precise geoid determination. The terrain aliasing effects are studied for the RTM topographic reduction, Pratt-Hayford topographic isostatic reduction, Helmert's second method of condensation, and the Rudzki inversion method. Because the terrain correction is a key quantity (as described in earlier chapters) in physical geodesy for both geoid and quasigeoid determination, a separate section in this chapter presents aliasing effects on terrain correction.

In this chapter, the term aliasing represents the loss of detail information as terrain reductions are evaluated from a high-resolution DTM to a coarse one. In other words, the results from the densest DTM are taken as "control values" and the differences between these results and the results obtained by using sparser DTMs are considered to be the aliasing effects.

6.1 Aliasing Effects on Terrain Correction

This section investigates the importance of using various DTM resolutions for terrain correction computation using constant and lateral density variation in flat and rough areas, within the context of precise geoid determination.

Numerical tests are carried out in two areas in Canada; the rugged area in the Canadian Rockies used in the previous investigations and a modest terrain area in Saskatchewan bounded by latitude between 49ºN and 54ºN and longitude between 110º W and 100ºW. The statistics of the DTMs in the test areas are presented in the tables 6.1 and 6.2 for different grid resolutions.

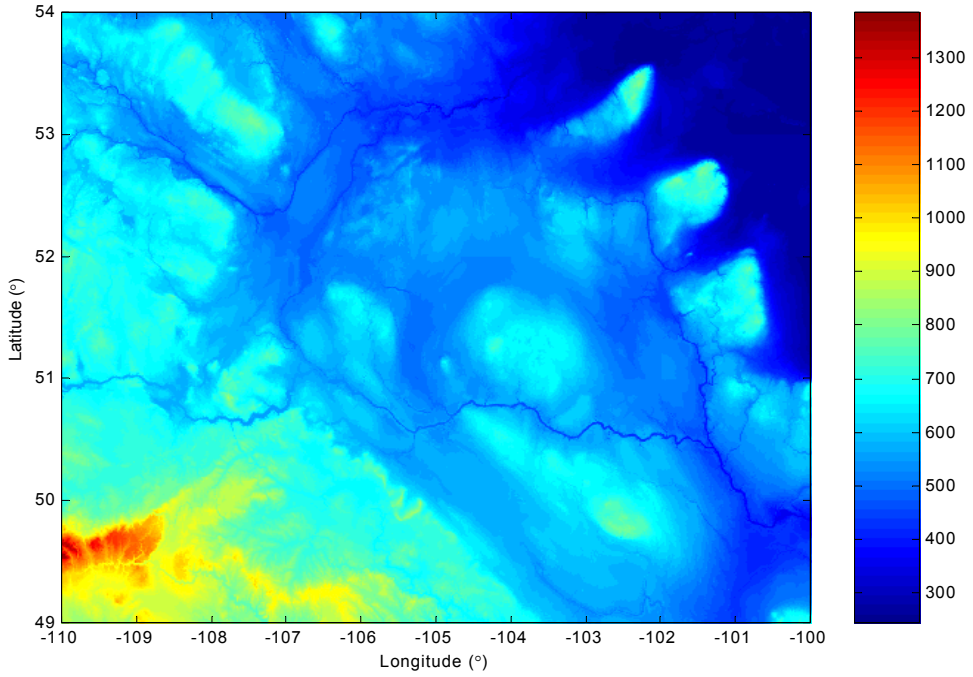

Fig 6.1 The topography in the Saskatchewan area (m)

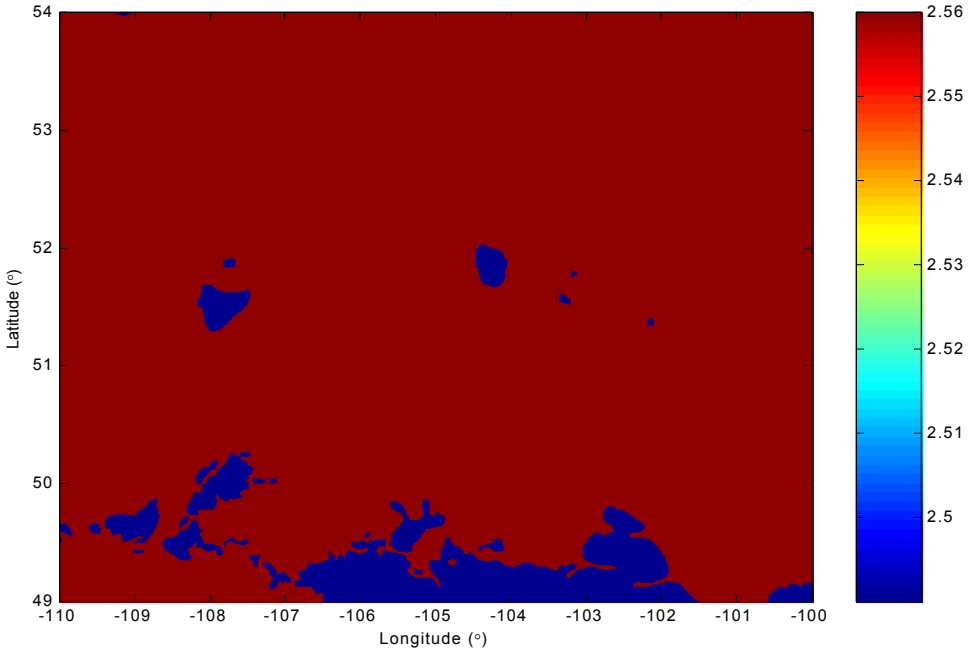

Fig. 6.2 The density model of Saskatchewan area (g/cm^3)

The original grid resolution available for this test is 3″, while 15″, 30″, 45″, 1′ and 2′ grid files are produced by selecting point height values from the 3″ grid. The resolution of the original DDM available for these test areas is 30″, while 1′ and 2′ grid resolutions of DDM are produced from the 30″ DDM by picking point density values for the corresponding grid levels. The topography and density models of the first test area are shown in Figures 4.2 and 5.2, respectively, whereas those of the second test area are shown in Figures 6.1 and 6.2, respectively. Saskatchewan has a smooth geological structure with constant density of 2.56 g/cm^3 except in some areas in the southern part.

Table 6.1 Statistical characteristics of DTMs in the Canadian Rockies (m)

Grid Resolution	Max	Min	Mean	STD
15″×15″	3840	0	1355	543
30″×30″	3785	0	1355	543
45″×45″	3656	0	1354	543
1′×1′	3429	0	1354	543
2′×2′	3275	0	1353	544

Table 6.2 Statistical characteristics of DTMs in the Saskatchewan area (m)

Grid Resolution	Max	Min	Mean	STD
15″×15″	1385	244	581	159
30″×30″	1381	244	581	159
45″×45″	1380	244	581	159
1′×1′	1379	244	581	159
2′×2′	1379	244	581	159

The TC computation is carried out using the mass prism model for different grid resolutions of DTM in both test areas for up to the second term in the Taylor series expansion. The kernel function is computed over the whole area and 100% zero padding is added around the matrices of heights in order to remove circular convolution effects. Table 6.3 summarizes the statistics of TC results using different grid resolutions of DTM.

Table 6.3 Terrain correction in the Canadian Rockies (mGal) (C1-first term, C2-second term, of Taylor series)

Grid resolution	Terms	Max	Min	Mean	RMS	STD
15″×15‴	C1	142.00	0.05	6.73	9.57	6.80
	C1+C2	108.76	0.05	7.06	9.89	6.93
30″×30″	C1	121.23	0.05	6.75	9.64	6.88
	C1+C2	100.06	0.05	6.96	9.77	6.86
45″×45″	C1	109.92	0.05	6.65	9.54	6.84
	C1+C2	83.38	0.05	6.71	9.44	6.64
1′×1′	C1	82.62	0.05	6.39	9.22	6.63
	C1+C2	59.83	0.05	6.36	8.98	6.34
2′×2′	C1	52.85	0.05	5.20	7.59	5.53
	C1+C2	42.73	0.05	5.09	7.31	5.24

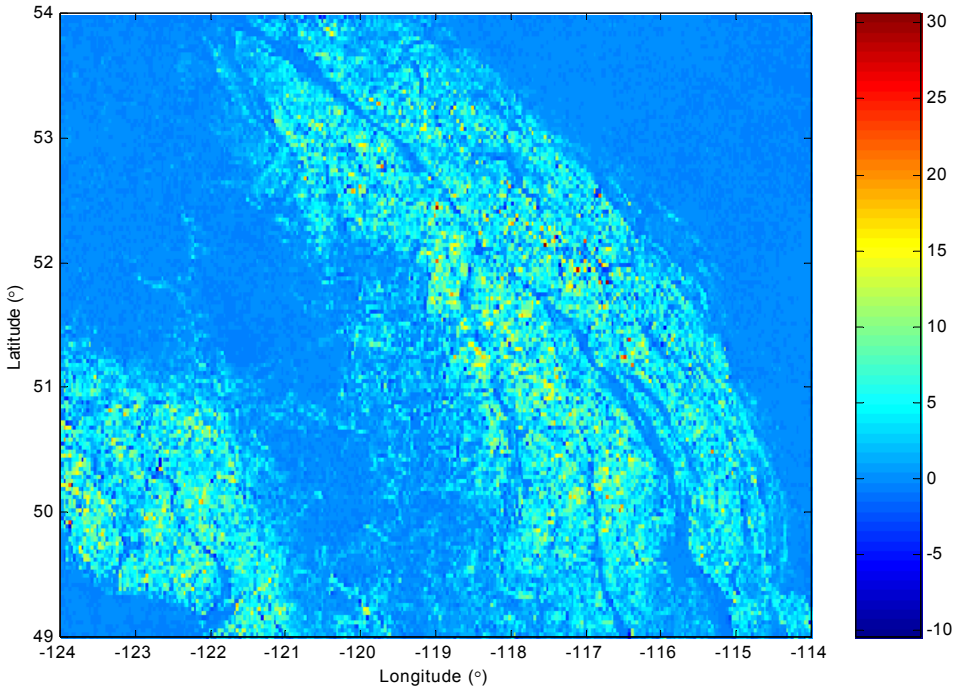

Fig 6.3 Difference in TC using 15″ and 2′ grid resolution (mGal)

Figure 6.3 shows the difference in TC using DTM grid resolutions between 15″ and 2′. The difference in TC using different DTM resolutions is correlated with the topography. TC varies from 109 mGal to 42.7 mGal in maximum value, and 9.9 mGal to 7.3 mGal in RMS in the Canadian Rockies, while there is no considerable difference in the statistics (which are shown in table 6.4) of Saskatchewan using DTMs from 15″ grid resolution level up to 2′ grid level. Maximum and RMS values of TC decrease from 2.6 mGal and 0.1 mGal to 1.5 mGal and 0.1 mGal, respectively, in Saskatchewan. Their effects on geoid undulations are given in Tables 6.5 and 6.6.

Table 6.4 Terrain correction in Saskatchewan (mGal) (C1-first term, C2-second term)

Grid resolution	Terms	Max	Min	Mean	RMS	STD
15″×15″'	C1	2.585	0.005	0.056	0.106	0.090
	C1+C2	2.653	0.005	0.058	0.108	0.092
30″×30″	C1	2.522	0.005	0.055	0.103	0.087
	C1+C2	2.533	0.005	0.055	0.104	0.088
45″×45″	C1	2.521	0.005	0.054	0.100	0.085
	C1+C2	2.521	0.005	0.054	0.101	0.085
1′×1′	C1	1.932	0.005	0.052	0.098	0.082
	C1+C2	1.928	0.005	0.052	0.098	0.082
2′×2′	C1	1.459	0.005	0.048	0.089	0.075
	C1+C2	1.457	0.005	0.048	0.089	0.075

Table 6.5. TC effect on geoid undulation (m) (Canadian Rockies)

Grid Spacing	Max	Min	Mean	RMS	STD
15″×15″	3.866	1.207	2.536	2.614	0.634
30″×30″	3.779	1.179	2.482	2.556	0.612
45″×45″	3.619	1.128	2.376	2.448	0.588
1′×1′	3.410	1.066	2.247	2.314	0.556
2′×2′	2.729	0.852	1.795	1.850	0.445

Table 6.6. TC effect on geoid undulation (m) (Saskatchewan)

Grid Spacing	Max	Min	Mean	RMS	STD
15″×15″	0.037	0.011	0.019	0.019	0.003
30″×30″	0.037	0.010	0.018	0.019	0.004
45″×45″	0.036	0.010	0.018	0.018	0.003
1′×1′	0.035	0.010	0.017	0.018	0.003
2′×2′	0.034	0.009	0.016	0.016	0.003

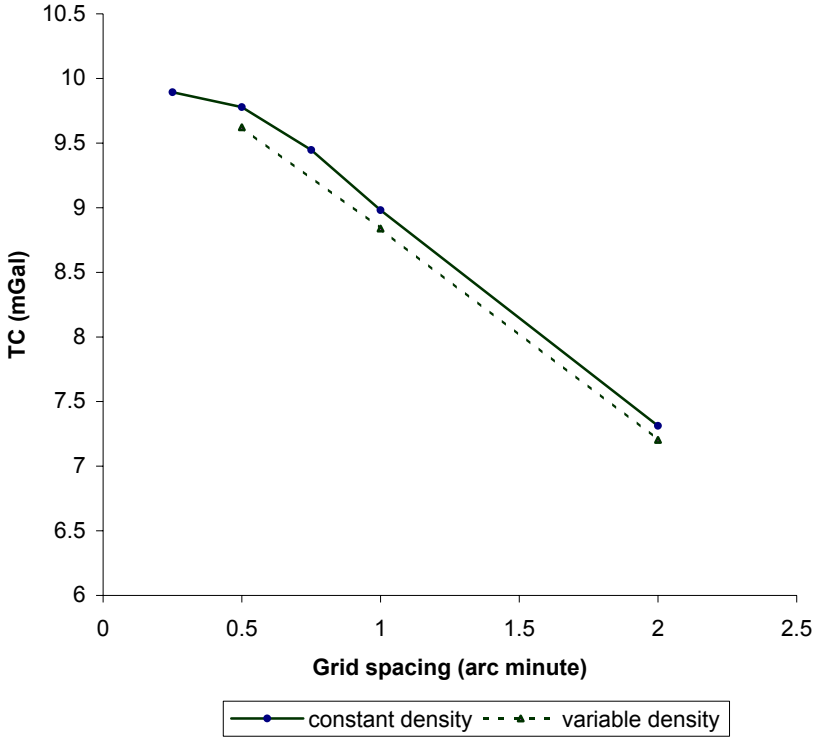

Fig 6.4 RMS value of TC using constant and variable density

Table 6.7 The difference in TC using constant and variable density (mGal) (Canadian Rockies)

Grid Spacing	Max	Min	Mean	RMS	STD
30″×30″	10.87	-4.91	0.13	0.38	0.36
1′×1′	3.26	-2.94	0.11	0.29	0.27
2′×2′	1.77	-2.46	0.08	0.23	0.22

Table 6.8 The difference in TC using constant and variable density (mGal) (Saskatchewan)

Grid Spacing	Max	Min	Mean	RMS	STD
30″×30″	0.105	0.002	0.002	0.004	0.004
1′×1′	0.079	0.000	0.002	0.004	0.004
2′×2′	0.055	0.000	0.002	0.004	0.003

Table 6.9 Effect of difference in TC using constant and variable density on the geoid (m) (Canadian Rockies)

Grid Spacing	Max	Min	Mean	RMS	STD
30″×30″	0.105	-0.011	0.046	0.052	0.024
1′×1′	0.085	-0.012	0.038	0.043	0.021
2′×2′	0.068	-0.010	0.029	0.034	0.016

Table 6.10 Effect of difference in TC using constant and variable density on the geoid (m) (Saskatchewan)

Grid Spacing	Max	Min	Mean	RMS	STD
30″×30″	0.002	0.000	0.001	0.001	0.000
1′×1′	0.002	0.000	0.001	0.001	0.000
2′×2′	0.002	0.000	0.001	0.001	0.000

The results from the first part of this test show that the effect of TC on geoid undulation using a 15″ grid spacing of DTM up to a 2′ spacing can vary from 3.88 m to 2.73 m in maximum value and 2.50 m to 1.73 m in RMS in the Canadian Rockies. These values can even be higher if 3″ grid resolution of DTM is used. On the other hand, there is just a change of 3-4 mm in maximum value and RMS in Saskatchewan. These results show that the high resolution DTM (15″ or finer) should be used in mountainous areas like the Canadian Rockies for geoid determination with an accuracy of a decimetre or higher. In the modest terrain areas like Saskatchewan, the high resolution DTM is critical only for geoid determination with the accuracy of a centimetre or higher.

The second part of this test is to study the same effect using variable density. The grid spacing of DTM and DDM used for this test are 30″, 1′ and 2′. Tables 6.7 and 6.8 show the statistics of the difference in TC using constant density and actual density information for different grid resolutions in the Canadian Rockies and Saskatchewan, respectively. Tables 6.9 and 6.10 show their effects on the geoid.

There is a difference of 3 cm in maximum value and 2 cm in RMS using constant and actual density information for grid spacing of DTM and DDM ranging from 30″ up to 2′ in the Canadian Rockies. There is no considerable difference in TC and their effects on geoid undulation using constant and actual density information in Saskatchewan. These results suggest that the finer DDM resolution (if available) should be incorporated in precise geoid determination with the accuracy of decimetre or higher in rugged areas. The use of DDM is not critical in the computation of terrain effect in non-mountainous regions for precise geoid determination.

6.2 Terrain-Aliasing Effects on Rudzki, Helmert, RTM, and PH Geoid Determination

This study investigates the importance of using various grid resolutions of DTM for different gravimetric mass reduction schemes within the context of precise geoid determination. The reduction methods used in this study are the Rudzki inversion method, Helmert's second method of condensation, the RTM method, and the PH topographic-isostatic reduction technique. The effect of using different DTM grid resolutions of 6″, 15″, 30″, 45″, 1′ and 2′ on gravity anomalies and absolute geoid undulations is studied for each of these reduction schemes. The same test area of the Canadian Rockies used in the previous investigations is selected for this study.

The geoid is computed from Stokes's integral formula with the rigorous spherical kernel by the one-dimensional fast Fourier transform algorithm. The 5′×5′ grid of gravity anomalies is used in Stokes's computation. The aliasing effects on gravity anomalies and on the geoid are not only due to the different DTM resolutions used in this test, but also to the use of 5′×5′ grid of gravity anomalies. Thus the results shown in this study should not be considered as absolute aliasing effects. The EGM96 is used as the reference global field for all schemes. The geoid computational procedure is the same as the one used in the investigation presented in Chapter 4. The only difference in this test is the

incorporation of different DTM resolutions for geoid determination in every gravimetric reduction technique.

First, the gravity anomalies are computed using different DTM grid resolutions for each mass reduction technique. The gravity anomalies obtained by using the highest DTM resolution are regarded as the control gravity anomalies for each reduction scheme. Figures 6.5 and 6.7 show the difference in maximum value and standard deviation, respectively, between control gravity anomalies and gravity anomalies obtained by using coarser DTM grid resolutions. The use of a 2′ DTM grid resolution instead of a 6″ one changes the gravity anomalies from 55 mGal to 123 mGal in maximum value, depending on the type of the gravimetric reduction technique chosen. Similarly, the difference in standard deviation changes from 8 mGal to 13 mGal. As the grid spacing decreases, we can note for every reduction scheme that the resultant map of gravity anomalies tends to get smoother. This can be easily seen by comparing the two figures of Rudzki gravity anomalies shown in Figure 6.6.

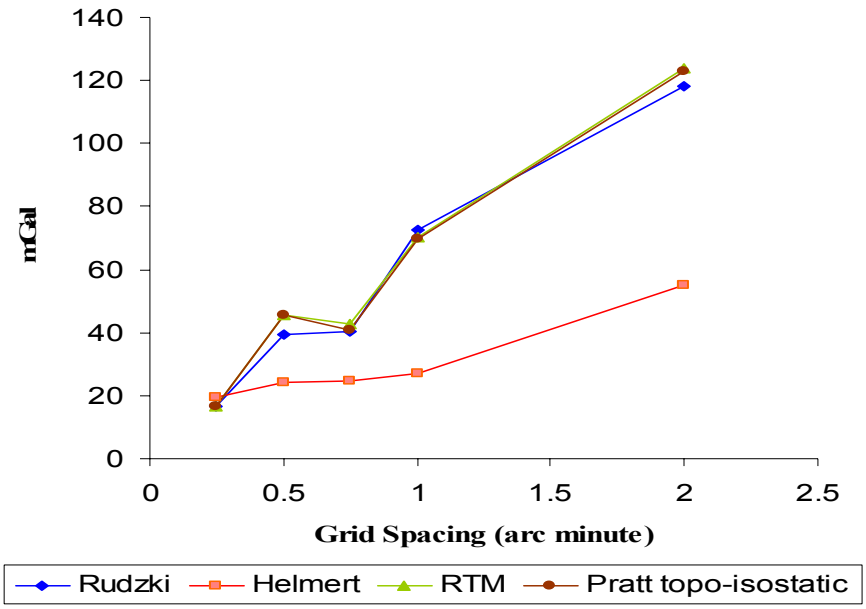

Fig. 6.5 The difference in maximum value between control gravity anomalies and anomalies obtained using different DTM resolutions

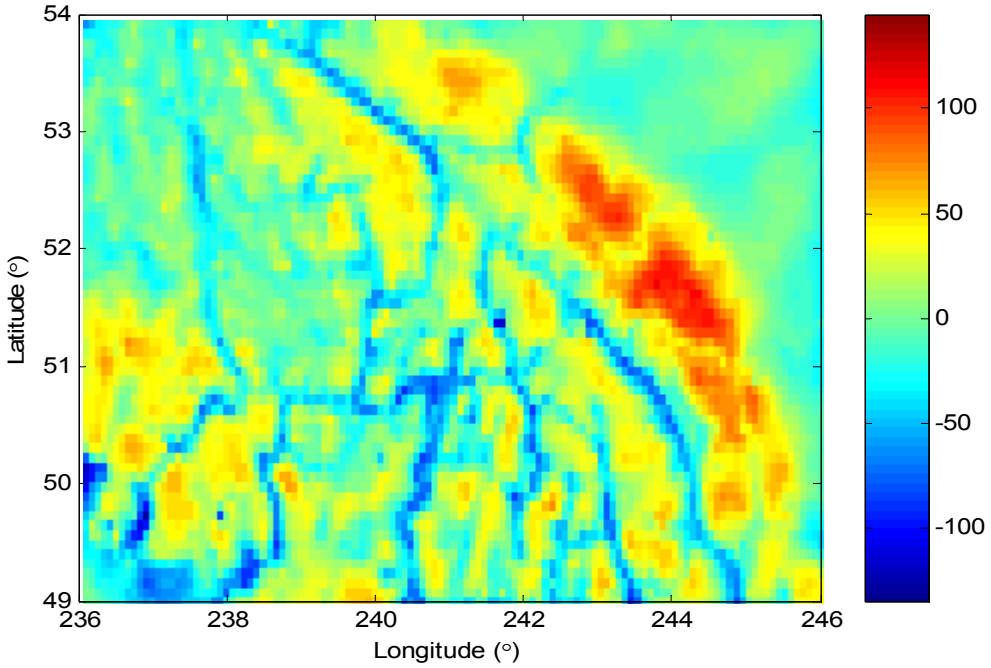

6″ DTM resolution

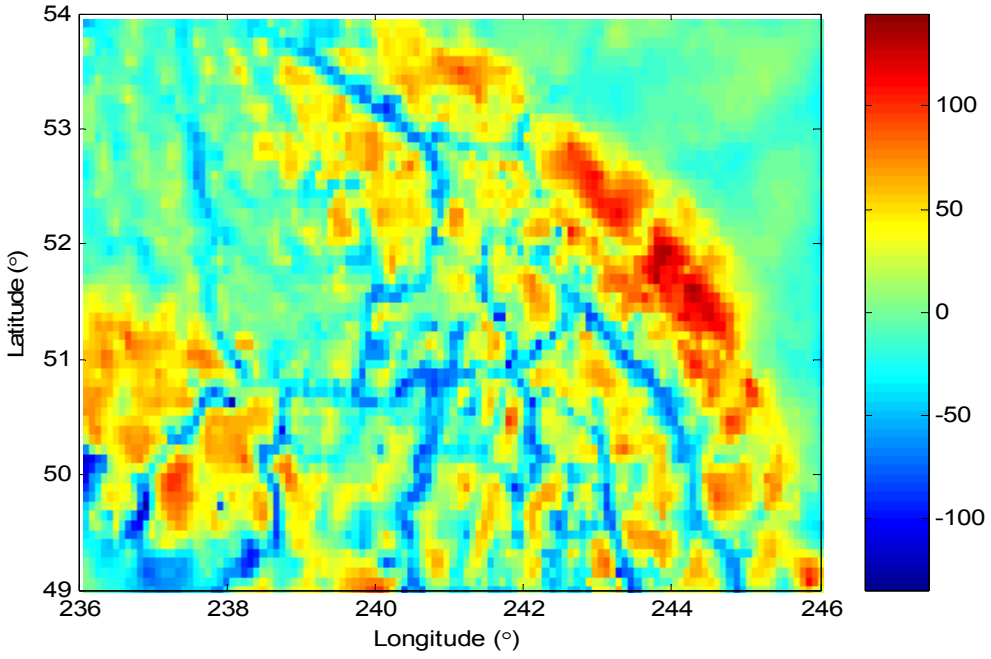

2′ DTM grid resolution

Fig. 6.6 5′×5′ Rudzki anomalies using 6″ and 2′ DTM grid resolution

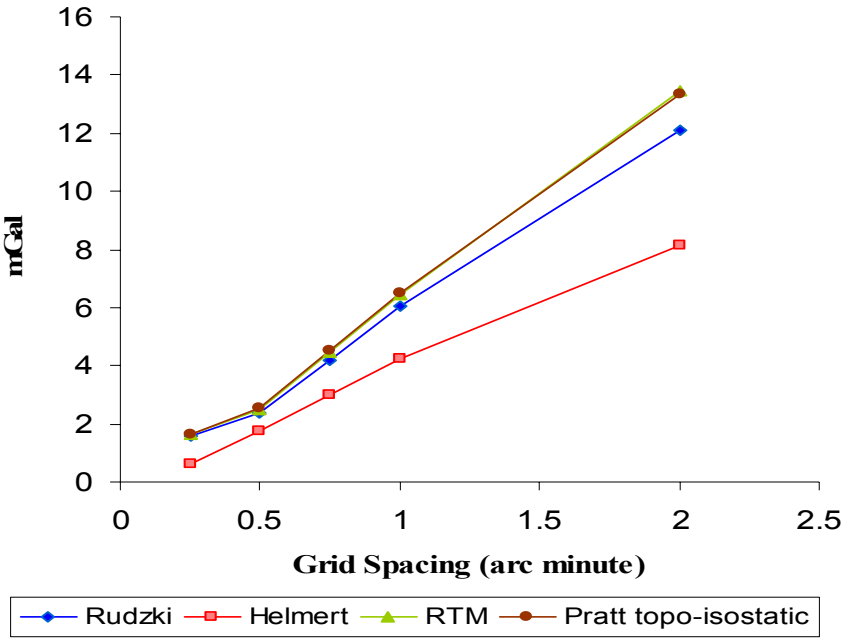

Fig. 6.7 The difference in standard deviation between control gravity anomalies and anomalies obtained using different DTM grid resolutions

Second in this investigation, the gravimetric geoid solution is carried out using each reduction scheme with different DTM resolutions. The geoid solution obtained by using the highest DTM resolution is regarded as the control geoid. Figure 6.8 shows the difference in maximum value between the control geoid and geoids obtained using different DTM resolutions. These differences can reach 2.05 m to 2.75 m in maximum value depending on the mass reduction scheme selected for geoid determination. These results in the Canadian Rockies suggest that a DTM grid resolution of 6″ or higher is required for precise geoid determination with an accuracy of a decimetre or higher for any gravimetric reduction method in rugged areas. A DTM resolution not coarser than 45″ is required for the geoid determination with an accuracy of a metre using Rudzki, Helmert, and RTM gravimetric reductions, whereas a DTM resolution not coarser than 15″ is required for geoid determination using Pratt Hayford topographic-isostatic reduction to gain the accuracy of a metre.

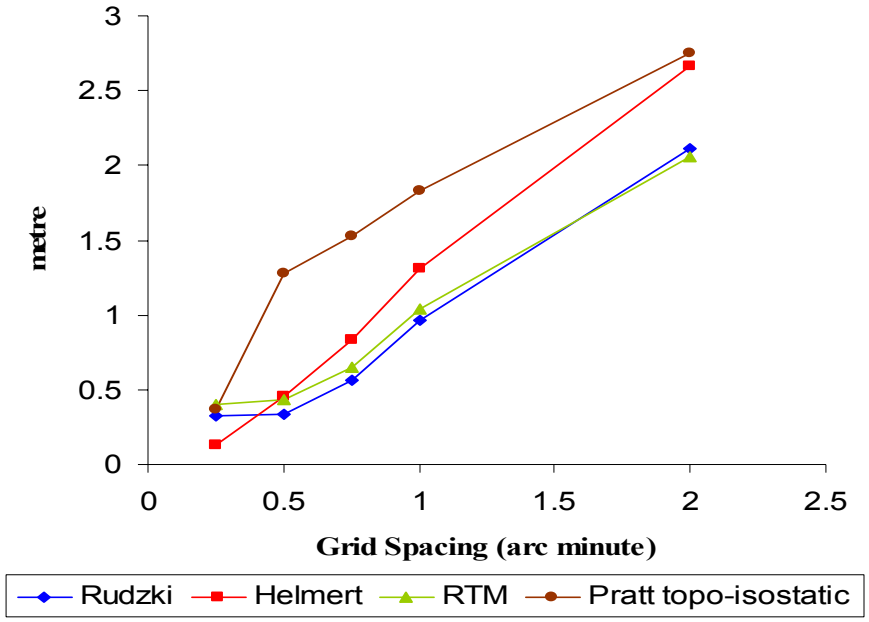

Fig 6.8 The difference in maximum value between the control geoid and geoids obtained using different DTM resolutions

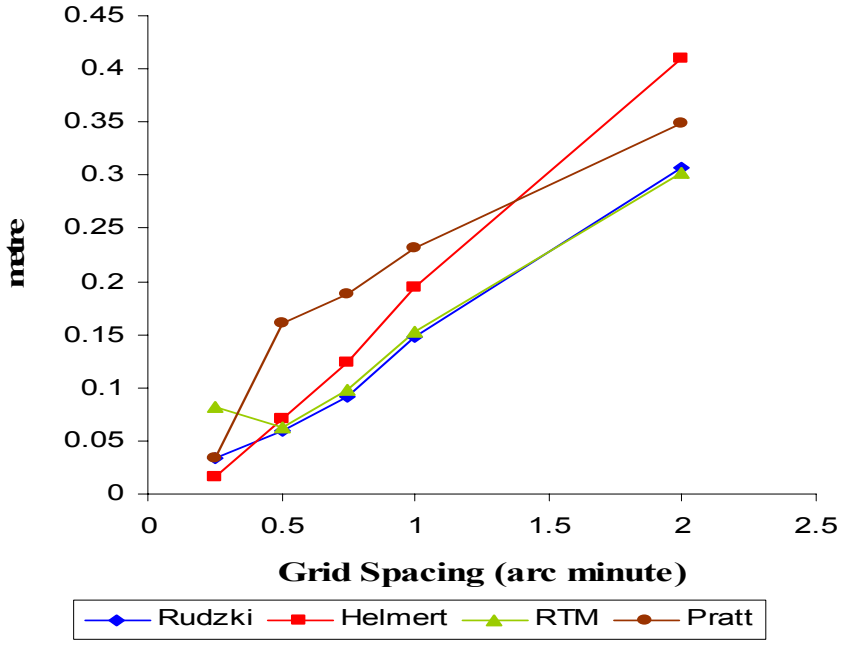

Fig. 6.9 The difference in standard deviation between the control geoid and the geoids obtained using different DTM resolutions

Figure 6.9 shows the trend of increasing the standard deviation with increasing DTM resolution, which is similar for all gravimetric reduction schemes. The difference in standard deviation between the control geoid and the geoids obtained using different DTM resolutions is between 3 and 4 decimetres depending on the reduction method selected. Comparing the Rudzki geoid using 6″ and 2′ DTM resolution shown in the figure 6.11, the geoid using 6″ DTM resolution is smoother as well as less correlated with the topography. This is true for all reduction methods used in this test.

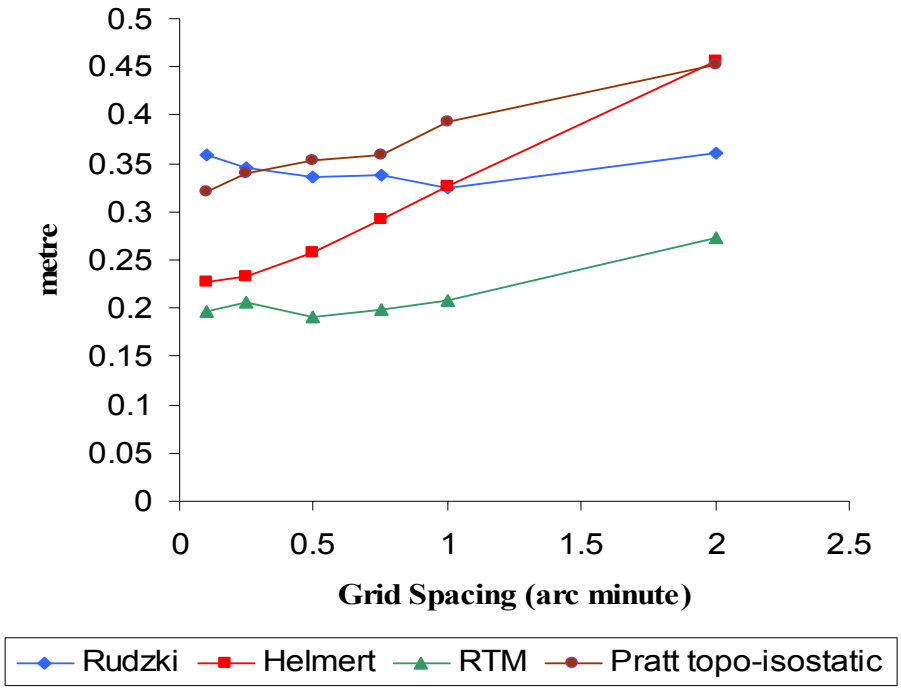

Fig. 6.10 Standard deviation of the differences between different geoid undulations with GPS-levelling geoid before fit

Finally, the gravimetric geoid solutions obtained from using different DTM resolutions for every reduction method are compared with the GPS-levelling geoid solution. Figures 6.10 and 6.12 present the graphs of standard deviation of the differences between

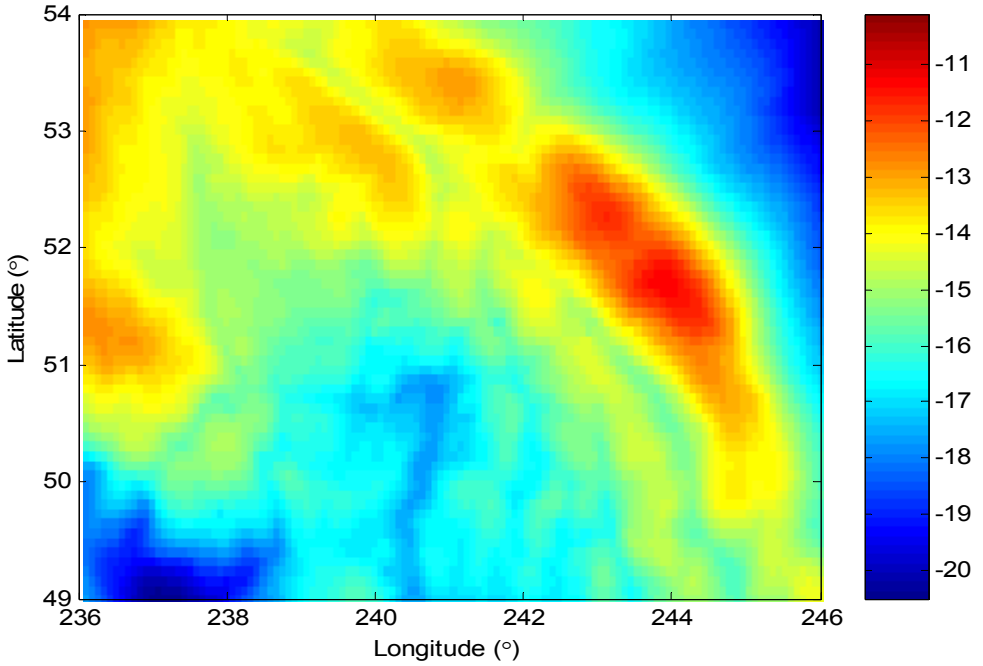

6″ DTM resolution

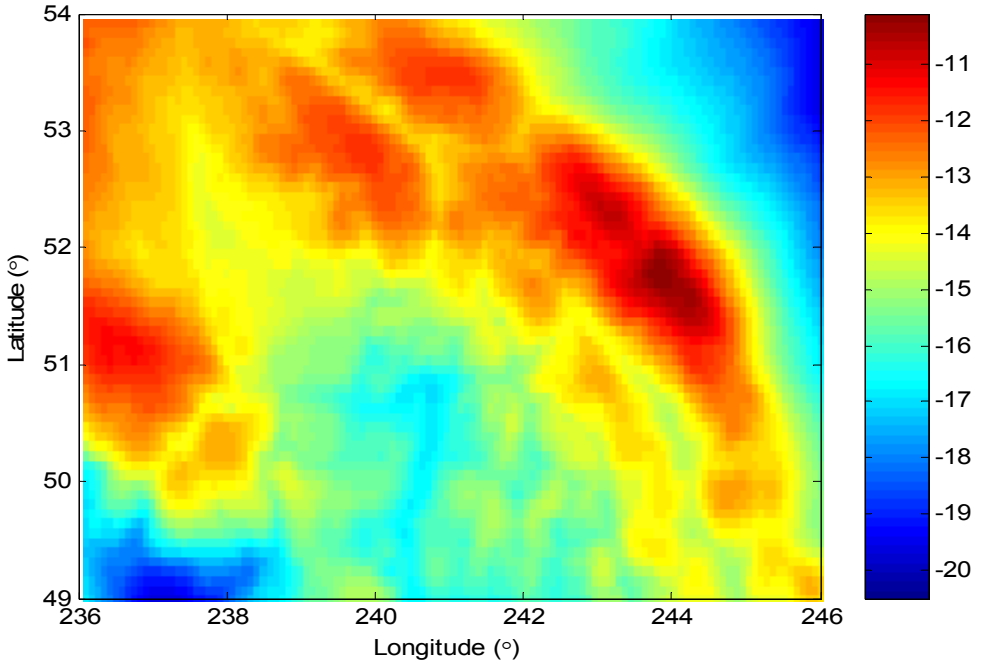

2′ DTM grid resolution

Fig. 6.11 5′×5′ Rudzki geoid using 6″ and 2′ DTM grid resolution

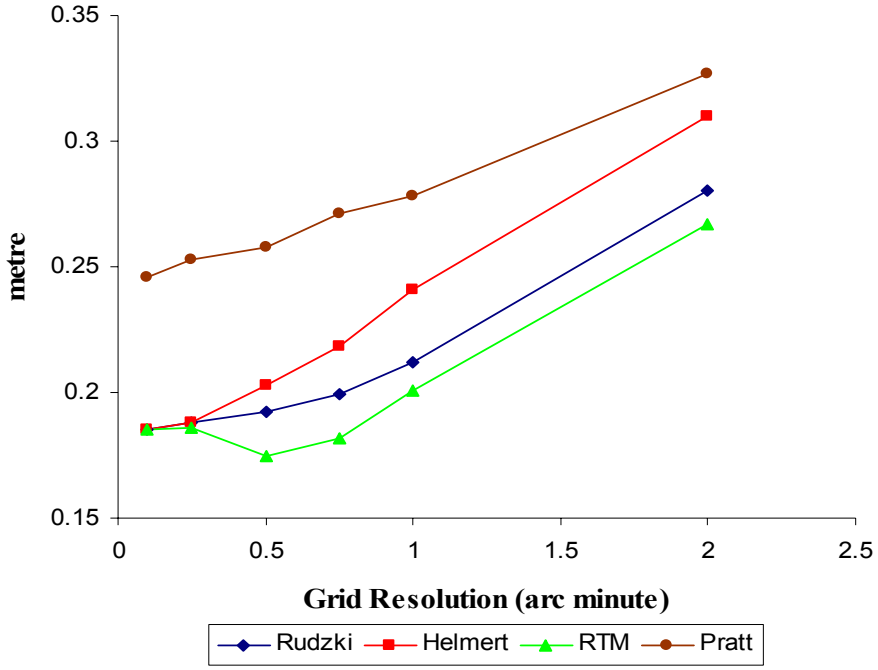

Fig 6.12 Standard deviation of the differences between different geoid undulations with the GPS-levelling geoid after fit

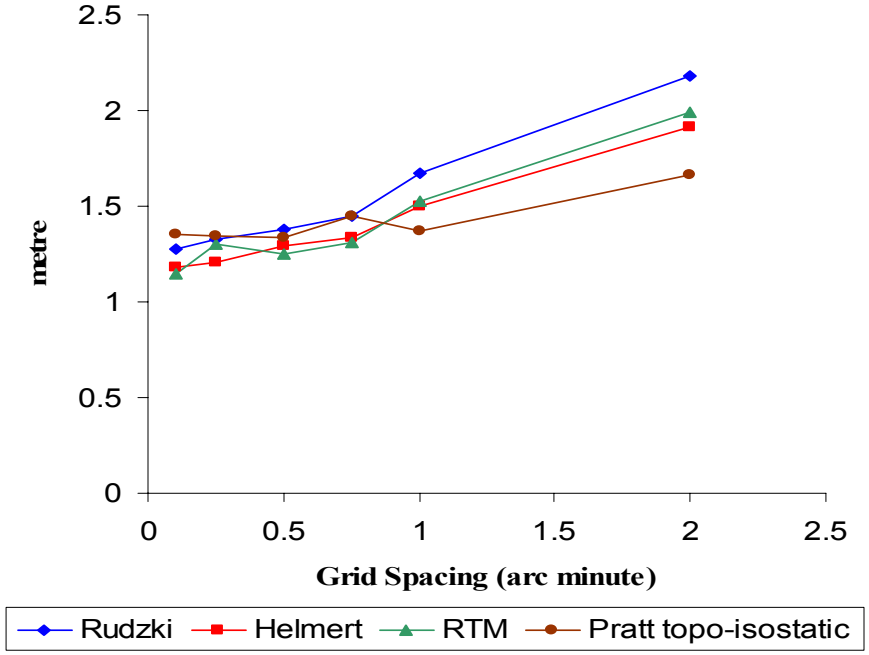

Fig 6.13 The range of differences between different geoid undulations with the GPS-levelling geoid after fit

different gravimetric geoid solutions with the GPS-levelling geoid before and after fit. The increasing trend of the standard deviation of the differences between gravimetric geoid solutions using different DTM grid resolutions with the GPS-levelling geoid looks similar for every reduction technique after fit. There is an increase of nearly a decimeter in standard deviation when using a 2′ DTM grid resolution instead of a 6″.

The most precise geoids obtained from this test are the ones obtained using Rudzki, Helmert, and RTM method with 6″ DTM resolution. The use of 2′ DTM grid instead of 1′ brings the change of nearly 7 cm in standard deviation for every reduction method. The finer the DTM grid resolution, the smaller the standard deviation and the range (as shown in Figure 13) of the differences between the gravimetric and GPS-levelling geoid.

6.3 Summary of results

This chapter investigated the terrain aliasing effects on geoid determination in two parts. First, the terrain aliasing effects in TC computation using constant and variable density variation were studied in two test areas. Second, the same effects on geoid determination using different gravimetric mass reduction schemes within the context of precise geoid determination were investigated. As earlier stated, the aliasing effects on gravity anomalies and on the geoid are not absolute since the 5′×5′ grid of gravity anomalies is used in Stokes's computation

The first investigation shows that a high resolution DTM (15″ or finer) should be used in mountainous areas like the Canadian Rockies for geoid determination with an accuracy of a decimetre or higher. The high DTM resolution is critical only for geoid determination with an accuracy of a centimetre or higher in modest terrain areas like Saskatchewan. The results in the Canadian Rockies show that the effect of different TC resolutions on geoid undulation using grid spacings between 15″ and 2′ can vary from 3.88 m to 2.73 m

in maximum value. The finer DDM resolution (if available) should be used for precise geoid determination with an accuracy of a decimetre or higher in the rugged areas, whereas it is not crucial in the computation of terrain effect in non-mountainous regions.

The second investigation showed the importance of using various grid resolutions of DTM for different gravimetric mass reduction schemes within the context of precise geoid determination. A DTM grid resolution of 6″ or higher is required for precise geoid determination with an accuracy of a decimetre or higher for any gravimetric reduction method chosen to treat the topographical masses above the geoid in rugged areas. A DTM minimum spacing of 45″ or dense is required for geoid determination with an accuracy of a metre using the Rudzki, Helmert, or RTM gravimetric reductions. A DTM not coarser than 15″ is required for geoid determination with metre accuracy when using Pratt Hayford topographic-isostatic reduction. The choice between using a 6″ and a 2′ DTM can alter the geoid from 2.05 m to 2.75 m in maximum value depending on the mass reduction scheme selected for geoid determination.

The most precise geoids obtained in this test are the ones obtained using Rudzki, Helmert, and RTM methods with 6″ DTM resolution. The standard deviation and the range of the difference between the gravimetric geoid and GPS-levelling geoid become smaller as the DTM resolution goes higher.

Chapter 7

Conclusions and Recommendations

6.1 Conclusions

The conclusions are drawn from three major investigations carried out in this thesis, i.e., (i) gravimetric geoid determination using different terrain reduction schemes; (ii) density and gravity interpolation effects on Helmert geoid determination; and (iii) terrain-aliasing effects on geoid determination using different reduction schemes. The following conclusions can be drawn

- The first investigation explored other gravimetric reduction schemes both in theory and in practice in the context of precise geoid determination, in addition to the usual Helmert's second method of condensation and RTM methods.
- The Rudzki geoid performs as well as, and has a smaller bias than, Helmert and RTM geoids, and better than the AH and PH geoids compared to GPS-levelling. The Rudzki reduction, therefore, can become a standard tool for gravimetric geoid determination.
- The main advantage of using this method is that one does not have to compute indirect effect on the geoid as required for the other reduction schemes. On the other hand, the Helmert and RTM methods not only require the computation of indirect effects on the geoid and restored terrain effects on the quasigeoid, respectively, but they also require some additional computations; in Helmert's second method of condensation, one needs to use different reduction methods for smooth gravity interpolation, while in RTM reduction, the transfer from the quasigeoid to the geoid is required for geoid determination.
- Rudzki anomalies have smaller standard deviation and the range than those of Helmert anomalies. Helmert anomalies yield the roughest gravity field in the test

area while topographic-isostatic anomalies with the AH and PH models produce smoothest field as well as have less correlation with the topography.

- The Rudzki, RTM, and Helmert anomalies seem to be in better agreement with EGM96 (which is based on FA coefficients) than the AH and PH anomalies, and thus are the best anomalies for geoid determination using a geopotential model such as EGM96.
- The indirect effect on geoid undulations with topographic-isostatic reductions reaches 10 metres, while the indirect effect of Helmert's method is only 47 cm. The maximum restored terrain effect on the quasigeoid for the RTM reduction is nearly a metre.
- The large bias in the topographic-isostatic geoid solutions indicates that one should use a corresponding topographic-isostatic global geopotential model to extract the low frequency part of the gravity signal.

The followings are the main conclusions drawn from the second investigation carried out in this research, which shows the density and gravity interpolation effects on Helmert geoid determination.

- The Pratt Hayford topographic-isostatic model and the RTM are the best gravimetric schemes for smooth gravity interpolation in the test area. The Pratt-Helmert and RTM-Helmert geoids fit better with GPS-levelling geoid than other-Helmert geoids. Also, their range is smallest compared to other ones before and after fit.
- The topographic-isostatic gravimetric reduction schemes like the PH or AH models or the topographic reduction scheme of RTM should replace the usual Bouguer reduction scheme for the interpolation of FA gravity anomalies in precise Helmert geoid determination especially in rugged areas like Canadian Rockies.

- The difference between direct-Helmert geoid and other Helmert-geoids can be as large as 10 metres with a standard deviation of more than a metre. Therefore, the direct Helmert geoid should not be used for Helmert geoid determination even with an accuracy of several metres.
- The investigation on the use of actual density bedrock information for Helmert geoid determination suggests that the actual density information should be used (if available) in precise geoid determination in high mountains, especially where large contrast in topographical density exists.
- The density information should be incorporated not only in the computation of TC, but also in all other steps of Helmert's geoid computational process. It should be used in the computation of Bouguer anomalies (if it is chosen for smooth gravity interpolation), which is commonly used for the interpolation of FA gravity anomalies and indirect effects on geoid.
- The difference in the direct effect of TC on geoid and indirect effect on geoid for Helmert's second method of condensation between using constant and actual density information reaches as much as 10 cm and 5 cm, respectively, in the test area.
- The final Helmert geoid solution using two dimensional digital density model in all steps of geoid computational procedure shows better results in terms of standard deviation (34 cm) compared to the one using constant density (56cm).
- It would be wise to use at least the mean density of the area, if available, for terrain correction computation in mountains if a DDM is not available.
- The knowledge of actual density information is not crucial in the TC computation of non-mountainous areas.
- The difference in TC using constant and lateral density variation is correlated with the topography.

The following conclusions are made from the final investigation of this thesis, which exhibits the importance of using various DTM grid resolution levels for different gravimetric mass reduction schemes within the context of precise geoid determination. These conclusions are based on the aliasing effects not only because of using different DTM resolutions but also because of using 5′×5′ gravity grid in Stokes's formula.

- A DTM grid resolution of 6″ or higher is required for precise geoid determination with an accuracy of a decimetre or higher for any gravimetric reduction method chosen to treat the topographical masses above the geoid in rugged areas.
- The DTM not coarser than 45″ is required for geoid determination with an accuracy of a metre using Rudzki, Helmert, and RTM gravimetric reductions, whereas a DTM not coarser than 15″ is required for geoid determination using the Pratt Hayford topographic-isostatic reduction with an accuracy of a metre.
- The difference between gravimetric geoid solutions using DTM resolution of 6″ and 2′ can reach from 2.05 m to 2.75 m in maximum value depending on the mass reduction scheme selected for geoid determination.
- The most precise geoids obtained from the test are the ones obtained using Rudzki, Helmert, and RTM method with 6″ DTM resolution.
- The differences between gravimetric geoid solutions and the GPS-levelling geoid are smaller in terms of the range as well as standard deviation as finer DTM grid resolution is used.

6.2 Recommendations

The following recommendations are made based on the research carried out in this thesis:

- Theoretical and practical research on direct and indirect effects on geoid undulations should be studied not only for Helmert's second method of condensation but also for other gravimetric reduction methods in the context of precise geoid determination. For example, the computation point of direct effect

on gravity either on the topography or on the geoid plays a great role in precise geoid determination for all reduction schemes. The optimal depth of compensation for PH and AH methods should be studied for geoid determination using topographic isostatic schemes.

- Theoretical and practical research should also be carried out in the spherical approximation to see the difference between planar and spherical approximation not only for Helmert's second method of condensation but also for all other mass reduction techniques.
- More practical studies using the Rudzki reduction scheme should be carried out in different parts of the world especially in the high mountains both in planar and spherical approximation.
- Further investigation using high density gravity measurements and homogenously distributed GPS benchmarks should be carried out in the test area. Some gravity points above the elevation of 2000 m would be very helpful to picture the better gravity map of a test area for geoid determination.
- It will be useful to establish a small test area in rugged area with local precise levelling not necessarily connected to a regional or national network to precisely evaluate the difference between GPS-levlling geoid solution and gravimetric geoid.
- More theoretical and practical studies on topographic-isostatic geopotential models should be conducted in the context of precise geoid determination.
- The studies incorporating actual density information should be carried out for different mass reduction techniques especially in high mountains where a large contrast in density exists.
- The study of using denser grid (3″ or finer) of DTMs should be carried out to study the terrain aliasing effects using different gravimetric solutions. Absolute aliasing effects should be studied using the same resolution of gravity grid as the DTM in Stoke's formula.

References

Abd-Elmotaal H (1998) Gravity reduction techniques and their comparisons applied to the gravity field in Egypt. Second continental workshop on the geoid in Europe. Budapest, Hungary, March 10-14, 1998.

Bajracharya S, Kotsakis C, Sideris MG (2002) Aliasing effects on terrain correction computation. International Geoid Service, Bulletin N. 12, April, 2002.

Bajracharya S, Sideris MG (2002) The Rudzki inversion gravimetric reduction scheme in geoid determination. Accepted by Journal of Geodesy.

Biagi L, De Stefano R, Sanso F, Sciarretta C (1999) RTC and density variations in the estimation of local geoids. Bolletino Di Geofisica Teorica ed Applicata. Vol.40, N.3-4, pp 589-595.

Biagi L, Sanso F (2001) TcLight: a New technique for fast RTC computation. IAG Symposia, Vol. 123 Sideris (ed.), Gravity, Geoid, and Geodynamics 2000, Springer – Verlag Berlin Heidelburg 2001, pp 61-66.

Blais JAR, Ferland R (1984) Optimization in gravimetric terrain correction in western Canada. Canadian Journal of Earth Sciences, Vol.20, pp 259-265.

Edward GA (1976) The effect of topography on solution of Stokes's problem. Unisurv report # S14, 1976. University of New South Wales, Kensington. N.S.W. Australia.

Forsberg R (1984) A study of terrain reductions, density anomalies and geophysical inversion methods in gravity field modeling. Report No. 355, Dept. of Geodetic Science and Surveying, The Ohio State University, Colombus, Ohio, April, 1984a

Forsberg R (1985) Gravity Field Terrain Effect Computation by FFT. Bull. Geod. Vol.59, pp.342-360.

Ferland R (1984) Terrain corrections for gravity measurements. M.Sc. Thesis, Department of Surveying Engineering, The University of Calgary, Calgary, Alberta, Canada

Haagmans R, De M, Gelderen VM (1993) Fast evaluation of convolution integrals on the sphere using 1D FFT and a comparison with existing methods for Stokes' integral. Manuscripta Geodaetica, 18: 227-241

Harrison JC, Dickinson M (1989) Fourier transform methods in local gravity field modeling. Bulletin Geodesique, Vol. 63, pp. 149-166

Heiskanen WA, Vening Meinesz FA (1958) The earth and its gravity field. Mcgraw-Hill Book Company, Inc. New York, Toronto, London.

Heiskanen WA, Moritz H (1967) Physical geodesy. W. H. Freeman and Company. San Fransisco.

Heck B (1993) A revision of Helmert's second method of condensation in geoid and quasigeoid determination. In: Montag H, Reigber C (eds) Geodesy and Physics of the Earth. IAG Symp no. 112. Springer, Berlin Heidelburg New York, pp 246-251

Heck B (2003) On Helmert's methods of condensation. Journal of Geodesy 77: 155-170.

Hipkin RG (1988) Bouguer anomalies and the geoid: a reassessment of Stoke's method, Geophysics Journal International. 92, 53-66.

Huang J, Vanicek P, Pagiatakis SD, Brink W (2000) Effect of topographical density on geoid in the Canadian Rocky Mountains

Kellog OD (1929) Foundations of potential theory. Cambridge.

Kotsakis C, Sideris MG (1997) Preliminary spectral analysis of gravity anomalies and geoid undulations using the EGM96 geopotential model and local 5' by 5' mean Helmert gravity anomalies. Contract report to Geodetic Survey Division, Geomatics Canada and Natural Resources Canada, Ottawa.

Kotsakis C, Sideris MG (1999) Spectral analysis and the modeling of Faye gravity anomalies and geoid undulations and geoid error modeling. Contract report to Geodetic Survey Division, Geomatics Canada and Natural Resources Canada, Ottawa.

Kuhn M (2000) Density modelling for geoid determination. GGG2000, IAG International Symposium, Banff, Alberta, Canada, July 31-August 4, 2000.

Lachapelle G (1976) A spherical harmonic expansion of the isostatic reduction potential, Bolletino di Geodesia e Scienze Affini, No. 35, 281-299.

Lambert WD (1930) The reduction of observed values of gravity to sea level, Bulletin Geodesique, no. 26, pp. 107-181.

Lemoine FG, Kenyon SC, Factor JK, Trimmer RG, Pavlis NK, Chinn DS, Cox CM, Klosko SM, Luthchke SB, Torrence MH, Wang YM, Williamson R, Pavlis EC, Rapp RH, Olson TR (1998) The development of the joint NASA GSFC and NIMA geopotential model EGM96. Tech rep NASA-TP-1998-206861

Li YC (1993) Optimized spectral geoids determination. M.Sc. Thesis, Department of geomatics Engineering, The University of Calgary, Calgary, Alberta, Canada.

Li YC, Sideris MG (1994) Improved gravimetric terrain corrections. Geophysics Journal International 119, 740-752

Li YC, Sideris MG, Schwarz KP (1995) A numerical investigation on height anomaly prediction in mountainous areas. Bulletin Geodesique 69 : 143-156.

Li YC, Sideris MG, Schwarz KP (2000) Unified terrain correction formulas for vector gravity measurements. PINSA, 66, A, No. 5, September 2000, pp. 521-535

Moritz H (1968) On the use of the terrain correction in solving Molodensky's problem. OSU Report No. 108, Department of Geodetic Science and Surveying, The Ohio State University, Columbus, Ohio.

Moritz H (1980) Advanced Physical Geodesy. Herbert Wichmann Verlag, Karlsruhe, Abacuss press, Tunbridge Wells Kent.

Moritz H (2000) Geodetic reference system 1980. Journal of Geodesy, 74, 128-164.

Macmillan WD (1958) The theory of the potential. Dover publications, Inc., New York.

Martinez Z, Vanicek P, Mainvelle A ,Veronneau M (1996) Evaluation of topographical effects in precise geoids computation from densely sampled heights, Journal of Geodesy, 70, 746-754.

Martinec Z, Vanicek P (1993) The indirect effect of topography in the Stokes-Helmert technique for a spherical approximation of the geoids. Manuscripta Geodaetica,19, 257-268.

Martinec Z, Matyska C, Grafarend EW, Vanicek P (1993) On Helmert's 2nd condensation method. Manucripta Geodaetica, 18, 417-421

Nagy D (1966) The prism method for terrain corrections using digital computers. Pure Applied Geophysics. Vol.63, pp 31-39.

Omang OCD, Forsberg R (2000) How to handle topography in practical geoid determination: three examples. Journal of Geodesy, 74: 458-466.

Pavlis NK, Rapp RH (1990) The development of an isostatic gravitational model to degree 360 and use in global gravity modeling. Geophysics Journal International 100, 369-378

Pellenin LP (1962) Accounting for topography in the calculation of Quasigeoidal heights and plumbline deflections from gravity anomalies; Bulletin Geodesique, Vol. 63, pp. 57-62

Peng M (1994) Topographic effects on gravity and Gradiometry by the 3D FFT and FHT methods. UCGE reports, Department of Geomatics Engineering, Calgary, Alberta, 1994

Rapp R (1882) Degree variances of the Earth's potential topography and its isostatic compensation. Bulletin Geodesique, pp 84-94

Rudzki MP (1905) Sur la determination de la figure de la terre dapres les mesures de la gravite, Bull. Astron., ser. B, vol. 22, 1905.

Schwarz KP (1984) Data types and their spectral properties. Proceedings of the International Summer School on Local Gravity Field Approximation, Beijing, China.

Schwarz KP, Sideris MG, Forsberg R (1990) The use of FFT techniques in Physical Geodesy. Geophysics Journal International Vol. 100, pp. 485-514.

Sideris MG (1984) Computation of gravimetric terrain corrections using fast Fourier transform techniques, UCSE Report #20007, Department of Surveying Engineering, The University of Calgary, Calgary, Alberta, Canada.

Sideris MG, Schwarz KP (1987) Improvement of medium and short wavelength features of geopotential solutions by local gravity data. Bolletino di Geodesia e Scienze Affini – No. 3, 1987

Sideris MG (1985) A fast Fourier transform method of computing terrain corrections. Manuscripta Geodaetica, 10, no.1, 66-73.

Sideris MG (1990) Rigorous Gravimetric terrain modeling using Molodensky's operator. Manuscripta Geodaetica, 15 : 97-106.

Sideris MG, She BB (1995) A new high resolution geoids for Canada and part of the US by the 1D-FFT method. Bulletin Geodesique, 69(2): 92-108

Sideris MG, Li YC (1993) Gravity field convolutions without windowing and edge effects. Bulletin Geodesique, Vol. 67:107-118.

Sideris MG, Quanwei L (2002) A wavelet compression method for terrain correction computation. Submitted to Journal of Geodesy.

Sjoberg LE (2000) Topographical effects by the Stoke's Helmert method of geoid and quasigeoid determination. Journal of Geodesy, 74 :255-268.

She BB (1993) A PC – Based unified geoids for Canada. UCGE report# 20051. Department of Geomatics Engineering, University of Calgary, Calgary, Alberta, Canada.

Sun W, Sjoberg LE(2001) Convergence and optimal truncation of binomial expansions used in isocratic compensations and terrain corrections. Journal of Geodesy, 74: 627-636.

Sunkel H (1985) An isostatic earth model. Rep 367, Department of Geodetic Science and Surveying, The Ohio State University, Colombus.

Strykowski G, Boschetti F, Horowitz FG (2001) A fast spatial domain technique for terrain corrections in gravity field modelling. IAG Symposia, Vol. 123 Sideris (ed.), Gravity, Geoid, and Geodynamics 2000, Springer – Verlag Berlin Heidelburg 2001, pp 67-72.

Tsoulis D (1998) A combination method for computing terrain corrections. Phys.Chem.Earth, Vol.23, No. 1, pp.53-58.

Tsoulis D (2001) A comparison between the Airy/Heiskanen and the Pratt/Hayford isocratic models for the computation of potential harmonic coefficients. Journal of Geodesy, 74: 637-643

Tsoulis D (2001) Terrain correction computations for a densely sampled DTM in Bavarian Alps. Journal of Geodesy (2001), 75: 291-307

Tziavos IN, Featherstone WE (2000) First results of using digital density data in gravimetric geoids computation in Australia. Paper presented in GGG2000, Banff, Alberta, Canada, 2000.

Tziavos IN, Sideris MG, Forsberg R, Schwarz KP (1988) The effect of the terrain on airborne gravity and gradiometry. Journal of Geophysical Research, Vol. 93, No. B8, pp.9173-9186.

Tziavos IN, Andritsanos VD (1998) Recent advances in terrain correction computations. Second continental workshop on the geoids in Europe. Budapest, Hungary, March, 1998. Report of Finish Geodetic Institute.

Tziavos IN, Sideris MG, Sunkel H (1996) The effect of surface density variation on terrain modeling – A case study in Australia. Proceedings, European Geophysical Society General Assembly. The Hague, The Netherlands, 6-10 May, 1996.

Vanicek P, Kleusberg A (1987) The Canadian geoid – Stoksian approach. Manuscripta Geodaetica, 12: 86-98.

Vanicek P, Martinec (1994) The Stokes – Helmet scheme for the evaluation of precise geoids. Manuscripta Geodaetica, 19, 119-128

Vladimir A (1994) A three dimensional gravity field model of the Kananaskis area. UCGE report # 20070, Department of Geomatics Engineering, Calgary, Alberta, Canada

Vermeer M (1992) A frequency Domain Approach to optimal geophysical data gridding. Manuscripta Geodaetica, Vol. 17, pp. 141-154.

Wang YM (1993) Comments on proper use of the terrain correction for the computation of height anomalies. Manuscripta Geodaetica, 18 : 53-57

Wang YM, Rapp RH (1990) Terrain effects on geoid undulations. Manuscripta Geodaetica 15 : 23-29.

Wang YM (1993) Comments on proper use of the terrain correction for the computation of height anomalies. Manuscripta Geodaetica, 18:53-57.

Wichiencharoen C (1982) The indirect effects on the computation of geoids undulations. OSU Rept. 336, Department of Geodetic Science and Surveying, The Ohio State University, Ohio, USA.